A new giant sauropod, *Australotitan cooperensis* gen. et sp. nov., from the mid-Cretaceous of Australia.

Scott Alexander Hocknull[1,2], Melville Wilkinson[3], Rochelle Ann Lawrence[1], Vlad Konstantinov[4], Stuart Mackenzie[3], Robyn Mackenzie[3]

[1] Geosciences Queensland Museum, 122 Gerler Rd. Hendra, Brisbane, Queensland, Australia 4011.

[2] Biosciences, University of Melbourne, Melboune, Victoria, 3010

[3]Eromanga Natural History Museum, 1 Dinosaur Drive, Eromanga, Queensland, Australia 4480.

[4] 65/168 Oktyabrskaya Street, Ryazan, Russia, 390010.

Corresponding Author:
Scott Hocknull[1]
122 Gerler Rd. Hendra, Brisbane, Queensland, 4011, Australia.
Email address: scott.hocknull@qm.qld.gov.au

Abstract

A new giant sauropod, *Australotitan cooperensis* gen. et sp. nov., represents the first record of dinosaurs from the southern-central Winton Formation of the Eromanga Basin, Australia. We estimate the type locality to be 270-300 m from the base of the Winton Formation, with a maximum depositional age of Cenomanian to ?earliest Turonian. The new titanosaurian is the largest dinosaur from Australia as represented by osteological remains. Based on limb-size comparisons it reached a size similar to the giant titanosaurs from similar-aged formations from South America. Using 3-D surface scan models we compare features of the scapula, humerus, ulna, pubis, ischium and femur that differentiate *Australotitan cooperensis* gen. et sp. nov. from the three named Winton Formation sauropods~~:~~: *Diamantinasaurus matildae* Hocknull et al. 2009, *Wintonotitan wattsi* Hocknull et al. 2009 and *Savannasaurus elliottorum* Poropat et al. 2015. 3-D morphological comparisons also ~~identify~~ allow identifying a mosaic of similarities shared between the four taxa. The ubiquitous presence of amphicoelous caudal vertebrae recovered from sites in the new southern-central Winton Formation replicates that observed in sauropod remains of the northern Winton Formation. These combined morphological similarities lend themselves to a hypothesis of shared ancestry for all four taxa, which is explored. However, due to the incomplete skeletal remains of each taxon, a new phylogenetic assessment of titanosaurian relationships is unhelpful. Instead, a comparative phylogenetic assessment is made using characteristics of the appendicular

skeleton for the four Winton Formation taxa. A key limitation of previous and to future studies of Australian sauropods, which mirrors similar problems globally, is the inability to easily and directly compare specimens. Therefore, 3-D digital models have, and will, become a more standard way to undertake direct comparisons. However, uncoloured, low resolution, and uncharacterized 3-D surface models can lead to misinterpretations, in particular identification of pre-, syn- and post-depositional distortions. We develop a method for identifying, documenting and illustrating these distortions directly onto the 3-D geometric surface of the models using a colour reference scheme. This new method provides a direct and repeatable option for researchers when observing and documenting specimen preservation, taphonomic alterations and geometric differences. Temporal, palaeobiological and palaeoenvironmental differences between the northern and southern-central sauropods are considered to explain the taxonomic and morphological diversity of sauropods from the Winton Formation. However, all explanations remain equivocal because of the poor local and regional chronostratigraphic resolution, with no sauropod taxa demonstrably sympatric.

Introduction

Australian dinosaur palaeontology has experienced somewhat of a resurgence of research over the last decade or so with several new taxa recorded from Cretaceous-aged localities across Australia, including *Wintonotitan wattsi*, *Diamantinasaurus matildae*, *Australovenator wintonensis* (Hocknull et al. 2009) and *Savannasaurus elliottorum* (Poropat et al. 2016) from Winton, Queensland; *Kunburrasaurus ieversi* (Leahey et al. 2015) from Richmond, Queensland; *Weewarrasaurus pobeni* (Bell et al. 2018) and *Fostoria dhimbangunmal* (Bell et al. 2019a) from Lightning Ridge, New South Wales; *Diluvicursor pickeringi* (Herne et al. 2018) and *Galleonosaurus dorisae* (Herne et al. 2019) from coastal Victoria; and six new ichnotaxa from Broome, Western Australia (Salisbury et al. 2016).

This increased naming of new taxa has mostly occurred due to more intensive study of previously described specimens and already established fossil collections, alongside a moderate increase in new discoveries from known fossil fields. Although a new 'wave' of research focus on Australian dinosaurs is underway, large regions of prospect for Cretaceous-aged fauna remain. Developing this potential both in terms of fauna and their geochronological context is

Comentario [MH1]: It seems that the document still contains Mendeley (or other reference manager) fields. You can export the plain text in a separate file, and then correct some citations. I marked up few of them along the text.

crucial to better understand the palaeobiogeography and biochronology of the Cretaceous-aged terrestrial faunal assemblages.

In the Winton Formation the dinosaurian fossil record is concentrated to a small number of sites near Winton and Isisford, located in the northern portion of the Eromanga Basin (Figure 1 & 2, A). This concentrated research effort is in spite of vast areas of mapped Winton Formation occurring throughout the central, southern and western Eromanga Basin, including much of western Queensland (QLD), large areas of interior and north-eastern South Australia (SA), south-eastern Northern Territory (NT) and north-western New South Wales (NSW) (Figure 1 & 2, A). These poorly developed regions comprise an area of approximately two thirds of the Eromanga Basin, but have currently only yielded isolated vertebrate faunal remains (Table 1). As such, major palaeobiogeographic gaps occur in our knowledge of these mid- to Late Cretaceous faunas, paralleling the vast gaps occurring in other high profile Australian vertebrate fossil records, such the Quaternary megafauna (Hocknull et al. 2020).

New fossil sites from the southwest Queensland portion of the Winton Formation, near the townships of Eromanga and Quilpie have recorded floral, faunal and ichnofossils, including the remains of sauropod dinosaurs (Hocknull et al. 2019) (Figure 2, A&B). Dinosaurian vertebrate fossils were first discovered in this area in 2004 by property owners of Plevna Downs Station. Subsequent excavations undertaken by Queensland Museum from 2006, and then between the newly established Eromanga Natural History Museum and Queensland Museum, have recovered vertebrate fossil remains that include the fossils described here. The new specimens described are lodged in the Eromanga Natural History Museum, a not-for-profit museum with a publically accessible palaeontological collection that represents vertebrate fossils from the southwest region of Queensland.

We describe a new taxon based on associated sauropod limb and girdle elements along with isolated remains referable to this new taxon. We compare these new finds with other sauropods world-wide sharing similar geological age and body-size, but we pay particular attention to comparisons with the previously described taxa from the northern Winton Formation; *Wintonotitan wattsi* Hocknull et al. 2009, *Diamantinasaurus matildae* Hocknull et al. 2009 and *Savannasaurus elliottorum* Poropat et al. 2016. ~~This~~ The new taxon represents the largest dinosaur so far found in Australia represented by osteological remains.

Institutional Abbreviations. AODF (Australian Age of Dinosaurs Museum of Natural History Fossil), AODL (Australian Age of Dinosaurs Museum of Natural History Locality) EMF (Eromanga Natural History Museum Fossil), EML (Eromanga Natural History Museum Locality), QMF (Queensland Museum Fossil), QML (Queensland Museum Locality).

Geological Settings

The new dinosaur sites reported here are located within the central Eromanga Basin as part of the southern-central Winton Formation. The sites occur 80-90 km west of the township of Eromanga on Plevna Downs Station (Figure 2, B). These new sites are approximately 500-600 km south of the Winton district, which represents the locations for all currently named dinosaurian taxa from the Winton Formation (Hocknull et al. 2009; Poropat et al. 2016) (Figure 2, A). Approximately 300 km to the north-east of Eromanga, an unnamed ornithopod has been reported from Isisford, representing the first central-eastern Winton Formation dinosaur (Salisbury et al. 2019) (Figure 2, A). As yet, no dinosaurian fossils from the south-western or western extremities of the Winton Formation have been found, excepting for a weathered bone from Munga-Thirri (Simpson Desert) that may be dinosaurian (Hocknull per. obs., 2002, 2011, & Yates pers. comms., 2019). A newly dated, now considered semi-contemporaneous dinosaurian fauna, from the Surat Basin Griman Creek Formation, occurs approximately 600 km southeast of Eromanga (Bell et al. 2019b) (Figure 2, A).

The new southern-central Winton Formation dinosaur sites are structurally dominated by the Mt. Howitt Anticline, a large anticline with associated Cooper Syncline that produces variable surface exposures of Winton Formation sediments, with a relatively thin cover of Cenozoic alluvium. Each fossil site is located on an alluvial plain with gullies and creeks that drain westward to form part of the greater Cooper Creek channel system. The floodplain forms part of the western portion of the Mount Howitt Anticline (Figure 2, B) and is surrounded by erosion-resistant flat-top hills comprised of Cenozoic silcretes and Glendower Formation that overlie extensively chemically-weathered Winton Formation sediments (Ingram 1971; Senior 1970; Senior 1968) (Figure 2, A; see also Figure 7, A).

Outcrop of Winton Formation is sparse and confined to resistant sandstones and calcite cemented siltstone-claystone concretions that form part of the resultant deeply weathered regolith (Figure 3, A). A relatively thin, 1 m to 2 m thick, soil profile containing a deflation lag

Comentario [MH2]: These should be within the same parentheses. Check it throughout the text after saving the document in plaintext.

of the Cenozoic-aged silcretes and Glendower Formation pebbles, covers most of the available Winton Formation (Draper 2002) (Figure 3, B). Faunal remains and silicified wood are initially found at the surface of this soil profile and are usually associated with broken up cemented concretions or rarely within sandstones.

The 'self-mulching' actions of the vertosol soils through the expansion and contraction of the smectite-rich clays (Grant & Blackmore 1991) offers a likely mechanism that evidently brings hard material from within the underlying Winton Formation up to the soil surface (e.g. fossilized bones, petrified wood and cemented rock). The vertosol profile itself is derived from the weathering of the underlying Winton Formation, as part of a wider process of cracking clays weathering the Rolling Downs Group surface expression (Vanderstaay 2000). Therefore, over time, as the Winton Formation weathers into a soil profile, the fossil remains rise and concentrate at the surface, breaking into pieces. This same mechanism was originally observed around the township of Winton and led to the discoveries of vertebrate remains at depth and the subsequent new dinosaur discoveries (Hocknull et al. 2009). This same process was observed at the Eromanga sites and subsequent excavations proved an essentially identical process yielding similar levels of success for recovering vertebrate fossils and discovering intact bonebeds subsurface.

Inclusions within the soil profile include alluvial sands, clays and gravels derived from major flooding of the Cooper Creek channel system that incorporates the material from the surrounding topographically higher Cenozoic cap rock. Therefore, the soil profile at most sites derives material from two separate sources.

Unlike the northern Winton Formation sites, buried Neogene-Holocene palaeochannels have been observed to cut and erode some of the southern-central Winton Formation dinosaur fossil sites. Therefore, at some time in the past, possibly during wetter periods of the Pliocene or Pleistocene, active channel down cutting likely exposed significant areas of Winton Formation at the surface. Subsequent to this, possibly during the intensifying aridity of the Late Pleistocene, burial of these palaeochannels occurred and vertosols dominated the landscape.

Winton Formation

The Winton Formation consists of interbedded volcanolithic sandstones, siltstones, mudstones, minor coals and intraformational conglomerates (Gray et al. 2002). Calcite cemented

concretions are common and in places the top approximate 90 m of preserved Winton Formation is highly chemically altered (kaolonitised and ferrugunised). The present-day thickness of the Winton Formation ranges from surface exposure on the basin margins that is associated with uplifted structures, to at least 1100 m of thickness toward the west-southwestern parts of the basin (Cook et al. 2013; Hall 2015).

The present-day surface expression, distribution and thickness of the Winton Formation is residual, reflecting modifications of its original distribution and thickness through multiple post-depositional structural and erosional events (Gray et al. 2002). It represents one of the largest formations (both in terms of thickness and areal extent) from the Cretaceous part of the Rolling Downs Group within the Eromanga Basin and occurs across three States (QLD, NSW, SA) and one Territory (NT) (Figure 1 & 2).

The Winton Formation forms the uppermost unit of the Rolling Downs Group and the Late Triassic to Cretaceous-aged Eromanga Basin (Exon & Senior 1976). It conformably and transitionally overlies the Mackunda Formation, however, due to the transitional nature of the Mackunda to Winton Formation it is difficult to establish the base of the Winton Formation, both in outcrop and in the subsurface (Cook et al. 2013; Draper 2002). In some successions in SA where these two formations are more difficult to differentiate, the superseded name Blanchewater Formation (Forbes 1966) was used in the past for the combined undifferentiated interval (Moore & Pitt 1985).

An informal convention has previously been used to define the base of the Winton Formation, using the first appearance of coals or rhizomiferous sediments to define the base (Draper 2002; Gray et al. 2002). However, coals are not always present and the majority of these transitions are only observable in cores and do not manifest in surface outcrop. This means there is uncertainty when determining the vertical and spatial distribution of the first appearance of coals or palaeosols and thus the base of the Winton Formation. Likewise, the last occurrences of marine shells, such as *Inoceramus*, are considered in numerous stratigraphic and petroleum well logs to be good indicators of the transition from the marine and tidally influenced Mackunda Formation to the freshwater fluvial and lacustrine deposits of the Winton Formation. However, in core samples, it is very difficult to confidently discern the difference between *Inoceramus*, or other marine invertebrate shells, in comparison to the freshwater-restricted invertebrate taxa, such as unionoid bivalves. Therefore, whether using the last presence of marine-tidal

invertebrate taxa and/or the first indications of palaeosols, freshwater taxa or coals, the clear distinction of the Winton Formation base remains equivocal.

Stratigraphic position of dinosaur sites. Due to the lack of contiguous Winton Formation outcrop it is practically impossible to directly trace and define the relative local stratigraphic position between any one of the many dinosaurian body-fossil sites found throughout the Winton Formation. Even at sites in relative close proximity to one another where the surface expression of fossilized bones is spaced 10s to 100s of meters apart it is impractical to define a local stratigraphic succession. Heavy earth-moving machinery must be used to create long and deep (4 m+) stratigraphic trenches that remove the 1 m+ soil and weathered vertosol-Winton Formation covering to expose enough primary sedimentological structure to enable bonebed layers to be traced laterally. This is both impractical and unrealistic in terms of developing a good understanding of local stratigraphic control between dinosaur bonebeds and site clusters. Ground penetrating radar has been trialed in places but with limited results. The clay-rich vertosol soil is variably moist at depth and possesses large voids and cracks, all of which impact the resistivity profiles and thus potential for accurate subsurface interpretations. The uniform sedimentological signature of the Winton Formation itself, being mostly siltstones to fine-grained sandstones, with small to large cemented concretionary zones also obscures lateral continuity.

Within the local context, the overall dip of strata is generally low; however, sites occur 100s of meters to several kilometers apart and are mostly associated close to poorly defined structural features such as concealed faults or the crests of anticlines (Figure 2, 4 and 5). Therefore, these local and poorly mapped structural features potentially create differences in vertical profile position of 10s to 100s of meters between individual fossil sites. ~~Therefore, a~~Although the sites may be regarded as topographically similar and assumed to be contemporaneous, this is unverified, and concealed stratigraphic differences could be greater than expected. Especially in terms of defining whether taxa recovered from one site are sympatric with taxa recovered from other locations, where there is no control on relative positions of bonebeds and the sedimentation rate of these deposits is unknown.

Regionally, defining the relative stratigraphic position of dinosaur fossil sites is equally difficult with the added complexity of; 1) regional subsurface structuring (Exon & Senior 1976;

Hoffmann 1989); 2) rapid exhumation and pre-Cenozoic erosion of the Winton Formation (Keany et al. 2016; Rodgers et al. 1991); 3) Cenozoic basin filling (Cook & Jell 2013; Day et al. 1983; Krieg et al. 1990); 4) deep Winton Formation chemical weathering (Idnurm & Senoir 1978; Senior & Mabbutt 1979); 5) broadly defined palynomorph zones with no refinement within the Winton Formation (Monteil 2006); and 6) considerable geographical distance between localities ranging from ~105 km to over 500 km apart.

The multiple levels of uncertainty at both local and regional scales, over such an extensive and thick geological formation, renders the level of stratigraphic accuracy needed for meaningful chronological comparisons between fauna difficult, and even more so when comparing fauna from semi-contemporaneous formations from separate basins. Such uncertainty requires a greater future effort to place each fauna within a local and regional context, currently leaving only broad-sweeping generalisations possible (Wilkinson et al. 2019).

We have attempted here to place the type localities of all four sauropod taxa into a regional stratigraphic context, but local stratigraphic context for each site is near impossible to ascertain. For the southern-central Winton Formation sauropod sites we begin by using a published interpretation of seismic and well data that produced an approximation of Winton Formation thickness (Hall 2015) (Figure 4, A). Importantly, it provides a NW-SE cross-sectional interpretation across the crest of the Mt. Howitt anticline, the key geological structure associated with all ~~of~~ the new dinosaur sites described here.

All of the new dinosaur sites occur within five kilometers of the western flank of the Mt. Howitt anticline with one locality (EML019) located close to the Mt. Howitt 1 well (Delhi Petroleum 1966). The thickness of the Winton Formation at Mt. Howitt 1 approximates 300 m, with thicker sections preserved on the flanks of the Mt. Howitt anticline (Figure 4, A),

Next, we used well and seismic data proximal to the sites to estimate the thickness of the Winton Formation closest to the dinosaur sites. The stratigraphic position of the type locality for *Australotitan cooperensis* gen. et sp. nov. (EML011(a)) relative to the base of the Winton Formation was estimated by examining data from nearby petroleum well bores, Wareena 1-5 (Gauld 1981; Lawrence 1998; Lowman 2010; Robinson 1988; Turner 1997) and Navalla 1 (Boothby 1989) with Wareena 4 located approximately 1.33 kilometers to the east of EML011. In addition to this, seismic data was investigated to determine the influence of faulting and

structural features within the vicinity of the dinosaur localities (Delhi Petroleum 1991; Finlayson 1984; Flynn 1985; Garrad & Russel 2014; Seedsman 1998).

Data from the petroleum well bores is limited, as no cores were taken, and the lithological descriptions do not indicate the clear presence of coal or palaeosols, thus determining the base of the Winton Formation or top of the Mackunda Formation was not possible. The closest stratigraphic core, GSQ Eromanga 1, occurs 130 km to the east, where the base of the Winton Formation is interpreted to be 164 m below ground surface (Almond 1983).

Without a good lithological control, we considered wireline petrophysical logs to interpret the base of the Winton Formation. Changes in petrophysical character of the gamma-ray, sonic, resistivity and self-potential wireline logs have previously been used to define the Mackunda and Winton Formations in the subsurface (Gray et al. 2002; Moore et al. 1986). We used these same features to pick the base of the Winton Formation with a thickness of 270-300 m for the Wareena and Mt. Howitt wells.

We correlated the petrophysically interpreted base of the Winton Formation at Wareena 1 and Mt. Howitt 1 wells with the uppermost prominent seismic reflection event for seismic line 83-NJZ (Figure 4, B). This seismic line includes the Mt. Howitt 1 and Wareena 1 wells and runs in a NNE-SSW direction close to the axis of the Mt. Howitt anticline (Figure 2, B). This seismic reflection event is not continuous which is likely due to small scale faulting. This again reflects the uncertainty likely to pervade local stratigraphic differences mentioned above. Interpretation of the seismic line indicates that the Wareena 1 and Mt. Howitt 1 wells are located near to the crest of the Mt. Howitt anticline and are therefore likely to contain the thinnest section of preserved Winton Formation. Therefore, on the basis of the four dinosaur localities (EML010-013) being located in close proximity to the Wareena 1 well on the crest of the Mt. Howitt anticline, the sites are likely to be 270-300 m from the base of the Winton Formation. This is supported by the interpretation by (Hall 2015) (Figure 4, A).

Comentario [MH3]: correct

Applying similar methods to the northern Winton Formation sauropod type localities, we focused our assessment of the Winton Formation base and thickness by assessing stratigraphic and petroleum wells found closest to the type localities of *Diamantinasaurus matildae* and *Australovenator wintonensis* at AODL85 (Hocknull et al. 2009); *Wintonotitan wattsi* at QML313 (Hocknull et al. 2009); *Savannasaurus elliottorum* at AODL82 (Poropat et al. 2016);

and the referred specimen of *Diamantinasaurus matildae* at QML1333 / AODL127 (Poropat et al. 2016) (Figure 5, A).

The type localities of *Diamantinasaurus matildae* and *Wintonotitan wattsi* are close to one another (~3.5 km apart) and occur 2.6 km and 1.1 km east of a concealed (unnamed) fault respectively. The closest petroleum wells are Minion 9 (Pangaea Resources 2013) to the west of the concealed fault and fossil sites, and Lovelle Downs 1 (Watson 1973) that occurs east of the concealed fault and east of the type localities. Lovelle Downs 1 is 4 km due east of the type locality for *Diamantinasaurus matildae*.

At Lovelle Downs 1, the base of the Winton Formation was assessed to be 880 feet (268 m) (Watson 1973); however, lithological descriptions indicate first coal at 1210 feet (368 m); therefore, we agree that the base of the Winton Formation is at least 268 m from surface but it is more likely to be 368 m or more from the surface. At Minion 9, west of the type localities and the unnamed fault, the base of the Winton Formation was assessed on first coals to be 352 m from the surface but with 31.6 m of overlying Cenozoic sediments; thus a thickness of 316 m (Pangaea Resources 2013). We agree with this assessment (Figure 5).

Both type localities are situated over a structural low termed the Lovelle Syncline / Depression, and occur about 18-20 km west and downthrown of a major fault, termed the Cork Fault, which would provide the structural means for a relatively thick Winton Formation across this area. Therefore, we propose a Winton Formation base from surface for the type localities of *D. matildae* and *W. wattsi* of at least 350 m (Figure 2, A).

The closest stratigraphic core to the type localities of *D. matildae* and *W. wattsi* comes from GSQ McKinlay 1 (Hoffman & Brain 1991), 70 km to the northwest and very close to the Winton Formation outcrop edge (Figure 5). The Winton Formation base at GSQ McKinlay 1 is interpreted to be approximately 112 m from the surface although no coals are present. *Inoceramus* shell is identified at ~125 m, therefore, we agree that the base of the Winton Formation is at around 112 m, but it could be higher in the core. Therefore, there is a difference of over 200-250 m of Winton Formation thickness between the Minion 9 and Lovelle Downs 1 wells (and type localities), relative to the closest stratigraphic core (GSQ McKinlay 1).

In contrast, the type locality of *Savannasaurus elliottorum* and another sauropod locality preserving a specimen referred to *D. matildae* (QML1333)~~,~~ occur~~s~~ approximately 70 km to the east of the Cork Fault on the upthrown section, and approximately 18 km west of the Eyriewald

Anticline. These sites are located closer to the Winton Formation outcrop edge than the type locations for *D. matildae* and *W. wattsi* and therefore we would expect them to be closer to the base of the Winton Formation.

The closest petroleum well is Wardoo 1 (Exoma Energy 2013), positioned 6-7 km south and southwest of the *S. elliottorum* type locality and QML1333 respectively. The base of the Winton Formation at Wardoo 1 is reported as 311 m, however, the first coals are indicated at 90 m (Exoma Energy 2013). Therefore, we treat the reported depth and thickness of the Winton Formation at Wardoo 1 with some caution and propose that it is more likely closer to 100 m (Figure 5). Wardoo 1 and the dinosaur localities are close to the Winton Formation outcrop edge, which is similar to that seen in the stratigraphic cores of GSQ McKinlay 1 (Winton Formation base at 112 m) (Hoffman & Brain 1991) and GSQ Manuka 1 (Winton Formation base at ~92 m) (Balfe 1978); therefore, we propose a 90 m depth based on the first appearances of coals as a more realistic estimate for the base of the Winton Formation at Wardoo 1. Therefore, we propose a depth to base of Winton Formation for the *S. elliottorum* type locality and QML1333 to be less than 100 m. (Figure 5).

Taken together, our assessment of the depth to base of Winton Formation in relation to the four sauropod type localities illustrates the uncertainty discussed above in relation to a lack of clear delineation for the base of the Winton Formation, and the relative stratigraphic positions of the sites both locally and regionally. On the available published data from stratigraphic cores, wells and seismic lines located closest to the type localities, we propose that; 1) the *Savannasaurus elliottorum* type and QML1333 sites are positioned less than 100 m above the base of the Winton Formation; 2) the new type locality for *Australotitan cooperensis* gen. et sp. nov. is positioned somewhere between 270 and 300 m above the base of the Winton Formation; and 3) the type localities of *Diamantinasaurus matildae* and *Wintonotitan wattsi* are positioned ~350 m (or somewhere between 316 and 368 m) above the base of the Winton Formation (Figure 5). Although this proposed series of positions above the base of the Winton Formation likely constitute real stratigraphic~~,~~ and thus chronological differences between the sauropod type localities, we urge caution in using this proposed stratigraphic sequence for palaeontological interpretations due to the uncertainty of it and the unknown spatiotemporal sedimentation rates across the Winton Formation.

Winton Formation Age

The Winton Formation was assigned a Late Albian to Cenomanian chronostratigraphic age on the basis of spore-pollen zonation (Monteil 2006). The presence of Late Albian index species *Phimopollenites pannosus* to Cenomanian index species *Hoegisporis uniforma* (=*Appendicisporites distocarinatus*) within the Winton Formation reflects this assessed chronostratigraphic age range (Helby et al. 1987). On the basis of well-preserved palynomorphs indicating the *Coptospora paradoxa* and *Phimopollenites pannosus* zones, a latest Albian age was interpreted for a surface locality located close to the type localities of *Diamantinasaurus matildae*, *Wintonotitan wattsi* and *Australovenator wintonensis* (Dettmann et al. 2009). The palynomorphs from this site indicated an age of no older than Late Albian. With the absence of Cenomanian indicator species such as *Hoegisporis uniforma* and *Appendicisporites distocarinatus* a Cenomanian age could not be given. The type localities for three dinosaurian taxa (*Diamantinasaurus matildae*, *Wintonotitan wattsi* and *Australovenator wintonensis*) from nearby sites were thus considered to be latest Albian in age (Hocknull et al. 2009).

Subsequent to this, two independent age assessments of the Winton Formation were conducted using modelled U-Pb radiometric assessments of detrital zircons, and calculated age probability distributions, to determine the maximum depositional age of dinosaurian fossil sites (Bryan et al. 2012; Tucker et al. 2013). Modelled interpretations from these probability distributions were used to propose true depositional ages for the layers from where the zircons were sampled and to construct an age profile for the Winton Formation, defined into lower, middle and upper Winton Formation (Tucker et al. 2017; Tucker et al. 2016). See Tucker (Tucker et al. 2016; Tucker et al. 2013) for explanations of each age model type and methodology used.

The reliability of the detrital zircon dating technique for sedimentary sequences will not be reviewed here, having been discussed and assessed by many others who have identified biases, methodological issues, and interpretative problems with detrital zircons (Allen & Campbell 2012; Andersen et al. 2019; Coutts et al. 2019; Horstwood et al. 2016; Johnstone et al. 2019; Klötzli et al. 2009; Košler et al. 2013; Sharman & Malkowski 2020).

Considering this uncertainty, the results so far produced for the Winton Formation need to be treated cautiously~~;~~. Nevertheless~~however~~, they all indicate a probable temporal age range of between 103 to 92 million years ago (Late Albian to earliest Turonian) for the maximal depositional ages of portions of the Winton Formation.

Key to determining the depositional age and age range for the Winton Formation is the source of the youngest zircon grains that likely came from eastern Australian volcanicity that continued throughout the Early to mid-Cretaceous (Bryan et al. 2012; Tucker et al. 2017). Substantial volumes of mostly silicic pyroclastic material and coeval first cycle volcanogenic sediment accumulated in the Eromanga Basin during deposition of the Winton Formation (Bryan et al. 2012). This material was transported over very large distances along with the semi-contemporaneous development of a southwest draining river system dubbed the 'Ceduna River'. The 'Ceduna River' depocentre was the Ceduna delta, a very large deltaic lobe that filled the tectonically subsiding southern Australian Bight Basin, which formed the contemporaneous paralic White Pointer supersequence (Espurt et al. 2009; King & Mee 2004; Lloyd et al. 2016; Sauermilch et al. 2019; Totterdell & Krassay 2003).

However, it is unclear, not only of the magnitude and continuity of explosive events, but also the ultimate cessation of volcanicity. If volcanicity ceased before the end of Winton Formation deposition, this raises the possibility of erosion and reworking of older zircons within the Winton Formation without the arrival of new zircons entering the system, which could obscure a more refined true depositional age, and this may impact the ages of the four type locality deposits.

Age of the dinosaur sites. A single population of detrital zircons has been published for the *D. matildae* type locality (Bryan et al. 2012), but no detrital zircon populations have been published for the other three type localities. The closest stratigraphically controlled detrital zircon populations for all three northern sauropod taxa, *D. matildae*, *W. wattsi* and *S. elliottorum*, comes from GSQ McKinlay 1 (2 samples) (Tucker et al. 2016). Whilst for the southern-central Winton Formation sites, the closest stratigraphically controlled detrital zircon population comes from GSQ Eromanga 1 (1 sample) (Tucker et al. 2016).

Of these four zircon populations recovered closest to our type localities, the two GSQ McKinlay 1 samples were taken closest to the Winton Formation base, at 102.7 m and 58 m from the Winton Formation base respectively. The lowest sample was defined to represent the 'middle' Winton Formation and the higher sample the 'uppermost' Winton Formation (Tucker et al. 2017; Tucker et al. 2016). The stratigraphically lower sample returned modelled zircon ages of between 92.1 ± 1.8 Ma (YC1σ (+3) to 95 Ma (YPP), whilst the stratigraphically higher sample

returned discordant older ages of between 93.5 ± 4.4 Ma (Weighted average (+3)) and 98 Ma +0.9/-4.1 Ma (TuffZirc (+6)).

The next highest zircon population was taken from GSQ Eromanga 1 within the core, at approximately 146 m above the Winton Formation base and defined as the 'lower' Winton Formation (Tucker et al. 2017; Tucker et al. 2016), 44 m higher than the 'uppermost' Winton Formation of GSQ McKinlay 1. This sample returned modelled maximum depositional ages ranging between 93.1 ± 1.1 Ma (YSG) and 101.1 +1.3/-1.4 Ma (TuffZirc (+6), representing a similar modelled age range compared to the 'uppermost' Winton Formation of GSQ McKinlay 1. Of note, a similar age range was also given for a sample taken between 20.8-35.8 m below surface at GSQ Blackall 2 stratigraphic core, to the north-east of GSQ Eromanga 1 (Tucker et al. 2016). This sample comes from the 'lower' Winton Formation, taken between 113-128 m from the Winton Formation base (~149 m below surface) (Coote 1987). This zircon population returned modelled ages ranging between 93.4 ± 1.8 Ma (YPP) and 98.7 +2.2/-5.3 Ma (TuffZirc (+6)).

Finally, the highest zircon population was sampled at the *D. matildae* type locality, which sits at least 350 m from the Winton Formation base. This sample sits twice to three times higher in the Winton Formation when compared to the 'lower' Winton Formation GSQ Eromanga 1 and GSQ Blackall 2 and 'middle' to 'uppermost' Winton Formation of GSQ McKinlay 1 (Tucker et al. 2017; Tucker et al. 2016). The ages for the type locality include a single youngest grain age of 94.29 ± 2.8 Ma and two youngest age peaks at ~95 Ma and ~102 Ma (Bryan et al. 2012; Greentree 2011).

Considering each zircon sample's stratigraphic position above the base of the Winton Formation with each sample's youngest single grain age, it would be expected that the sample taken closest to the base of the Winton Formation would return the oldest youngest single grain age, and that the sample taken furthest from the Winton Formation base would have the youngest single grain age. This is not the case, the lowest sample, taken 58 m from the Winton Formation base has a single grain age of 93.4 ± 1.5 Ma, which is within the error of the highest sample (350 m+) single grain age of 94.29 ± 2.8 Ma. The youngest single grain ages for the intermediate samples are also within error of the lowest and highest zircon populations; therefore, the maximal depositional age based on youngest single grain detrital zircons is similar throughout the 350 m

Comentario [MH4]: is this a single parenthesis?

+ sampled Winton Formation and does not indicate a change in age with the stratigraphic position.

Taking the youngest age peak for the zircon populations, a similar situation exists, with the sample taken closest to the base of the Winton Formation returning an age of 95 Ma and the sample taken furthest from the base of the Winton Formation also returning an age of 95 Ma. Such similarities in ages across 350 m+ of Winton Formation can potentially be reconciled in several ways.

The similarities in ages could represent the loss of new zircons entering the system after the cessation of volcanicity, resulting in reworking of the youngest available grains up the profile. Or, the sedimentation rate across the Winton Formation was exceptionally variable across the basin producing considerable differences in depositional thicknesses across relatively small geographical areas. Alternatively, the base of the Winton Formation may be diachronous across the basin, resulting in areas with similar positions relative to the base of the Winton Formation being of dissimilar ages. It is conceivable that one or more, or even all, of these processes were operating during deposition of the Winton Formation. We note that all samples within the Winton Formation contain recycled detrital zircons and as yet no in situ pyroclastic beds have been recorded.

The ~~closest~~ detrital zircon samples taken closest to our new dinosaur sites is GSQ Eromanga 1 (Almond 1983) and as discussed above the sample comes from close to the base of the Winton Formation (~146 m). The type locality for *Australotitan cooperensis* gen. et sp. nov. is estimated to occur 270-300 m above the base of the Winton Formation, therefore, twice as high within the sequence relative to GSQ Eromanga 1, located 130 km east of it. The age range for this detrital zircon population is also within the error of the samples from the northern Winton Formation, with a youngest single grain of 93 ± 1.1 Ma, and ranging up to 101.1 +1.3/-1.4 Ma (Tucker et al. 2016). The youngest population peak sits at 96 Ma, slightly older than the lowest samples from the northern Winton Formation stratigraphic cores. We therefore consider that the age of the type locality EML011(a) and other associated localities have a maximum depositional age of between 93-96 Ma.

The combined uncertainties expressed above in regards to the stratigraphic positions of all of the type localities, uncertainties with detrital zircon dating, and the lack of other techniques to better refine the absolute ages of the deposits, the ~~true~~ actual age of all four taxa remains equivocal. A

Con formato: Resaltar

Con formato: Fuente: Cursiva

maximum depositional age of mid-Cenomanian (~95-96 Ma) for the four type localities discussed here is favoured. Any further refinement will require much greater control of both stratigraphy and age. We note that the uncertainty of the maximum depositional age has been suggested to range for the 'lower', 'middle' and 'upper' Winton Formation of between 92-94 Ma (Tucker et al. 2016). We generally agree with this level of uncertainty but propose a slightly greater range (92-96 Ma).

The uncertainty surrounding the chronometric dates for the maximum depositional age of either portions of, or the whole, Winton Formation presents significant difficulties when proposing testable hypotheses focused on local or regional sauropod biogeography, palaeoecology and evolution. Additionally, these stratigraphic and age uncertainties further render chronological comparisons of the Winton Formation dinosaurian fauna with the semi-contemporaneous Griman Creek Formation at Lightning Ridge (Bell et al. 2019b) of limited value.

Depositional & Taphonomic Settings

The dinosaurian skeletal remains from these southern-central Winton Formation sites are exclusively represented by sauropods. In spite of a large number of sites having been excavated over the last decade, only the remains of a freshwater turtle (?chelid) and an isolated poorly preserved hyriid bivalve represent fauna not attributable to sauropods (Hocknull et al. 2019). There is a distinct lack of higher taxonomic representation relative to the fauna from the northern Winton Formation sites. Currently missing fauna from the southern-central Winton Formation include gastropods, insects, teleost fish, lungfish, crocodilians, pterosaurs, theropods, ornithopods, ankylosaurs (Table 1).

Preservation of sauropod remains range from isolated, fragmentary remains that have undergone considerable pre- and post-depositional modifications through to articulated partial skeletons preserved within thick cemented siltstone concretions (Figure 6, I & K). Preserved alongside these sauropod remains are macrofloral remains ranging from isolated leaves to thick layers of woody debris (Figure 6, A-I). In addition, ichnological evidence points to considerable bioturbation (dinoturbation) at EML011, which includes the type locality of *Australotitan cooperensis* gen. et sp. nov. (Figures 6, J; Figure 7, C & D and Figure 8, A-N). One such feature is a near 100 m long trampled silt and bonebed unit, also preserving a partial associated skeleton.

Site Descriptions

At least fourteen dinosaur bone-bearing fossil sites have so far been discovered in the southern-central Winton Formation. These sites are divided into two areas of northern and southern Plevna Downs Station, located 85 km west of the Eromanga township (Figure 2, B). The type ~~locality~~ specimen? ~~for~~ of *Australotitan cooperensis* gen. et sp. nov. comes from the southern Plevna Downs Station, EML011(a), with referred remains from EML010 and EML013.

EML 010. Material; EMF106 & EMF164. EML010 surface scatter was discovered in 2005 within the present-day anastomosing channelled creek system. The bones occur between two weathered units of resistive siltstone-mudstone cemented rock both running in a general East-West direction. The bone scatter occurs between these two units with no surface bone found to the north or south of them. It represents a discrete site with the entire deposit being confined to a single area of surface scatter approximately 1500 m^2. The majority of the surface scatter was made up of fragmented, rounded and winnowed cortical and cancellous bone fragments indicating a long period of surface exposure, but relatively little distal transport from its subsurface source matrix.

Bone preserved with adhering cemented siltstone-mudstone indicates that the bones originated from one of the cemented units and subsequent surface exposure and weathering has broken up the remains into small pieces. Collections of surface specimens in 2005, 2006, 2010 and 2014 along with excavated subsurface collections in 2006 and 2014 revealed a large number of bone fragments representing pieces from sauropod axial and appendicular elements.

There is no obvious element duplication; however, some remains indicate the presence of two different-sized sauropod individuals within the deposit. At this point, we have separated the identifiable elements of the large individual from those that are from a smaller individual, or those pieces that are unidentifiable. The identifiable remains from the large individual include pieces of a massive femur, pieces of at least one very large somphospondylous presacral vertebra, fragments of appendicular limb (ulna) and rib shaft pieces. The putative smaller individual is represented by a partial caudal vertebra and fragments of podial elements.

Few fragments could be pieced together with most suspected joins having long weathered away due to long-term exposure. Most are of limited morphological use due to their poor

preservation; however, on comparison with other ~~better~~ better-preserved specimens from other sites, the large individual represents the largest sauropod specimen so far recorded.

Winnowing and rounding through sand-blasting of the ~~cancellous internal~~internal cancellous bone is present in most surface collected elements. At depth, the bone fragments are found within a lag of Paleogene-aged silcrete gibber stones close to the transition between the vertosol and underlying Winton Formation siltstone. These gibber stones most likely became incorporated within the vertosol during soil formation processes as lag and channel fill. Therefore, the bone deposit can be considered to be a lag and redeposit derived from the breaking down of the cemented Winton Formation siltstone unit containing the vertebrate fossil remains. Subsequent mixing within the channel has concentrated bone fragments within the vertosol profile, and recycling of these fragments within the soil profile makes it impossible to determine the original relationship of the bones to one another within the siltstone unit itself. However, the total confined spread of the fragments and uniform preservation indicates no secondary bone mixing from other localities. We conclude from this that an in situ siltstone shelf preserving the dinosaur skeletal remains was broken apart through the combined weathering and development of the vertosol with the recycling actions of a small palaeochannel sometime during the Quaternary.

One additional possible taphonomic agent at this particular site is bioturbation of the deposit by wombats. A tooth of a wombat, probably a species of *Lasiorhinus* (Hairy-nosed Wombat), was recovered within the vertosol during initial excavations in 2005. Although there are no preserved indications of burrows, the presence of wombats in the area in the past does offer an alternative mechanism for dislocation of fossil remains at depth and transport of these remains to the surface. The burrowing behaviour of wombats may have also contributed to the surface expression and bone fragments in Winton, at QML1333 (Hocknull 2005).

Once exposed at the surface, lateral movement of the bone fragments has been limited due to the very low topographic relief and channel velocity during flooding events. It was observed in 2011 that exposed bone fragments can withstand high volume flow during large-scale flood events, whereby the specimens move very little during the event and remain exposed at the surface on pedestals of sediment. So although flooding occurs within the channel system, the impact of this on the surface expression of dinosaur bones seems minimal. Together, these

observations suggest that EML010 represents the longest-term surface expression of dinosaur fossils so far found in the region.

EML010 is unique within the sites so far recovered from Eromanga having experienced the greatest amount of surface weathering of any of the sites and the only site demonstrating the impact of winnowing by windblown abrasion. This form of bone weathering is unique in all of the sites so far observed in the Queensland section of the Winton Formation. Thus, EML010 probably represents one of the most weathered dinosaur localities from the Winton Formation that still preserves bone at the surface.

Fossil bone observed by SAH in 2002 and 2011 at the Museum of Central Australia, Alice Springs, Northern Territory, and via Yates pers. comm. (2019), represent vertebrate fossil remains from the Winton Formation located in the Munga-Thirri (Simpson) Desert. These bone fragments show similar levels of surface weathering and wind-blown sand abrasion. The proximity of the Eromanga and Northern Territory sites to the sand dunes of the Munga-Thirri Desert provides adequate mechanisms for sand abrasive conditions to be present especially throughout the intensified aridity of the late Quaternary (Hocknull et al. 2007; Hollands et al. 2006; Maroulis et al. 2007). In comparison, the dinosaur localities of Winton and Isisford to the north and east are distal to these dunes and probably did not experience this kind ~~or~~ of abrasive surface weathering.

EML011(a-c). Material; EMF102, EMF103 & EMF111. EML011 was first thought to be a single large surface scatter over an area of 5000 m^2. It was treated as a singular entity whilst excavations proceeded from 2007-2010. However, during this period, three discrete subsurface fossil beds were recognised representing semi-contemporaneous deposits, but containing different associated skeletons representing three individual sauropod specimens and including unusual ichnological features that indicate a trampled surface (Figure 6-8).

The trampling is localized to EML011 and is not observed in other northern or southern Plevna Downs sites. EMF102 from EML011(a) and EMF103 from EML011(b) are two associated skeletons recovered 72 m apart, and are divided by an approximately 100 m linear ichnological feature interpreted to be a sauropod ‘trample zone’. Silty sediments have been turbated and compressed by the footsteps of numerous heavy tetrapods, likely sauropods walking single file, creating a trodden ‘pathway’ or ‘pad’ (Hocknull et al. 2019). Partial tracks are discernable, and

resemble sauropod foot-prints, along with clear deformation structures and subsurface sediment deformation. However, complete tracks or trackways are difficult to decipher due to the similarity of the siltstone matrix infilling the depressions made within the trampled sediment. The siltstone has preferentially cemented along the compressed 'pathway' as seen in Figure 6, J. This feature, along with other ichnological features, will be fully described elsewhere. EMF103 was located within the middle of this linear trampled features and is represented by a series of associated dorsal vertebrae and isolated teeth. The vertebrae are heavily compressed from trampling, making referral of it to known sauropod taxa difficult, and erection of a new taxon is premature at this stage. It will be described fully in a future study.

EML011(a) (Figure 7). Material; EMF102, Holotype of *Australotitan cooperensis* gen. et sp. nov. EML011(a) was located in 2005 as a small surface scatter of bone fragments that were able to be joined with unweathered fits indicating that this locality was likely to preserve in situ fossil remains that were better preserved in comparison to the heavily weathered remains 1 km to the south at EML010. The total area of EML011(a) is approximately 480 m^2.

Excavations ~~recovered~~ allowed recovering several massive sauropod appendicular elements including a partial left scapula, partial left and complete right humeri, a complete right ulna, partial left and near complete right femora, both pubes and ischia and indeterminate corticocancellous bone that was originally suspected to be of osteoderm origin. In total, ten elements were recovered in association with the pelvic elements in semi-articulation. No duplicate bones were found, and each element corresponds to a sauropod individual of comparable size. Therefore, these elements are treated as the same individual and thus can represent a describable holotype specimen (EMF102) and new taxon, *Australotitan cooperensis* gen. et sp. nov.~~.~~

The ~~upward~~ upward-facing surface of each bone has experienced a greater degree of cortical bone weathering than the ~~downward~~ downward-facing bone surfaces due to the actions of the vertosol ~~soil~~ soil-forming processes active at the site. The bone surfaces are split into a mosaic of pieces, superficially resembling the mosaic weathering stages of exposed bone (Behrensmeyer 1978; Lyman 1994).

Instead of cracking occurring prior to fossilisation, the surface splitting of the cortical bone observed on these specimens occurred after fossilisation and during the period of weathering at

the vertosol-Winton Formation transitional zone. The cracking vertosol penetrated the cemented mudstone matrix encasing the surface bone. Expansion and contraction of theses clays split the cemented matrix into quadrangular sections. The surface cortical bone is indurated with the matrix above it which indicates that when these cracks penetrated the cemented matrix, they also cracked the surface bone, lifting these sections off of the main body of the specimen. The weaker corticocancellous bone layer is a region of weakness and splits before the matrix-cortical bone interface does.

Subsequent infilling of these cracks with vertosol sediment widens the cracks and eventually lifts the cemented matrix with surface bone off of the main body, exposing cancellous bone from inside. As the matrix lifts, sediment penetrates below the surface bone and forms a soft clay infill. Subsequent gypsum precipitation within this clay infill creates a crystalline surface between the lifted matrix-surface bone and the underlying corticocancellous bone. Preparation of the matrix removes the cemented matrix from the thin adhering surface bone, and removal of the gypsiferous layer allows the original cortical bone surface to be repositioned back onto a cleaned surface. These quadrangular pieces present themselves as a mosaic-like pattern across the surface of the bone in a similar way to sauropod remains reported from Argentina (González Riga & Astini 2007).

Most of the bones show post-burial to pre-induration distortion created by localised directional compression forces exerted from above the bone and specifically focused above the area of distortion. These distortions do not occur uniformly across all of the bones or across the entire surface of a single bone~~, t~~. Therefore, the distortion is not a result of diagenetic and lithostatic compression. Instead, the bones are crushed in localised areas, and this direction of crushing is from above and locally generated by forces orthogonal to the in situ horizontal orientation of the bones (Figure 7 & 8). The best interpretation of these distortions is as a result of crushing through dinoturbation, which involves the actions of trampling by dinosaurs, likely sauropods (Britt et al. 2009). Clear evidence of this crushing has been observed in the right femur, which preserves a ~~well~~ well-delineated sauropod manus-shaped crush mark within the proximal diaphyseal shaft (Figure 8, A-H).

The forelimb elements (scapular blade, humeri and ulna) were all found together with each element touching one of the other elements. Their long axes were oriented in a NW-SE direction for the humeri and ulna and in a N-S direction for the scapular blade. The hind limb elements

Comentario [MH5]: This cracking is also present in *Bravasaurus* and *Dreadnoughtus* from AR, *Mansourasaurus* from Egypt, *Shingopana* from Tanzania,

Comentario [MH6]: A bit difficult to figure out this from Fig. 8. Maybe a a dashed line on Fig. 8A could help.

(puboischial complex and right femur) were found close to one another, whilst the left proximal femoral head was found disassociated from this group, at the surface and downslope from the right femur's position. Between the two appendicular bone groups, a small patch of indeterminate corticocancellous bone was recovered, likely the internal corticocancellous remains derived from within the femur nearby.

The orientation of the in situ bones shows a degree of skeletal sorting by water flow with the long axis of the bones oriented horizontally in either a NW-SE, or a near-normal to this (N/NE-S/SW), direction. The right femur was oriented with a NE-SW long axis direction whilst the pelvis was oriented in a NW-SE long axis direction.

Due to the flat aspect of these broad bone elements, they are oriented either with their long axis in the direction of flow or perpendicular to it, indicating the direction of water flow was the key driver of their final orientations (Kreutzer 1988; Lyman 1994; Voorhies 1969). Based on the dominant direction of orientation, the palaeocurrent was in a NW-SE direction.

Much of the fine primary sedimentary structure has been destroyed by the cementation and concretion formed around the bones, along with significant post diagenetic growth of gypsum throughout the sediment. The bones are preserved in a fine siltstone-mudstone matrix which is cemented, predominantly on the undersides of the bones. There is very little structure to the sediment surrounding the bones other than gross horizontal laminations. These laminations have been compressed in parts, likely through dinoturbation (Figure 7, D).

Below the bonebed, a very thin lens (<10 cm) of cross-laminated yellow-orange coloured sandstone occurs with a scoured top surface that is filled with the overlying siltstone that preserves the bones. This layer was most evident underneath the preserved pelvic elements but was also observed below the ulna and scapula (Figure 7, D-F).

The cross-laminations indicate a palaeocurrent parallel to the long- axis of the pelvic elements (NW-SE) suggesting higher energy flow which was followed by a scouring event with the subsequent deposition of silts along with sparse plant remains and bones. Settling of finer muds produced the gross horizontally laminated siltstone-mudstone matrix which entrained the bones. Following deposition of this thick silty-mud unit with the entrained bones, the water-saturated soft bones were deformed via trampling (dinoturbation) of the sediment. This, along with post-depositional processes, destroyed much of the primary sedimentary structures available.

Small-sized pieces of woody plant debris covered the top surface of the bones, having settled out with and onto the exposed bone surfaces prior to burial. The largest pieces of wood debris have a preferred long axis orientation of a NW-SE direction, therefore, supporting the dominant NW-SE palaeocurrent direction.

The woody debris is found in close proximity to the surface bone and was most evident during preparation of the femur and scapula, suggesting that these elements formed an obstacle for water flow allowing woody debris to settle. Both these limb elements are oriented normal to the main axis of flow providing a leading edge that would have slowed flow and provided an opportunity for the woody plant remains to settle out.

EML013. Material**;** EMF105 (femur), EMF165 (humerus), EMF166 (metacarpal).

EML013 was discovered in 2007 and is located 860 m northwest of EML011. A small patch of bones within cemented mudstone was found at the surface including a fragmented anterior caudal vertebra and partial ribs. There was no immediate subsurface connection of this scatter to a bonebed; however, after extensive excavation, a line of bones was discovered at depth and within the Winton Formation. This bonebed lay just below a thick rock unit preserving densely packed woody debris, that was well-sorted with a dominant long-axis orientation, NW-SE.

The rock unit shows sorting of the plant debris from large log-jams with directional orientation, with isolated and broken bones, at the base, overlain by smaller suspended plant pieces in matrix, and densely packed woody fragments in the upper-most section (Figure 6, G-H). The entire unit has been cemented within a siltstone-mudstone that sits above the underlying bonebed. Isolated and broken bones were found at the base of this cemented woody debris unit (Figure 6, I). Transitioning below this level into the un-cemented Winton Formation a series of well-preserved sauropod bones was found. Four limb elements were found lying side-by-side, offset to one another in an east-west direction by approximately 20-40 cm. Each bone was similarly oriented in a NW-SE direction, parallel with the observed orientations of the overlying woody debris.

The bones include a partial humerus, femur, metacarpal and yet-to-be prepared large limb element. Each of these elements was differentially cemented, but clearly isolated within the uncemented Winton Formation siltstone layer below the main debris level. Stratigraphically

below and south of this bonebed a thin fine mudstone lens ranging from 5-15 cm in thickness preserved leaf and cone scale impressions. The floral remains exclusively preserve leaves and cone scales from gymnosperms, and pinnae and pinnules of pteridophytes and a possible bennetitalean (Figure 6, A-F).

Macrofloral fossils occur at all of the southern-central Winton Formation sites associated with the sauropod bonebeds, and are predominantly represented by thick plant debris strands of well-sorted woody remains. Occasional clay lenses exclusively preserve pterydophyte and gymnosperm leafy remains with no indication of equisetaleans, ginkophytes, angiosperms or cycadales macroflora typical of northern Winton Formation sites.
The combination of predominantly thick sections of well-sorted woody remains with rare near-monospecific leaf deposits has not been observed by us from any of the faunal or floral sites in the northern Winton Formation, or the Surat Basin Griman Creek Formation.
The combined depositional, taphonomic and ichnological observations here represent a distinct departure from what would be expected based on observations from the northern Winton Formation sites. The combined bias to sauropod skeletal remains, disturbance by trampling over large areas, and the low diversity of flora, indicates either a unique taphonomic bias that has removed these remains from preservation potential, or it establishes the base for palaeoenvironmental differences observed between northern and southern Winton Formation sites. Palaeoenvironmental differences between the two regions are likely the reasons for these differences and will be discussed later.

Materials & Methods

Fossil Preparation. The sauropod remains described herein were prepared using pneumatic air-scribes and pneumatic chisels. All remains were preserved within varying thicknesses of siltstone-cemented matrix that also included layers of gypsum-rich mineral precipitation. Mechanical preparation was used to prepare the holotype using a variety of pneumatic air scribes and an electric high-speed diamond wheel cutter. A combination of the following air scribes were used~~;~~: WEN pen, HW50, HW10, No 6 & 4 microjacks and Aro. The preserved

747 elements were partially encased in the concretionary mudstone and buried in the surrounding
748 clays. Gypsum crystals had fractured the surface of some of the preserved elements, and in
749 some areas, a thin iron-oxide crust covered the bone surface.
750
751 **Specimen 3-D Surface Geometry Creation.** Undertaking comparative assessments of
752 morphology for the key taxa during this work came with specific difficulties because of the
753 specimen's geographical location, physical attributes and conservation considerations. In this
754 particular work, three museum collections house the four holotypes referring to the taxa of
755 specific interest here. *Wintonotitan wattsi* QMF7287 is reposited in the collection of the
756 Queensland Museum, Brisbane, southeast Queensland; *Diamantinasaurus matildae* AODF603
757 and *Savannasaurus elliottorum* AODF660 are reposited in the collection of the Australian Age
758 of Dinosaurs Museum of Natural History, Winton, central Queensland, and the proposed
759 holotype of the new taxon described here, EMF102, is reposited in the collection of the
760 Eromanga Natural History Museum, Eromanga, southwest Queensland. From Brisbane, each
761 location is around 1000 km apart, representing a next to impossible logistical means for direct
762 specimen comparisons. Traditional plaster or polyurethane replicas do not exist.
763 Each type specimen presents its own specific difficulties when undertaking comparative work
764 because of their physical location, very large size and great mass, fragility, and conservation
765 needs. For such large specimens simply viewing individual elements from multiple sides (e.g.
766 proximal, distal, anterior and posterior) can be a fraught process both for the specimen, the
767 researcher and the collection staff. These difficulties in comparative analysis have been manifest
768 since the discovery of dinosaurs, and since then, concessions have had to be made based on the
769 primary protection and conservation of the type specimens relative to access for assessment by
770 researchers.
771 Advances in three-dimensional (3-D) scanning technology, in particular, the relatively easily
772 learned and affordable process of photogrammetry (Bates et al. 2010; Falkingham 2012; Otero
773 et al. 2020), have allowed many of these limitations of comparative work to be resolved by
774 creating three-dimensional models of specimens. Digital 3-D models allow multiple
775 comparisons with multiple specimens in a virtual sense, helping to augment direct observations,
776 and more frequently superseding them.

Since 2011, we (SAH & RAL) have collected photogrammetric data of the four taxa used in this work which has allowed regions of morphological interest to be directly compared between the taxa. During this process, it has become evident that changes and damage sustained to the specimens during events occurring pre- and post-deposition, during preservation, exposure and weathering, during excavation and throughout preparation and display, have all altered the specimens and have influenced comparative capabilities and interpretations.

In the past, many of these taphonomic and preparatory changes to the specimens have been unintentionally or intentionally 'rectified' and 'restored', resulting in what might be considered to be a more realistic representation of the specimen prior to alteration. Thus, providing the researcher with a different morphological starting point for comparisons versus what was originally preserved. Many intentional restorations occur in response to display or by connecting isolated portions of a specimen together to estimate a whole. Restorations of this manner can preclude morphological features or unintentionally fabricate morphology that ~~didn't~~ did not exist in the original element.

Such restorations occurred to the holotype specimen of *Wintonotitan wattsi* (QMF7292), prior to its establishment as a holotype, which included plaster-based restoration of bones and bolting of elements for display armature. Such restorative work was removed for the purposes of description of *Wintonotitan wattsi*, ~~however~~although~~,~~ this process also meant the loss of some surface bone. This type of specimen alteration is not uncommon, but it does serve to alter the specimens, sometimes irreversibly from what it was in situ in the field. 3-D digital reconstruction and restoration allow~~s~~ a reversible and testable way of assessing and restoring alterations evident in the specimens so that more meaningful comparative assessments can be made. Demonstrating that a feature does or does not exist, or potentially could, but has been altered from some taphonomic or preparatory reason, impacts all interpretations and needs to be communicated in some way.

3-D digital reconstruction, retrodeformation and restoration is becoming a more common element in palaeontology, whereby a 3-D digital restoration or reconstruction is used to assist in morphological, ichnological, body-size and biomechanical studies (Otero et al. 2020). Whilst this process is becoming more common place, new standards of reporting are required when utilizing these datasets, especially considering the initial limitations that come with accessing specimens to undertake scanning in the first place. In particular, digital capture and restoration

requires several tradeoffs including capacity of hardware, software and personnel, along with financial and time constraints.

Tradeoffs also include ease of access to capture the specimens in the first instance, which includes lighting, physical location, speed of capture and ultimately resolution and fidelity of the final digital 3-D geometry. This has led to the development of some standards and procedures of capture that may assist collection managers, curators and researchers when deciding about the relative advantages and disadvantages of different scanning procedures and taking into account these tradeoffs (Bitelli et al. 2020; Brecko & Mathys 2020; Lautenschlager 2016; Le Cabec & Toussaint 2017; Otero et al. 2020; Vidal & Díez Díaz 2017). However, it is unlikely that all standards can be met at all times, and in our present experience, this was the case.

Here we will take the opportunity to describe the methods and processes used as a way to describe the limitations of resulting 3-D models, but also how they provide clear advantages over traditional methods of morphological comparison.

We generated 3-D surface models of the fossil specimens using digital photogrammetry and surface rendering from Computed Tomography (CT) X-ray scans. The process of 3-D model creation using photogrammetry and CT data is well documented across many disciplines and readily available through software manuals, online tutorials, YouTube demonstrations and simple, but iterative, trial and error.

From 2011-2014 specimens in this study were captured using two Panasonic Lumix DMC-TZ30 cameras. These cameras were chosen due to their portability, affordable price, rapid shooting, tough body, and image LED review screen. This allowed them to serve multiple purposes for capturing specimen and field site photogrammetry. Their small compact size with LED review screen allowed us to position and focus on specimens quickly and evenly, and in very awkward and tight positions, such as on darkly-lit shelves, within fiberglass cradles in preparation laboratories, on display, or in very small spaces within cramped working spaces.

The settings were set to ‘Fine JPG’ resolution, using f-stop settings between F12-18, ISO Auto or 100, under autofocus. Lighting was balanced as best possible during each shooting session; however, individual bones may have been captured over a period of several months or years depending on the point of preparation of each available side of the specimen. The difference in lighting and colour can be seen on a number of specimens where the shooting occurred at

different times with different lighting arrangements, creating dissimilar coloured surfaces. This did not affect the geometric reconstruction.

Rapid and close-range images were taken of each specimen with the user moving around the specimen. Foreground and background elements were initially recorded for alignment control, ~~then~~and then later removed from the dense point cloud. We also opted to 'over-shoot' each specimen, focusing on capturing as much fine surface detail as possible.

Due to the massive size and impossibility of building a large enough turn-table, undertaking standard turn-table techniques were not employed. In addition, due to the location of many of the specimens occurring either in a preparation facility or within close range to very dusty environments, it was impossible to control dust and therefore, creating a uniform coloured background was not possible. Instead, we opted to include the foreground and background elements within the photograms, so that although the main focus of the reconstruction was on the specimen, the shooting included elements that would assist in alignment and would be removed later. We found the more irregular these features, the better the overall alignment. Therefore, in future, if a uniform clean background and stage with turntable is not possible, we suggest creating a very geometrically complex stage and remove unwanted dense point cloud data after this phase of reconstruction.

Although we understood the tradeoff of the number of images taken relative to additional geometry, digital storage space, and processing time, we opted to 'over-shoot' each specimen. This created close to two or three times as many images as was generally required for a usual turn-table approach where all factors such as light, camera stability, camera resolution and processing time are all controllable. We also focused on capturing as much fine surface detail as possible each session within the timeframes available.

Due to the large number of images captured per specimen and long processing time, subset image batches were processed in Agisoft Photoscan Standard versions 0.8.2 (June 2011) to 1.0.4 (April 2014 and then in Agisoft Metahape 1.6.1 build 10009 (20 January 2020)), retrieved from http://agisoft.com. All images of each specimen were reprocessed in Reality Capture software, retrieved from http://capturingreality.com (beta 2014 onwards) due to its faster processing speed of greater numbers of images whilst using the same processing power. This new process returned a greater detail of surface geometry, especially in areas with detailed image clusters.

Each specimen needed to be captured from at least two sides due to their large size, fragility and housing cradle. If possible, a significant overlap of an area was captured from each side so that both could be neatly aligned later. Images were aligned and positions reconstructed in the software, with a dense point cloud generated from these positions. Surface geometry was reconstructed in Reality Capture using Normal Settings with vertex and polygon colouration. All outputs were exported as Stanford Triangle Format (i.e. .ply files).

Removal of unwanted geometry, such as background structures and specimen housing was undertaken in Reality Capture and Agisoft Photoscan at the dense point cloud stage, leaving only the geometry representing the specimen and the included scale bar. If poorly reconstructed geometry was observed, usually below the edges of specimens where there was overhang or shadowing, this geometry was also removed to reduce the production of inaccurate additional geometry when the surface models were aligned to one another.

The scanned components of the specimen were scaled to real-world dimension in Meshlab (Callieri et al. 2012; Cignoni et al. 2008), by measuring the included scale bar or a known distance on the specimen using the measuring tool. The real-world measurement was then divided by the measurement given in Meshlab, thereby, providing a scaling factor. This scaling factor was then used to scale the object in Meshlab using the Scaling option, whereby the scaling factor occurred in all directions (x, y and z). The scale of the specimen was then re-checked by measuring within Meshlab the included scale bar or known length. We then 'Freeze the Current Matrix' so that the new scaling factor is coordinated to the vertex positions. Finally, we export the model as a .ply file.

Each component of the specimen model is then aligned together in Meshlab (Cignoni et al. 1998; Pietroni et al. 2009) using the alignment tool by point picking multiple corresponding positions of overlap on each component and adjusting this alignment for maximum best fit. Ideally, specifically corresponding geometries or specimen numbering written on the specimen are chosen to allow for quick and accurate point picking to occur. The two aligned meshes are more precisely aligned using the default alignment parameters within Meshlab. If alignment is not clear, we cross-check this in Cloud Compare software (Girardeau-Montaut 2016), using the alignment tools of this software. Once aligned, the two separate components (layers), are merged using the 'Flatten Visible Layers' tool and exported, creating a single model.

This combined, merged model is re-meshed using the Poisson Surface Mesh reconstruction tool with the Reconstruction Depth set to 12, and the Adaptive Octree Depth set to 8 (Cignoni et al. 2008; Kazhdan & Hoppe 2013). We have found that these meshing parameters produce the most accurate resulting full surface geometry. However, some components may create additional geometry along the seams between two parts that had limited overlap. For example, the large limb elements that are fixed within firm housing ~~fiberglass~~ fibreglass cradles are missing approximately 5-10 mm of overlap due to the obscuring nature of the cradle. Therefore, alignment needed to take this into account, and the Reconstruction Depth using the Poisson reconstruction method may need to be reduced to 10 or 8. Although this reduces the overall detail in the surface geometry, it also removes the false geometry. A tradeoff is required to attain the best re-meshed model.

Finally, the fully aligned and re-meshed model is colourised by transferring the vertex colour attributes from the original components onto the new uncoloured mesh geometry. We do this using the Vertex Attribute Transfer tool in Meshlab (Cignoni et al. 1999). The finalized, coloured model is then exported as a .ply model. We once again take measurements from the included scale bar or known distances to verify correct scaling. We then remove the scale bar from the model and undertake a final model clean using the 'Remove Isolated Pieces' tool in Meshlab (Cignoni et al. 2008). We then re-align the model to the correct bounding box position and use the manipulator tool to reorient the model so that the dorsal anatomical direction is aligned to the z-axis within the 3-D model space, and the anteroposterior anatomical direction is in the x-axis plane. The final model is exported again as a .ply file.

In addition to photogrammetry data, where possible we collected CT scan data for the holotype of *Wintonotitan wattsi* and particular remains associated with EMF102. The ischium of *Wintonotitan wattsi* was digitized using CT scan data that was aligned and processed in Dragonfly 3.6 (Computer software), from Object Research Systems (ORS) Inc., Montreal, Canada, 2018 retrieved from http://www.theobjects.com/dragonfly.

The ischium was too large to be scanned as one piece, ~~therefore,~~ so we scanned the specimen twice, moving it across the gantry to allow all of it to be captured. These two scan datasets were then aligned in Dragonfly 3.6 using the image stack alignment tool. A surface model was then generated from these aligned CT scan datasets.

Specimen 3-D digital restoration, retrodeformation, reconstruction and annotation. A benefit of 3-D digital geometry of specimens in palaeontology is the capacity to manipulate these specimens in a way not possible with the original specimen. In addition, digital techniques can help restore bones to reflect the known and predicted original shape (Lautenschlager 2016; Vidal & Díez Díaz 2017). In particular, skeletal remains when components of the right and left elements are preserved, but are not complete, can be used together to restore a whole singular bone. Here we undertook similar processes to assist in reconstructing the bones we compared. Before restoration or reconstruction can be accomplished the specimens need to be assessed for matrix obscuration, bone damage and loss, along with deformation. High fidelity models that possess realistic and detailed colour allow the user to see features and textures with the geometry that colourless surface scans cannot, which is a distinct advantage of photogrammetry. Specimens that are digitized in pieces provide an extra level of data if each individual piece is reconstructed, because they can provide cross-sectional information such as cortical and cancellous bone thickness, that a completed bone may not reveal.

Computed Tomographic (CT) scans provide another level of detail that can show difficult to distinguish matrix coverage or bone damage, surface corrosion and loss. Together, using these different lines of evidence, each bone can be restored. However, prior to any restoration, the obscured, altered, missing or damaged areas need to be clearly identified on the 3-D model geometry.

To do this, we colourised a duplicate 3-D model of each specimen and digitally painted onto the surface geometry areas of alteration, damage and deformation using a pre-defined colour scheme (Figure 8, O). Meshlab (Cignoni et al. 2008) was used to undertake this surface geometry painting, including singular colour choices without gradation or feathering, with the brush set to 100% opacity and 100% hardness. This provided a clear distinction between a painted surface and the colour data from the original surface scan, thereby indicating clearly what has been intentionally coloured and what has not.

The colour scheme used the following preferences using the Meshlab (Callieri et al. 2012; Cignoni et al. 2008; Cignoni et al. 1999) standard HTML HEX colour coding: Brown (#aa5500) indicating obscuring matrix; Purple (#aa55ff) indicating bone deformation; Red (#ff0000) indicating significantly broken/missing surfaces; Magenta (#ff55ff) indicating corroded surfaces; Dark Green (#55aa00) indicating loss of cortical bone surface; Very light orange

(#ffaa7f) indicating mosaic broken surface (cortical bone); White (#ffffff) indicating plaster fill; Yellow (#ffff00) indicating poorly rendered 3-d model geometry; Light Blue (#55aaff) indicating pneumatic pores and cavities (Figure 8, O). All images rendered from these models for the figures used herein were produced in Meshlab using natural vertex colour, ambient occlusion, x-ray or radiance scaling rendering (Cignoni et al. 2008; Vergne et al. 2010), or by using the edge detect feature in Dragonfly 3.6 with the 3-D model placed in orthogonal projection and 100% transparent.

After completion of the 3-D specimen model, the regions of deformation and alteration were identified and segmented into separate components using the model cutting tool in Agisoft Metashape. The lasso cutting tool was used to trace the line of deformation, which then broke the model into at least two components. If this region was deformed further, additional segments were created. Each segmented piece was saved as a separate model to be re-aligned in Meshlab. After identifying the greatest degree of deformation, usually in the downward direction relative to the field site position, the segmented components were rotated in the x- or y-axis to align to the un-deformed portion of the model. Once the new alignment was determined, all of the components were merged using the 'Flatten Visible Layer' tool in Meshlab. The resulting merged model was then re-meshed using the same process described above and the resulting closed mesh exported as a new model.

Bone retrodeformation was undertaken by SAH where such deformation would clearly influence comparative understanding. The focus of this procedure was to retrodeform the surface scan models of EMF102 elements so that they could be compared to other taxa without the influence of distortions leading to misinterpretation of similarities or differences between taxa (Figure 8). If the bone was undeformed, or the deformation features did not alter the overall shape of the element substantially, or a better preserved contralateral pair existed, comparative assessments were undertaken directly between these elements as preserved. These regions included the scapula (excluding the acromion plate), humerus, (excluding the deltopectoral crest), ulna (excluding the diaphyseal curvature), pubes and ischia (excluding the right ischium) and femur (excluding the proximal half of the diaphysis).

Retrodeformation was applied to the humerus to restore the deformed deltopectoral crest of the left humerus. The deltopectoral crest was deformed during removal at the point of excavation where the crest relaxed outward from its original position due to the compressive weight of the

specimen and lack of reinforcement of the plaster jacket. The preserved extent of the right humerus (digitally mirrored) provided a guide to the direction of the distal end of the deltopectoral crest for the left humerus. Field images prior to removal provided additional guidance as to the shape of the overall element. Finally, each segment could not overlap each other, which provided the key limitation to the overall shape of the crest and the proximal margin.

The right ulna diaphysis was clearly bent downwards in the site, through the processes of trampling. The diaphysis was segmented into components and realigned so that the shaft was straightened. The pubes and ischia were segmented apart due to each element being slightly dislocated from their articular margins. They were then relocated, re-articulated along their articular margins. It was evident that the right pubis and ischium had suffered most deformation and crushing so the left puboischium (and its duplicate mirror) was used as the base model for the reconstruction of the pelvic floor and comparisons of this element.

The right femur was deformed downwards in the site having also been crushed from trampling. The proximal half of the shaft was segmented into components and realigned so that the shaft was straightened. The distal end was not deformed but some areas of the condyles had been lost post-deposition. To restore the proximal region of the femur, the isolated and associated left femoral head of EMF102 along with a referred proximal femoral head (EMF164) were used to reconstruct an entire femur. We subsequently used the referred complete femur (EMF105) to compare our resulting reconstruction.

With the elements of EMF102 retrodeformed and/or reconstructed using specimens referable to the new taxon VK undertook to digitally sculpt complete bones using these retrodeformed elements as the basis for the models. VK used ZBrush digital sculpting software retrieved from https://pixologic.com/ to generate a new geometry for each element, using the retrodeformed models as a subtool basis for this new geometry (Figure 27). Also at this stage, any additional small deformations, weathering features or cracked surfaces were digitally ‘repaired’. The overall geometric shape and size ~~was~~ were not altered. Where areas of articulation were missing articular surfaces, these were estimated based on the preserved trajectory of such features in the reconstructed models or by reference to ~~better~~ better-preserved titanosaurs from the literature. To be clear, these sculpted ZBrush models were not used in any comparative assessments between taxa, or for the establishment of the diagnostic characteristics of the taxon. They serve

only as a guide to the overall shape and size of the reconstructed bones, allowing us to produce 3-D printed 1:1 scale versions of them and to assist in recreating a skeleton for exhibition.

New Taxonomic Name

The electronic version of this article in Portable Document Format (PDF) will represent a published work according to the International Commission on Zoological Nomenclature (ICZN), and hence the new names contained in the electronic version are effectively published under that Code from the electronic edition alone. This published work and the nomenclatural acts it contains have been registered in ZooBank, the online registration system for the ICZN. The ZooBank LSIDs (Life Science Identifiers) can be resolved and the associated information viewed through any standard web browser by appending the LSID to the prefix http://zoobank.org/. The LSID for this publication is urn:lsid:zoobank.org:pub:AF1FA65A-5351-45B1-B0CB-EC1225590A0F. The online version of this work is archived and available from the following digital repositories: PeerJ, PubMed Central and CLOCKSS.

Results

Systematic Palaeontology

Dinosauria Owen, 1842

Saurischia Seeley, 1887

Sauropodomorpha von Huene, 1932

Sauropoda Marsh, 1878

Eusauropoda Upchurch, 1995

Neosauropoda Bonaparte, 1986

Macronaria Wilson and Sereno, 1998

Titanosauriformes Salgado et al., 1997a

Somphospondyli Wilson and Sereno, 1998

Titanosauria Bonaparte and Coria, 1993

Australotitan gen. nov.

Type Species. *Australotitan cooperensis* gen. et sp. nov.

Diagnosis. As for species.

Australotitan cooperensis gen. et sp. nov.

Material. Holotype: EMF102, consists of ten appendicular elements and pieces of corticocancellous internal bone. The appendicular elements include a partial left scapula, partial left and complete right humerus, right ulna, right and left pubes and ischia, and partial right and left femora.

Referred Specimens: EMF164, a fragmented femur, a fragmented ulna, presacral vertebral centrum fragments and rib fragments. EMF105, a complete femur and EMF165, a distal humerus.

Age & Horizon. Cenomanian-? Turonian, Winton Formation.

Type Locality. EML011(a). Referred Specimen Localities, EML010 & EML013.

Etymology. *Australo* – meaning southern in Greek and in reference to the southern continent of Australia; *titan* – from the Greek mythological Titan Gods and in reference to its gigantic size; *cooperensis* – being from the Cooper-Eromanga Basin, Cooper Creek system & "Cooper Country".

Diagnosis

A large titanosaurian sauropod with the following combination of characters that differentiate this new taxon from all others. Proposed autapomorphies indicated by an asterisk. Scapular blade, narrow and straight with sub-parallel dorsal and ventral margins with lateral ridge situated near the ventral margin. Humerus with a rounded ridge that extends from the distal end of the deltopectoral crest to a just proximal of a tri-lobate distal epiphysis. Ulna with heavily reduced anterolateral and olecranon processes relative to much enlarged and elongate anteromedial process. Ulna with a distinct radial interosseous ridge within the distal half of the radial fossa*. Anterolateral process of the ulna with a~~n accessory distal~~ distal accessory

projection* proximal to a proximally beveled distal epiphysis*. Pubes and ischia broad and contact each other medially and centrally forming a cohesive pelvic floor. Distal ischial blades curve ventrally to produce a dorsal face that is posteriorly directed. Femur with a medially sloped proximolateral margin, diaphysis narrow anteroposteriorly, and distal condyles directed anterolaterally to posteromedially.

Description

Holotype, EMF102. *Scapula* (Figures 9, A-B & G and 10, A; Table 2). The scapula will be described with the long axis of the blade held horizontal and the short axis of the blade held vertically (dorsoventrally) with the acromion process vertical (dorsally oriented). A partial left scapula is represented in the holotype preserving from the mid-section of the anterior supracoracoideus fossa, including the acromion ridge and process, to a large proximal portion of the scapular blade. The anterior portion of scapular plate that articulates with the coracoid, including the proximal portion of the supracoracoideus fossa, coracoid suture (articulation), glenoid fossa and proximal portion of the supraglenoid buttress are not preserved having been broken off before fossilisation. It is missing the distal portion of the scapular blade including the distal-most margin. The proximoventral margin of the scapular blade base has been crushed and pushed dorsomedially into the medial side of the scapular blade.

The surface cortical bone of the scapular plate and blade is broken into a mosaic-like fracture pattern with minor distortions due to collapse and some crushing from trampling; however, the overall morphology is intact.

The preserved section of the scapular plate proximal of the acromion ridge is very thin in mediolateral thickness and is deflected medially. This makes what would have been the anterior fossa, very shallow and angled medially, thus the coracoid articulation was also most-likely medially positioned and coracoid angled medially. The bone thickness of the preserved scapular plate is very thin and broken along its proximal and proximoventral margins indicating that the missing regions of the supracoracoideus fossa, coracoid suture (articulation) and the glenoid were very gracile parts of the scapula.

The proximal dorsoventral expansion of the acromion region is hard to estimate; however, the thickness of the bone at the preserved proximal margin suggests that it wasn't expanded to a level seen in similarly large and gracile scapulae like that of *Dreadnoughtus schrani* (see Figure

Comentario [MH7]: There is something missing here. Bone thickness cannot be "broken".

2 in (Ullmann & Lacovara 2016)). Instead, it is most similar to the scapula of *Yongjinglong datangi* (see Figure 11 in (Li et al. 2014)).

Lateral View. The acromion is not fully preserved, with the ventral margin missing, therefore, the relative acromion dorsoventral height to minimum dorsoventral height of the scapular blade is not precisely known. However, based on the preserved extremities, the proximal region of the acromion at its broadest part was not significantly expanded dorsoventrally. Based on our reconstruction, the ratio of minimum scapular blade dorsoventral height to acromial plate dorsoventral height would be 0.48 (Table 2). -*Y. datangi* (see Figure 11 in (Li et al. 2014)) approaches this with a ratio of 0.5 derived from a minimum scapular blade dorsoventral height of 230 mm and an acromial plate dorsoventral height of 460 mm. Comparing this ratio across other titanosauriform sauropods, there is variation from 0.29 to 0.5 (e.g. *Muyelensaurus pecheni*: 0.29 (Calvo et al. 2007)-; *Elaltitan lilloi*: 0.30 (Mannion & Otero 2012); *D. schrani*: 0.34 (Ullmann & Lacovara 2016); *Patagotitan mayorum*: 0.38 (Carballido et al. 2017); *Saltasaurus loricatus*: 0.4 (González Riga et al. 2019);, *W. wattsi*: 0.42 (Hocknull et al. 2009; Poropat et al. 2015a); *Jiangshanosaurus lixianensis*: 0.42 (Mannion et al. 2019a); *Suuwassea emilieae*: 0.43 (Harris 2007); *Vouivria daparisensis*: 0.45 (Mannion et al. 2017)), with *Y. datangi* and the estimate of *A. cooperensis* of 0.5).

The dorsal process of the acromion is short, straight and oriented perpendicular to the long axis of the scapular blade. The acromion ridge is near straight along its dorsoventral length expressed as a low and rounded lateral face. The ventral-most portion of the acromion ridge is missing; however, what is preserved is a broad low rise that becomes slightly steeper along its dorsal length where it terminates at the dorsal-most region comprised of roughened surface bone texture. This may be interpreted as a tuberosity; however, we cannot exclude taphonomic alteration of the dorsal margin. The posterior surface of the acromion process is a flat plate running from the acromion ridge to the scapular blade base. There is no posterior acromion fossa or notch present. The posteroventral corner of the acromion is not preserved in the holotype so it is not possible to determine whether it possessed a subtriangular posteroventral process, similar to that seen in *D. matildae* (Figures 9, E, F, I and 10, B; see also Figure 4, A in (Hocknull et al. 2009) and Figure 8, B in (Poropat et al. 2015b)), and *W. wattsi* (Figures 9, C, D,

Comentario [MH8]: Mistake due to the reference manager. Check it throughout the whole ms.

Comentario [MH9]: Correct ref parentheses

Comentario [MH10]: Correct parentheses

Comentario [MH11]: Something missing here?

H and 10, C; ~~also~~ see also Figure 16, G-H in (Hocknull et al. 2009) and Figure 7, B in (Poropat et al. 2015a)).

The scapular blade is dorsoventrally narrowest just distal of the scapular blade base where it meets the acromion plate; in comparison with *W. wattsi* and *D. matildae* where the narrowest point is further distally along the blade. The entire scapular blade is narrow along its entire length with sub-parallel dorsal and ventral blade margins with only a slight expansion of the preserved distal portion of the blade. The distal-most end is not preserved and there is no indication of significant expansion relative to the main blade plate; therefore, it is likely that there is a significant portion of the distal blade missing (Figure 10, A).

On comparison with sauropods possessing mediolaterally thin scapulae with parallel dorsal and ventral margins such as *Y. datangi* (Li et al. 2014) and *Lirainosaurus astibiae* (Díaz et al. 2013) the scapular blade could conceivably be much longer than is preserved. *D. matildae* (Hocknull et al. 2009; Poropat et al. 2015b) and *W. wattsi* (Hocknull et al. 2009; Poropat et al. 2015a) have shorter, robust, and distally expanded scapular blades by comparison.

A ventral ridge runs along the lateral side of the blade (Figures 9, A and 10, A). This feature is most prominent toward the distal half of the blade. A similar ridge is seen in *L. astibiae* (Díaz et al. 2013) in comparison to the centrally located scapular blade ridge of *D. matildae* (Hocknull et al. 2009; Poropat et al. 2015b) (Figures 9, E and 10, B) and *W. wattsi* (Hocknull et al. 2009; Poropat et al. 2015a) (Figures 9, C and 10, C), which runs close to the midline of the blade, as observed in many titanosaurs (González Riga et al. 2019).

In *A. cooperensis* the acromion ridge is near straight, curving only slightly at its ventral extent. Both *W. wattsi* and *D. matildae* partially preserve the acromion plate; however, the acromion ridge is only observable in *W. wattsi*. In *W. wattsi* it is curved anteriorly toward its ventral margin and terminates about the midline of the scapular plate and blade. The posterior margin of the acromion process is rounded and narrower in *W. wattsi* compared to the flat and relatively broad region of *A. cooperensis*. In both *W. wattsi* and *D. matildae* the acromion plate is thicker mediolaterally and less medially deflected compared to *A. cooperensis*.

Medial View. The scapular plate preserves a deep fossa created by the medial curvature of the scapular plate and an excavated medial side of the acromial ridge and scapular blade base. This large fossa is interpreted to be a proximal location for the M. subscapularis (Figure 9, B). The

Comentario [MH12]: Correct parentheses here

fossa in *D. matildae* (Hocknull et al. 2009; Poropat et al. 2015b) (Figure 9, F) and *Wintonotitan wattsi* (Hocknull et al. 2009; Poropat et al. 2015a) (Figure 9, D) is not as deep, and in both of these taxa there exists a small and distinct medial tuberosity muscle scar distal to the fossa near the midline of the scapular blade. This feature has not been observed in other taxa illustrating the medial view of the scapula, so it could be considered a shared characteristic of these two taxa. Such a medial tuberosity is missing from *A. cooperensis* and helps differentiate it from *D. matildae* and *W. wattsi*.

The bone making up the acromion process is thin and excavated from the medial side of the scapular plate to be level with the dorsal margin of the scapular blade. The bone then thickens mediolaterally toward the dorsal margin of the acromion process, forming a rounded buttress for the process. The scapular blade base is straight with sub-parallel dorsal and ventral margins. The ventral margin has been crushed and the bone making up the proximoventral margin of the scapular blade has been deformed vertically and medially. The ventral margin of the blade is rounded and slightly thicker than the dorsal margin toward the scapular blade base, which on the lateral side, forms a slightly raised ridge running along the ventrolateral margin of the blade. There is no indication of this ridge occurring on the medial side; therefore, the ridge is a lateral expansion of bone only along this lateral margin.

Distal View. The scapular blade bends only slightly laterally along its length toward the distal end. Half-way along the shaft, the blade is slightly laterally deformed~~,~~. ~~however~~However, this does not alter the overall form of the blade being very straight and only slightly curved laterally. The distal end of the blade is not preserved, so it is difficult to estimate the distance from the broken margin to the scapular blade's distal extremity. The bone thickness does not alter significantly along its length suggesting the blade could have continued significantly further than what is preserved, especially when comparison is made to the same area of cross-sectional shape in *D. matildae* and *W. wattsi* (Figure 10), and in comparing the distal cross-sectional shape of *Y. datangi* (see Figure 11, E in (Li et al. 2014)). The cross-sectional shape along the length of the scapular blade is shallowly curved and sub-rectangular with no distinct lateral ridge along the midline of the scapular blade or any medial excavation or fossa (Figures 9, G-I and 10, A-C).

Comentario [MH13]: Correct parentheses

Although not completely preserved, the scapula possesses a combination of features that warrant comparison across titanosauriforms. The taxa that exhibit some of the suite of features seen in the scapula of *A. cooperensis* include *Y. datangi,*(Li et al. 2014), *L. astibiae* (Díaz et al. 2013), *D. schrani* (Ullmann & Lacovara 2016)*, C. hubutisaurus insignis* (Carballido et al. 2011a) and *V. daparisensis* (Mannion et al. 2017). They all possess relatively narrow scapular blades that have close to parallel dorsal and ventral margins with poorly expanded distal margins and lack a central scapular blade ridge.

Considering the diversity of scapulae shape across titanosauriformesTitanosauriformes, taxa tend to possess either; 1) a dorsoventrally broad acromion plate with a dorsoventrally narrow scapular blade that is markedly expanded posteriorly (e.g. *Tehuelchesaurus benitezii*, see Figure 14 in (Carballido et al. 2011b); 2) a broad acromion plate with a dorsoventrally narrow scapular blade that is not expanded posteriorly with sub-parallel dorsal and ventral margins (e.g. *D. schrani*, see Figure 2 in (Ullmann & Lacovara 2016); 3) a broad acromion plate with a dorsoventrally deep scapular blade that is expanded posteriorly (e.g. *P. mayorum*, see Figure 2, h in (González Riga et al. 2019); 4) a dorsoventrally narrow acromion plate with a dorsoventrally narrow scapular blade that is not expanded posteriorly with subparallel dorsal and ventral margins (e.g. *Y. datangi*, see Figure 11, E in (Li et al. 2014)); and 5) a narrow acromion plate with dorsoventrally broad scapular blade that is expanded posteriorly (e.g. *Mendozasaurus neguyelap*, Figure 2, g in (González Riga et al. 2019)). *A. cooperensis* shares features most closely with the titanosaurs similar to *Y. datangi* in scapular morphology, whilst the other Winton Formation taxa that have comparative scapulae (*W. wattsi* and *D. matildae*) more closely resemble each other and titanosaurs with scapulae like *M. neguyelap*.

Humeri (Figures 11, 15 & 16) (Table 3). The humerus will be described with the diaphysis long axis oriented vertically and the distal condyles horizontal and perpendicular to the diaphysis long axis. The holotype preserves both humeri; a partial left and a nearly complete right humerus. The left humerus is missing the proximal epiphysis and much of the medial margin of the diaphysis. Most of the lateral margin of the limb is preserved from just distal of the proximolateral corner along the deltopectoral crest, including the distal portion of the diaphysis and distal epiphysis, from the distolateral flange and ectepicondyle to the distomedial flange and entepicondyle. The cortical bone is heavily split, forming three main sections that

join together. Portions of the deltopectoral crest were collected as surface scatter, having been dislodged from the main distal epiphysis and weathered and exposed at the ground surface. These elements click together and also click to the main piece recovered within the transitional horizon between the overlying vertosol and the underlying Winton Formation.

The right humerus is relatively well preserved although the cortical surface bone is heavily split into a mosaic-like pattern similar to the left humerus. A thin crust of cemented siltstone with plant woody debris covered the element prior to preparation. The posterior side? face? of the right humerus was facing up in the deposit as the top surface and has suffered significant weathering of the surface bone through the actions of the vertosol. The anterior face was oriented downwards and had been somewhat protected from this weathering. The right deltopectoral crest is flattened laterally due to collapse that occurred during plaster jacket removal during excavation~~, h~~. However, the relative positions of each distorted region are identifiable and this enables us to reconstruct the pre-collapsed state of the deltopectoral crest and thus understand the shape of the proximolateral corner. By combining the 3-D photogrammetric models created ~~of~~ from both humeri, we retrodeformed the deltopectoral crest so that accurate description of the humerus would be possible (see Methods) (Figures 8, K-N and 11, H).

Anterior view. The proximal and distal epiphyses are widely expanded relative to a narrow midshaft, as seen in most sauropod humeri, but further expanded mediolaterally as seen in titanosauriform sauropods. The proximal epiphysis is rounded, with the humeral head proximomedially directed and the proximolateral corner is rounded, similar to *V. daparisensis* (Mannion et al. 2017), *Zby atlanticus* (Mateus et al. 2014) and *Alamosaurus sanjuanensis* (Lehman & Coulson 2002), in comparison to a distinct right-angled 'corner' that is seen in the outlines of *D. matildae, S. loricatus, Epachthosaurus sciuttoi, Neuquen~~o~~saurus australis* and *M. neguyelap* with *Panamericansaurus schroederi, Tornieria africana* and *Kotasaurus yamanpalliensis* (see Figure 16 in (González Riga & David 2014)).

The distorted (flattened) proximolateral margin makes the specimen look like it possesses a distinct proximolateral corner; however, this is an artefact of deformation. When reorienting the deltopectoral crest the proximolateral margin exhibits a more rounded appearance in comparison to taxa showing the distinct proximolateral corner. The proximal anterior fossa forms a shallow

Comentario [MH14]: Saltasaurids like *Saltasaurus* and *Neuquensaurus*, as well as *Bravasaurus* also have widely expanded epiphyses.

Comentario [MH15]: This does not seem to connect with the rest of the sentence.

Comentario [MH16]: Correct Ref parentheses

and broad ~~fossa~~ depression from the proximomedial margin of the deltopectoral crest to the proximolateral margin of the humeral head. A small raised rugosity is just medial ~~of~~ to the center of the proximal anterior fossa.

The deltopectoral crest rises anteriorly from the proximolateral corner, thickens toward the midshaft of the diaphysis and is thickest at approximately a third the maximum proximodistal length measured from the proximal margin. This thickening at the apex of the deltopectoral crest is rugose and forms a tuberosity on the crest. The deltopectoral crest forms a shallow curve originating from the proximolateral margin in a distomedial direction onto the anterior face of the diaphysis where it expands into a shallowly rounded ridge that continues distally and expands mediolaterally toward the medial condyle of the radial-ectepicondylar region.

The medial margin distal to the humeral head curves laterally toward the midshaft of the diaphysis, then straightens along the midshaft and curves medially toward a medially expanded entepicondylar margin of the distal epiphysis. At the midshaft of the diaphysis the lateral margin extends distolaterally from underneath the deltopectoral crest into a broad ectepicondylar flange that curves slightly laterally toward the rounded distolateral corner. The distal epiphysis is broad due to both the medial and lateral margins expanding distally to respective epicondylar regions.

The ectepicondylar region comprises two main articular regions, the radial condyle and the flattened ectepicondyle. The radial condyle consists of two small condyles coalesced on the distal articular surface. The medial condyle is rounded and smaller than the sub-triangular lateral condyle, they are split apart by a crack. The ectepicondyle is separated from the radial condyles by a shallow distal anterior fossa; however, it too is connected to the radial condyles through the distal articular surface. The distal articular surface is anteroposteriorly convex curving up onto the distal margin of the distoanterior face. The entepicondylar region comprises a large rounded ulnar condyle that is mediolaterally expanded and rounded medially. The distal articular surface curves anteroposteriorly onto the anterior face, but not to the extent seen in the radial condyle. A shallow and elongate fossa divides the anterior face of the ulnar condyle from the radial condyle and the ~~central low~~low central ridge that extends from the deltopectoral crest.

Posterior view. The proximal epiphysis is poorly preserved, missing portions of the humeral head; however, based on the distribution of the surface bone preserved it indicates a relatively thick posterior expansion of the humeral head, thicker than the anterior humeral head bulge.

There is a large, broad and rounded posterior ridge that expands from the medial flange laterally to approximately the midline of the shaft. The medial fossa (medial fossa for the M. scapulohumeralis) is significantly reduced to a small flat region along the medial flange. The lateral fossa (lateral fossa for the M. scapulohumeralis) is large, broad and shallow. The lateral margin of the diaphysis, distal to the level of the deltopectoral crest, is curved medially and expanded distolaterally to the ectepicondylar region. This region lacks any representation of a tuberosity or strong bulge as seen in *Opisthocoelicaudia skarzynskii* (see Figure 7 in (Borsuk-Bialynicka 1977)), but could be preservational loss.

The medial margin of the diaphysis has been distorted by internal collapse to form a narrow fissure along the mid-length of the shaft in a proximodistal orientation. The surface cortical bone is still traceable along the margins of this fissure and shows that the fissure is an artefact of preservation. The olecranon (=anconeal or cuboid) fossa is elongate and subtriangular in shape with the tallest apex starting at the level of the midshaft of the diaphysis, just distal to the level of the deltopectoral crest termination. The fossa broadens distally and is shallow along its length. The distolateral expansion for the distal condyles creates a steep medial margin for the fossa, whilst the medial side of the fossa remains broadly shallow.

Proximal view. Proximal epiphysis cross-section through the mid-level of the anterior fossa is anteroposteriorly narrow, elliptical, and slightly curved posteriorly. Midshaft diaphysis cross-section is bi-lobed subrectangular in shape, taking into account the internal collapse along the medial margin and distal extremity of the deltopectoral crest. The distal epiphysis cross-section through epicondylar region is tri-lobed with shallow fossae dividing each lobe. The anterior portion of the humeral head is anteroposteriorly moderately expanded and rounded anteromedially. The posterior face of the humeral head is poorly preserved with indications of thickening in a posterior direction to form a relatively broad humeral head. The deltopectoral crest is near perpendicular to the proximal anterior fossa and curved medially. The deltopectoral crest remains vertical along its length and its base curves medially toward the center of the anterior face of the diaphysis. The vertical projection and apex of the crest remains vertical and does not curve medially to project across the anterior face of the humerus.

Comentario [MH17]: Correct me if I am wrong. Could be the same as thte ridge present in the humerus of *Patagotitan* and interpreted by Otero et al (2020; Fig 3G-I) as the latissimus dorsi insertion scar?

Otero A., Carballido JL., Pérez Moreno A. 2020. The appendicular osteology of Patagotitan mayorum (Dinosauria, Sauropoda). *Journal of vertebrate Paleontology* 40:1–19.

Distal view. The distal condylar region is tri-lobed and sub-equal in size. The radial condylar region is made up of a rounded radial condyle, which is divided into two small condyles, and a large ectepicondyle that is similar in size to the radial condyle itself. The ulnar condyle is offset posteromedially from the radial condylar region via a shallow groove. The ulnar condyle is similar in size to the radial condyle. The entepicondylar region is rounded and not as expanded relative to the ectepicondylar corner.

Three of the four currently recognised Australian Cretaceous sauropod taxa possess humeri: (*D. matildae* (Figure 12), *W. wattsi* (Figure 13), and *S. elliottorum* (Figure 14) do, whilst *Austrosaurus mackillopi* does not. Only *D. matildae* is complete enough with minimal deformation for good comparisons. Both *W. wattsi* and *S. elliottorum* can only be compared for central diaphysis shape and relative proportions (Figures 12-16, Table 3). Both are missing the proximal and distal epiphyses due to significant pre-depositional breakage and surface weathering (i.e., *W. wattsi*) or pre-diagenetic loss and crushing (i.e., *S. elliottorum*).

The proximal region of the humerus in *A. cooperensis* differs from *D. matildae* by possessing: a more rounded proximolateral corner; a more rounded proximal articular margin in anterior view; a relatively thinner, more vertically oriented and more distally terminating deltopectoral crest; a relatively narrower humeral head and shallower proximal anterior fossa. Posteriorly, the posterior ridge is broader medially, and the medial fossa is reduced in *A. cooperensis*. *A. cooperensis* has more laterally and medially flared distal condyles (Figures 15 and 16).

The diaphysis of *A. cooperensis* differs from *W. wattsi* and *S. elliottorum* by being considerably more elliptical in cross-sectional shape where *W. wattsi* and *S. elliottorum* present a much more ovo-rectangular cross-sectional shape relative to *A. cooperensis* and *D. matildae* (Figure 16).

The humerus is hour-glass shaped, as is typical of most sauropods. The proximal margin compares most favorably with *Alamosaurus sanjuanensis* (Gilmore 1946; Lehman & Coulson 2002), *Turiasaurus riodevensis* (Royo-Torres et al. 2006), *V. daparisensis* (Mannion et al. 2017), *Haestasaurus becklesii* (Upchurch et al. 2015) and *Z. atlanticus* (Mateus et al. 2014). These similarities are based on the outline curvature in anterior view of the proximal margin, differing from the 'sigmoidal' or 'sinuous' outline characterising other sauropods with similarly broad proximal epiphyses (e.g. *D. matildae*, *S. loricatus*, *N. australis* and *O. skarzynskii*). The distal epiphysis in distal view forms a tri-lobate articular cross-sectional profile which is not seen in *D. matildae* (Figures 11, 12 and 16), but is similar to *E. lilloi* (see Figure 6, E in

Comentario [MH18]: This sentence sounds a bit confusing. Could be separated as:

The diaphysis of *A. cooperensis* differs from *W. wattsi* and *S. elliottorum* by being considerably more elliptical in cross-sectional shape, in contrast to the much more ovo-rectangular cross-sectional shape present in the latter taxa (Figure 16).

Besides, it is not clear to me what is the difference between elliptical and ovo-rectangular cross sectional shape.

Comentario [MH19]: The outline curvature can change among individuals of different sizes. The following picture corresponds to three *Saltasaurus* specimens of different sizes (and ages?) from Museo Miguell Lillo, Tucumán, Argentina. The curvature of the proximal margin increases as they get bigger.

(Mannion & Otero 2012), *Giraffatitan brancai* and *E. sciuttoi* (see Figure 4, F-G in (Upchurch et al. 2015). Contributing to the tri-lobate distal epiphysis is a deep olecranon fossa which is longer and deeper than in *D. matildae* but is similar to that of *E. lilloi*.

Considerable variation exists across titanosauriformes in regards to the overall shape of the humerus as illustrated by the outline drawings in Figure 7 of (Lehman & Coulson 2002), Figure 16 of (González Riga & David 2014) and Figure 4 of (González Riga et al. 2019). The humeri of *A. cooperensis* share a combination of characteristics that are missing from more derived titanosaurs ~~compared~~. The gently curved proximodorsally convex outline of the epiphyseal head is similar to that seen in *Tehuelchesaurus benitezii* and *V. daparisensis* and differs from the proximodorsally projecting sub-quadrangular outline typical of many titanosaurians like *C. insignis*, *D. matildae*, *N. australis*, *Notocolossus gonzalezparej~~s~~asi* and *Paralititan stromeri*. The distal epiphyses of *A. cooperensis* is mediolaterally broad, with clearly defined articular condylar areas that are anteroposteriorly compressed. This overall shape is similar to that seen in *D. schrani*, *P. stromeri* and *Malawisaurus dixeyi,* but differs from titanosaurs like *D. matildae*, *N. australis*, *E. lilloi*, and *N. gonzalezparej~~s~~asi*, that possess a more rotund humerus that is not mediolaterally expanded, but anteroposteriorly deep.

Ulna (Figures 17-19) (Table 4). The ulna will be described with the longest proximodistal length, taken from the distal articular surface to the olecranon process, oriented vertically. The main processes of the ulna are oriented anterolaterally and anteromedially with the radial fossa considered anterior. The holotype preserves a single almost complete right ulna. It is one of the best preserved and distinctive bones of the holotype specimen. The proximal region has experienced some weathering; however, much of the articular surfaces remain. The cortical bone of the anteromedial process and anterior and posterior faces of the diaphysis are heavily split into mosaic-like pieces; however, they are tightly arranged and have not moved significantly post-burial and excavation. The diaphysis has been deformed and bent in an anterolateral direction prior to preservation and is unlikely a result of subsurface movement and more likely a result of trampling. Digital retro-deformation of the shaft was possible and ~~allows~~ allowed a more accurate description of the bone and its dimensions. Referred ulna fragments

Comentario [MH20]: See the distal end of the *Saltasaurus* specimen 4017-67. An "extra lobe" is barely interpretable from Powell 1992, Fig 31, although is evident in the largest humerus (right) of the photo in last comment.

Comentario [MH21]: Correct the parentheses

Comentario [MH22]: Some authors consider that is better to use titanosaurians instead of titanosaurs, like in the next sentence.

Con formato: Resaltar

Con formato: Resaltar

from EMF164 include parts of the proximal diaphysis and the interosseous ridge of the distoanterior face.

Anterior view. Three distinct processes extend from the proximal epiphysis, the anterolateral, anteromedial and olecranon processes, in an arrangement typical of sauropods. The anterolateral and olecranon processes are of similar length with the anteromedial process being much longer than either of these. The anteromedial process is shallowly concave along its length ending at its extremity as a triangular point. The anterolateral process is short and broad with a rounded extremity whilst the olecranon process is constricted mediolaterally and angled proximally into a tapered articular surface. Between the anterolateral and anteromedial processes, a deep radial fossa extends distally toward a distinct radial interosseous ridge. The lateral side of the fossa is steep, made up by the medial face of the anterolateral process. The medial side of the fossa is shallow and slightly curved, made up by the broad lateral face of the anteromedial process. The radial fossa extends distally to the beginning of the distal epiphysis.

The distal half of the fossa is shallow and a distinct and thick proximodistally oriented interosseous ridge extends along its center, terminating just proximal of the distal articular end. This feature is present in fragments of a large ulna of EMF164; therefore, such a unique feature allows us to confirm referral of EMF164 to this same taxon.

The anterolateral process is ~~broadest~~ broader proximally, but is not a thick process. It extends the length of the diaphysis tapering along its length into a tall thin crest and terminates just proximal of the distal articular end. At the distal end of the anterolateral process a distinct crest of bone, an interosseous crest, smaller than the process itself extends slightly posterolaterally with a small rounded tuberosity at its apex. This tuberosity sits above another ridge of bone that extends anteriorly along the distal edge of the diaphysis and connects anteriorly to the distal articular region. There is no indication on the surface of the bone or surrounding this region to suggest that this unique set of features is distortion through preservation or from pathology.

Lateral to the anterolateral process is a narrow and deep posterolateral fossa bounded by the lateral face of the anterolateral process and the anterolateral face of the olecranon process. The fossa is broadest proximally and extends distally to about the midshaft level where it tapers to a shallow point before meeting the distal epiphysis. The anteromedial process curves steeply from

its proximomedial extremity to the distal articular surface. The olecranon process is the highest of the three processes with its articular face oriented anteroproximally.

Posterior view. The anteromedial process is broad and flat with a shallow medial fossa extending across the process and distally to approximately two thirds of the proximodistal length. The olecranon process extends distally making a shallow sigmoidal curve, convex proximally and concave distally to the distal articular surface. The anterolateral process is straight in profile and sharply tapers distally to the distal tuberosity and accessory process and ridge.

Proximal view. Tri-radiate anterolateral, anteromedial and olecranon processes. Olecranon process smallest of the three, anterolateral process second largest whilst the anteromedial process is much longer than both extending approximately two and a half times the length of the anterolateral process. The angle created between the long axes of the anteromedial and anterolateral processes is approximately 50°.

Distal view. The distal articular surface is beveled proximally, and made of two clear lobes, a posteriorly placed mediolateral lobe and a small anterolateral lobe. The overall shape in distal view is oblong for the posterior lobe and rounded for the anterior lobe. The whole articular area is compressed anteroposteriorly so that the posterior region is not prominently expanded and more 'comma' shaped.

Overall the ulna possesses the characteristic shape seen in many sauropod taxa. The stout nature of the ulna is similar to many titanosaurs like *D. matildae, S. loricatus, N. australis, Y. datangi* and *O. skarzynskii.* The presence of an accessory interosseous crest on the mediolateral process and an interosseous ridge within the radial fossa is unique to this taxon. An accessory interosseous crest has been recently observed in the brachiosaur *V. daparisensis* (see Figure 20, A in (Mannion et al. 2017)); however, this feature does not originate from the anterolateral process as it does in *A. cooperensis*~~,~~ ~~i~~. Instead, the crest originates separately from it in a more medial position. Distinct interosseous ridges within the radial fossa of the ulna are observed in *Z. atlanticus* (Mateus et al. 2014), *Rapetosaurus krausei* (Curry Rogers 2009), *Bonitasaura*

Con formato: Resaltar

Comentario [MH23]: A very similar ridge is present in the radial fossae of at least two ulnae of *Neuquensaurus* (see Otero 2010, Fig. 4, A_1-A_3 and B_1-B_2)

Otero A. 2010. The appendicular skeleton of *Neuquensaurus*, a Late Cretaceous saltasaurine sauropod from Patagonia, Argentina. *Acta Palaeontologica Polonica* 55:399–426.

Comentario [MH24]: Also seen in *Diamantinasaurus* (Poropat 2015a, Fig. 11b, c) and Figs 17F and 18B of this ms.

salgadoi (Gallina & Apesteguía 2015) *Narambuenatitan palomoi* (Filippi et al. 2011); and to a lesser degree of development in *N. robustus* (Otero 2018) and *D. schrani* (Ullmann & Lacovara 2016). With the exceptions of *A. cooperensis* and *N. robustus*, the interosseous ridge originates at approximately one third distal of the proximal epiphysis. In *A. cooperensis* and *N. robustus*, the ridge originates in the distal third of the shaft.

The ulna of *D. matildae* differ from *Australotitan* by both possessing a similar combination of features not present in *A. cooperensis*; including a relatively shorter anteromedial and relatively longer anterolateral and olecranon processes (in proximal view) (Figures 17, E-H, 18 and 19); a taller and broader olecranon process; a less sinusoidal posterolateral ridge (in anterior view); the absence of an anterolateral distal interosseous crest or interosseous ridge within the distal radial fossa; a more inflated and rounded anterolateral and anteromedial~~ly~~ margins of the distal epiphysis producing an inflated bean-shaped articular end in distal view; and a deeper fossa between the anteromedial and posterior processes.

The ulnae of *W. wattsi* are both poorly preserved missing the proximal and distal epiphyses and cannot be easily compared with *A. cooperensis* (Figure 17). The reconstructed ulna (Figure 18, C) shows clear differences between *W. wattsi* and *A. cooperensis* along with *D. matildae* in regards to cross-sectional thickness of the anteromedial and anterolateral processes (Figures 18 and 19). *W. wattsi* is distinctly more robust in cross-section. Previously it has been reported that the left ulna of *W. wattsi* preserves the proximal and distal epiphyses (Hocknull et al. 2009; Poropat et al. 2015a), however, on inspection, both the left and right ulnae lack preserved proximal or distal articular ends or preserved epiphyses (Figure 17-19). The proximal end of the left ulna is missing significant portions of the anteromedial and anterolateral processes. The olecranon is also missing the articular end with the surface exhibiting a pitted and corroded surface that can also be seen along the diaphyseal shaft (Figure 17, M & O). The distal end is missing and there is some indication of plant-debris adhering to this broken surface. Therefore, observations about the morphology of the ulnar condyles of *W. wattsi* are likely misinterpretations.

Pelvis. The right and left pubes and ischia were recovered together in semi-articulation and semi-life position with the dorsal side facing up in the deposit. The ilia were not found. Both pubes are well preserved; however, the cortical bone surface has been split into small mosaic-

Comentario [MH25]: Also check Otero 2010. The ridge is also present in *N. australis* (as seen in Otero 2010 and 2018).

Comentario [MH26]: I got confused in this sentence. *A.* means *Australotitan*, right? Rephrasing could help here.

like pieces across the broad anterodorsal plates of the pubes and posterodorsal plates of the ischia. The pubes and ischia have split along the medial symphysis and reoriented sub-horizontally within the deposit, the cause of which is likely dinoturbation through trampling. The pubic blades are oriented slightly above horizontal. The ischial blades have been dislocated slightly from their life position relative to the pubes; however, remain in near contact along their articular surfaces between each ischium and pubis.

Pubes (Figure 20-22) (Table 5). *Lateral view.* The lateral (ventrolateral) views of both pubes represent the sides facing downward in the site resulting in this side being better preserved than the medial (dorsomedial) side. The left pubis is best preserved and will be used as the basis for most of the pubic description. The iliac peduncle sits dorsal of a shallow fossa that runs posteroventrally to the obturator foramen. Posterior of the obturator foramen the ischial peduncle is broken with matrix infill obscuring the lateral connection to the ischium. The anterior margin of the proximal blade extends ventrally from the iliac peduncle curving slightly ventrally toward the distal blade expansion. The ischial peduncle is connected and was co-ossified to the ischium along its entire length extending ventromedially to the midline, then joining with its contralateral pair. The ventral margin of the distal blade is divided into two regions of differing bone thickness with a line of collapsed bone forming an irregular groove from the ventral margin of the ischial peduncle across the pubic blade at about a third of the distance from the ventrolateral margin. This line of collapse indicates a distinct change in bone thickness from the main distal and proximal blade to the internal (medially directed) thin bone connection between the two contralateral elements.

Medial view. The medial (dorsomedial) view of both pubes represent the face exposed upwards in the site, therefore, the medial surface preserves a number of post-burial alterations to the bone surface. The right pubis has been affected more so than the left, with the surface cortical bone fractured into a mosaic tile of pieces with some collapse of internal bone and compression observed. Both pubes have some distortion to the central portion of the distal blades having been affected by crushing through trampling.

The iliac peduncle is better preserved in the left pubis. In medial view, it is broad and flat, taking up almost the entire proximal portion of the acetabulum. The peduncle is slightly

expanded dorsally of the proximal blade plate which extends ventrally and curves medially to the central symphyseal surface. The posterior margin of the proximal blade is made up of the ischial peduncle which was fused to the pubic peduncle of the ischium along its entire length during life. In the left pubis the connection has been split and broken prior to fossilisation with the pubis medially and ischium laterally displaced relative to life position. The medial margin of the ischial peduncle has been split and dislodged vertically above the anterodistal margin of the pubic peduncle of the ischium. The opposite has occurred on the right side element with the pubis displaced laterally and the ischium medially.

Ventral of the posterior margin of the iliac peduncle and anterior of the ischial peduncle is an enclosed ovoid obturator foramen with a long axis oriented posterodorsally to anteroventrally. The symphyseal margin is thickest at both the posterior and anterior ends and has broken away from its contralateral pair exposing broken and open internal bone along its length, indicating that both blades were originally fused together. The bone connecting the contralateral elements is very thin along their length and curves ventrally to the massively expanded distal articular surface.

The distal articular surface is dorsoventrally thickened with a central fossa (preserved best in the left pubis). A shallow fossa runs along the distomedial surface behind the distal expansion. The lateral margin of the proximal blade begins lateral ~~of~~ to the anterior margin of the iliac peduncle and curves ventrally at a very low angle toward the distal blade and distal expansion. In the left pubis, two abnormal indentations occur at the junction of the proximal and distal blades and just proximal of the distal expansion. These indentations appear to be the result of bone trampling. The original lateral margin would have been a smooth curved surface along its length as seen in the right pubis.

Based on the ~~better~~ better-preserved left pubis, the iliac peduncle is oval in shape with tapered anterior and posterior margins, thickest in an anteromedial to distolateral direction. The region for the ambiens process is indistinct as the pubic blade runs directly ventral of the base of the iliac peduncle. Only a short acetabular surface is present posterior of the iliac peduncle on the pubis.

Ischia (Figures 20-22) (Table 6). The left ischium is the least deformed of the ischia, preserving good and near complete margins and iliac and pubic peduncles. The iliac peduncle of

the ischium is teardrop shaped with a rounded posterior and tapered anterior margin that runs into the acetabular surface. The acetabular surface is shallowly concave and approximately the same length as the iliac peduncle.

The anterior corner of the acetabular surface where it meets the pubic peduncle is dislocated posterodorsally from the corresponding puboischial articular surfaces, offsetting this articulation in a dorsoventral and mediolateral direction. The distal ischial symphysis is broken along its anteromedial margin indicating that these two elements were connected in life. However, complete bone is observed close to the central connection of both paired elements, suggesting that the four elements were fused along their respective articular surfaces except for the central point where all four elements meet (Fig. 21).

Instead, we reconstruct this area as having a slight opening that would have resembled a diamond-shaped gap between the four elements or exceptionally thin bone that has not preserved. The posteroventral margin of the ischium is unfused, but when mirrored form a distinct ‘v’ shaped margin (notch) between the mediodistal ends of each ischium when viewed dorsally. The proximal ischial plate is anteroposteriorly broad along its entire length and continues to retain this breadth distal of the pubic articulation, creating a broad posterodistal, but ventromedially projecting ischial shaft. A lateral tuberosity along the middle of the posterior ischial margin is a long thin buttress of bone.

When compared to other sauropods, the preserved portions of the pelvis are closest in morphology to all three previously described Winton Formation taxa (i.e. *D. matildae*, *W. wattsi* and *S. elliottorum*). The ischium is preserved for all taxa and warrants specific comparison (Figures 22 and 28). The ~~iliac~~ articular surface of the iliac peduncle is poorly preserved in all taxa; however, the shaft just ventral of this articular surface indicates that all taxa bear a similar tear drop-shaped process that was anteroposteriorly longer than mediolaterally wide. The iliac peduncle is dorsoventrally elongate in *D. matildae*, *W. wattsi* and *A. cooperensis*, with that of *W. wattsi* being the most elongate~~,~~. ~~however~~However, this could be a reflection of the significant bone loss around the peduncle in *W. wattsi*, creating an illusion of a more elongate feature (Figure 22). This feature is fore-shortened in *S. elliottorum* and seems real. However, the iliac peduncles of both the pubis and ischium are somewhat dorsoventrally compressed, suggesting this feature might be due to taphonomic crushing.

The proximal ischial plate is broad anteroposteriorly with a ventromedially curved posterior margin in all taxa, following the curvature of the pubic articulation and co-ossified fusion. Ventromedially the ischial shaft is indistinct from the proximal plate and is best described as a distal plate because it is broad anteroposteriorly along its entire length, and is not differentiated into a posterior process as seen in *O. skarzynskii* (Borsuk-Bialynicka 1977). The distal ischial plate contacts its co-lateral partner medially and was clearly fused to one another in all the Australian taxa, although broken apart during fossilization in *W. wattsi*, *D. matildae* and *A. cooperensis*. This fusion is clearly preserved in *S. elliottorum*, and partially observable in *D. matildae* and *A. cooperensis*. This feature is likely to have been present in *W. wattsi* as well because the distal ischial plate is similarly broad along its entire length and posteriorly foreshortened, with no sign of a completed medial margin. This indicates that bone co-ossification likely occurred with its contralateral pair. Although the medial margin is missing, the thickness of bone suggests a significant area of missing distal ischial plate in *W. wattsi*.

A broad and foreshortened distal ischial plate without a posteriorly projecting blade-like process is not well defined in titanosauriformes; however, *M. dixeyi*, *A. sanjuanensis* and possibly *Uberabatitan ribeiroi* approach this morphology (Gomani 2005; Silva et al. 2019; Tykoski & Fiorillo 2016). However, they still retain a posterior process of the ischium shaft blade. *O. skarzynskii* possesses a similar central fusion and broad distal ischial plate~~;~~ , ~~however~~although~~,~~ the distal plate continues posteriorly to form a distinct straight and posteriorly projecting blade-like process (Borsuk-Bialynicka 1977). We therefore consider this combination of features of the ischium a potential synapomorphy for *D. matildae*, *S. elliottorum* and *A. cooperensis*, with the possibility ~~that~~ of? this feature also uniting the only other Winton Formation taxon, *W. wattsi*, within this group (see Discussion).

When viewed posteriorly, the distal ischial plate retains a gentle medial curvature to meet and fuse medially with its contra-lateral partner in *D. matildae*. However, in *S. elliottorum*, *A. cooperensis* and possibly in *W. wattsi*, the distal plate curves medially to meet its partner, as in *D. matildae*, but before doing this the distal ischial plate curves steeply ventrally creating a posteriorly facing dorsal surface of the distal ischial plate (Figure 22).

Femur (Figures 23-24) (Table 7). The femur will be described with the long axis of the shaft vertical and the distal condyles orientated so that they lie flat along a mediolateral horizontal plane. Portions of both the right and left femur are preserved in the holotype. The right femur preserves the diaphysis and distal epiphysis. It is missing the proximal epiphysis and the proximal section of the diaphysis is crushed and distorted, having been pushed downwards from a horizontal position (Figure 8). This vertical displacement and crushing has distorted the diaphysis from about the midshaft proximally. The crushing is likely due to trampling as discussed above (Hocknull et al. 2019) (Figure 8) and has distorted the longitudinal axis of the diaphysis. The distal half of the diaphysis and distal epiphysis remain undistorted~~;~~, although ~~however,~~ the distal medial condyle is damaged with loss of structure on both the anterior and posterior surfaces.

The left femur was recovered on the surface in a large number of fragments and was pieced back together. Surface exposure has removed much of the surface cortical bone; therefore, the femoral head would have been larger and ~~preserved~~ had more of the bulbous femoral head articular surface than what is preserved. Reconstruction of these fragments recovered the proximal epiphysis and the proximal region of the diaphysis to just above the lateral bulge. Both elements preserve overlapping regions of the proximal diaphysis, which allows reconstruction of the femur (Figure 23-24).

In addition to EMF102 (holotype), two other femora, EMF164 and EMF105, are referred to ~~*Australotitan*~~ *A. cooperensis* due to significant shared overlap in morphology. EMF164 is highly fragmented but represents a larger femur preserving the proximomedial margin of the proximal epiphysis, along with portions of the lateral bulge, diaphysis, fourth trochanter and medial and lateral condyles. The proximal epiphyseal portion (greater trochanter) has been useful when reconstructing the femur. EMF105 is a complete femur, with some loss of cortical bone around the proximal epiphysis and medial distal condyle. This femur, although smaller than the holotype, provides an accurate independent guide for overall femoral shape when scaled isometrically to the size of EMF102 (Bonnan 2007; Bonnan 2004; Kilbourne & Makovicky 2010). It also provides the best guide to the shape of the dorsomedial portion of the femoral head. The following descriptions of the femur will be based on the holotype but will reference the referred femora where appropriate.

Anterior view. The proximal epiphyseal head is rounded and projects proximomedially with preserved articular surface extending across the proximal-most margin from just above the greater trochanter and is assumed to include the missing femoral head. The fourth trochanter is positioned slightly more proximally than the medial margin of the femoral head. The lateral margin of the femur is shallowly sigmoidal in overall outline shape, made up of the abductor crest (lateral bulge) that curves laterally in a shallow convex outline, distally from the greater trochanter, encompassing approximately a third of? the proximal length of the entire lateral margin of the diaphysis. Distal of this, the lateral margin of the diaphysis then curves medially in a shallow concave outline along the remaining two thirds of the shaft where it meets the lateral epicondyle. The medial margin curves laterally in a shallow concave outline from the medial margin of the femoral head position to the fourth trochanter and then curves laterally again in another shallow concave outline from the distal margin of the fourth trochanter to the tibial (medial) condyle.

The distal condylar region is mediolaterally wide with an anteroposteriorly narrow distal epiphysis with the lateral condyle mediolaterally broader than the medial condyle. The articular surface of both condyles extends onto the anterior face of the diaphysis and both condylar articular surfaces on the anterior face are dorsolateral to ventromedially directed, the medial condyle more so than the lateral condyle.

Posterior view. A low rounded ridge (trochanter shelf) runs from the greater trochanter along the lateral bulge and merges with the diaphysis approximately 1/3 the length of the shaft. The fourth trochanter is best visible in posterior view and is proximodistally ovoid in shape and positioned on the poster~~i~~o~~r~~-medial face of the diaphysis. The distal end of the diaphysis expands mediolaterally and houses a shallow broad fossa proximal to the distal epiphysis. The distal articular region is divided into two regions, the tibial (medial) condyle and the fibular (lateral) condyle, which includes the lateral epicondyle. The posterior origin of the fibular condyle and lateral epicondyle extends further proximally on the posterior face than the tibial condyle. The fibular condyle and lateral epicondyle are divided by a distinct and deep fossa. The lateral margin of the lateral epicondyle expands from the main articular surface creating a small shallow fossa on the distolateral corner. The tibial and fibular condyles are divided by a deep and wide intercondylar fossa.

Proximal view. Although poorly preserved, the femoral head is expanded anteroposteriorly and rounded medially. The greater trochanter is constricted anteroposteriorly with a mediolaterally tapered articular region. A shallow 'D'-shaped transverse cross-sectional outlines the proximal diaphysis, being broad mediolaterally and very narrow anteroposteriorly. The midshaft transverse cross-section outline is anteroposteriorly deeper forming a more distinct 'D'-shape.

Distal view. The long axes of the tibial and fibular condyles in distal view are oriented anterolaterally to posteromedially. The tibial (medial) condyle is anteroposteriorly longer than the fibular (lateral) condyle. The crural extensor fossa on the anterior side of the distal epiphysis is broad and similarly as deep to the intercondylar fossa of the posterior side. The anterolateral to posteromedial orientation of the condyles is similar to the distal condyles described for *Daxiatitan binglingi* (You et al. 2008), *D. schrani* (Ullmann & Lacovara 2016), *L. astibiae* (Díaz et al. 2013) and cf. *L. astibiae* (Vila et al. 2012). In *D. binglingi*, a combination of this feature with dorsolateral bevelling of the distal condyles was considered both unique features of this taxon (You et al. 2008). This feature was considered to be one of a number of features that could identify femora to *L. astibiae* (Vila et al. 2012). However, in *D. schrani* (Ullmann & Lacovara 2016) the medially oriented distal condyles were considered to be oriented in this plane due to taphonomic distortion through lithostatic compression. Therefore, in some taxa this seems to be a real feature, whilst in others it is taphonomic. The anterolateral to posteromedially directed condyles in *A. cooperensis* are unlikely to be taphonomic, although there has been loss of surface bone to the condyles indicating some damage but crushing is restricted to the proximal half of the holotype femur. The same condylar feature is observed in the referred femur EMF112, which has not been crushed.

When comparing the distal condyles of specimens referred to *A. cooperensis* with other femora from the Winton Formation there are clear differences in distal epiphyseal shape (Figures 25 and 26). Other than the considerable larger size, the femur of *A. cooperensis* also differs from the femur of *D. matildae*, the only described Winton Formation taxon to preserve a femur, in a number of ways. These differences are also observed when comparing several additional isolated femoral elements from the Winton Formation not currently assigned to a taxon (Figures 25 and 26), and include: 1) A more proximomedially directed femoral head; a mediolaterally

Comentario [MH27]: This condition is also present among saltasaurids, such as *Saltasaurus*, *Opisthocoelicaudia*, *Neuquensaurus* and *Rocasaurus*. It has been proposed originally as a synapomorphy of Saltasauridae by Wilson and Carrano 1999. This proposal was then followed by several authors. There is a brief discussion on this feature (bevelled condyles) in Otero 2010, p. 417.
If it is not the same character, you should clarify it to avoid possible confusion.

broader and anteroposteriorly narrower diaphysis along the entire length; 2) A relatively larger and more posteriorly positioned fourth trochanter; 3) a less sigmoidal lateral margin and more convex medial margin; and 4) Anterolateral to posteromedially oriented distal condyles (in distal view). These features not only differentiate the two taxa possessing femora, but also differentiate the southern-central from the northern Winton Formation femoral specimens. Therefore, the femur may be of taxonomic value when differentiation of taxa between regions. This also suggests closer morphological similarities to those taxa found within a particular region, relative to between regions. These differences do not seem to relate to overall element size because the differences are seen in specimens from Eromanga and Winton that are very different in size (Figures 24, 26 and 35).

Overall, the femur of *A. cooperensis* is similar to titanosauriform sauropods and more derived titanosaurs. Comparing the outline shape of the anterior and posterior views across titanosauriform sauropods similarities in overall shape are found in *D. schrani* (Ullmann & Lacovara 2016), *Traukutitan eocaudata* (González Riga et al. 2019), *L. astibiae* (Díaz et al. 2013), *Aegyptosaurus baharijensis* (Stromer 1932) and *Ampelosaurus atacis* (Le Loeuff 2005). These similarities reflect a broad femoral shaft relative to proximal and distal condylar breadths, along with a long shallowly curved lateral bulge and less bulbous proximal femoral head. The femora are also narrow anteroposteriorly along the diaphyseal length, but possess expanded proximal and distal epiphyseal regions.

The northern Winton Formation femora, including *D. matildae*, all have narrower and deeper diaphyseal shafts, more bulbous proximal femoral heads, anteroposteriorly thicker lesser trochanter, and anteroposteriorly rotund distal epiphyses (Figures 25 and 26). The femoral shaft is relatively narrower and dorsoventrally straightened in the northern Winton Formation sauropods compared to the southern-central specimens. Such variation in femoral shaft morphology is present in several titanosaurs, ranging from stout and robust diaphyses in taxa like *N. robustus* (Otero 2010), *S. loricatus*, *E. sciuttoi* (Martínez et al. 2004) and *Bonatitan reigi* (González Riga et al. 2019), to straight and deep diaphyses in taxa like *P. mayorum* (Carballido et al. 2017), to anteroposteriorly compressed and mediolaterally broad, sinuous diaphyses in taxa like *A. cooperensis*, *L. astibiae* (Díaz 2013) and *D. schrani* (Ullmann & Lacovara 2016).

Con formato: Resaltar

Referred Specimens

EMF164. *Axial remains.* The type specimen for *A. cooperensis* does not possess associated vertebrae; however, the referred specimen EMF164 from EML010 includes isolated pieces of presacral vertebrae preserving distinctly camellate somphospondylous internal centrum bone. The internal cavities filled with matrix are large and indicate derived somphospondylous architecture similar to that seen in all other Cretaceous-aged sauropods from Australia. The camellate bone structure is very thin, reticulated ~~thin~~ with? bone struts held within a mudstone matrix, approximating the same degree of camellate structuring seen in the holotype dorsal vertebrae of *A. mackillopi*, *D. matildae*, *W. wattsi* and *S. elliottorum*. The thickness of the trabeculae and the size of the vacuities observed in the isolated pieces of EMF164 are larger than those from these previously described taxa, thus indicating that the vertebrae were much larger in overall size. Large pieces of plank-like rib shafts are also present, ~~however,~~although no proximal rib articular ends have been identified.

Comentario [MH28]: How can be identified as presacral? Some anterior caudal centra can be heavily pneumatized.

Comentario [MH29]: The size of the trabeculae and vacuities not always correlate with body size.

Appendicular remains. Identifiable pieces of ulna include sections of diaphysis and a fragment preserving a thick ridge that represent the prominent interosseous ridge of the radius, similar to that present in holotype (EMF102). These ulna fragments are too poorly preserved to provide additional information that the holotype provides; however, the thickness of the cortical bone seen in cross-section of EMF164 when compared to that of the holotype (EMF102) indicates that EMF164 was a larger individual.

The larger size of EMF164 is best represented by the fragments of a right femur (Figure 35). A large number of fragments represent diaphyseal pieces of the femur that are clearly anteroposteriorly narrow indicating a broad, but narrow diaphysis for the femur, similar to that seen in EMF102. However, these pieces have much thicker cortical bone in cross-sectional comparison. As with the ulna pieces, this thickness of cortical bone indicates an individual of larger size than that of EMF102.

The elements of the EMF164 femur do not provide any additional details of the femur from a comparative point of view, other than its larger size. Estimating the size of this larger femur provides some additional information in regards to the overall variation in the size of these elements and estimates of body-size in this taxon. Therefore, we have undertaken three different estimations of the femur length of EMF164 and will report the average and range.

We directly matched the largest fragments of the femur of EMF164 to the femora of the *A. cooperensis* holotype, EMF102 and referred EMF105. We first did this by sight and then digitally by aligning and scaling the 3-D surface meshes of the smaller femora (EMF102 & 105) to match the size of the combined 3-D surface meshes of the EMF164 femoral pieces. This was achieved in Meshlab (Cignoni et al. 2008) and Cloud Compare (Girardeau-Montaut 2016) by point picking, rotation/translation, then isometrically scaling the 3-D surface mesh of EMF102 and EMF105 to match the size and position of the EMF164 pieces.

The resulting isometrically scaled reconstruction returned maximum total lengths of the femur when scaled to EMF102: maximum medial length of 2117 mm; maximum central length of 2134 mm; maximum lateral length of 2160 mm. The reconstructed surface mesh of EMF102 does not include the proximal-most femoral head articular surface because this is missing portions of the proximal-most cortical bone, therefore, these estimates could be considered underestimations.

Second, we undertook the same process, but this time we matched the 3-D restored femur that was based on the surface mesh of EMF102 (Figure 35). Therefore, when scaling the reconstructed model isometrically, this universal scaling was automatically applied to the associated 3-D modelled femur. The resulting isometrically scaled model returned total lengths of the femur: maximum medial length of 2125 mm; maximum central length of 2176 mm and; maximum lateral length of 2140 mm. The modelled surface mesh of EMF102 includes estimations of the proximal-most femoral head articular surface by continuation of the surface bone shape, therefore, these estimates could be considered accurate.

Finally, we used the 3-D surface mesh created of the referred femur, EMF105, and aligned and scaled this mesh to match the surface meshes of EMF164 pieces. The resulting isometrically scaled model returned total lengths of the femur: maximum medial length of 2133 mm; maximum central length of 2187 mm and; maximum lateral length of 2147 mm. EMF105 is a complete femur missing some of the proximal and distal condyles making this estimate likely a slight underestimate.

Together, taking all nine measurements we arrive at an average length of 2146 mm with a range of 2117-2187 mm. Considered together, this provides an estimated length of the EMF164 femur of approximately 2.15 m in length, which is approximately 20 cm longer than the reconstructed femur of the holotype (EMF102) (Figure 35).

Comentario [MH30]: Use uniform units (mm or m) along the text.

Comentario [MH31]: This seems like a mix of methods plus results. The explanation of the different approaches to estimate maximum sizes should be in methods.

EMF105 (Figure 23 and 24, Table 7). EMF105 is a complete right femur, measuring 1412 mm in maximum proximodistal length. The femur conforms closely to the overall morphology of the holotype femora EMF102; however, it is better preserved and includes a well-preserved proximal femoral head. Post-depositional scouring of the distal condyles has truncated them in the anteroposterior plane. Excavator damage during removal of overburden has occurred to the distal diaphysis shaft with loss of preserved bone in a triangular wedge-shape.

EMF165 (Figure 29). EMF165 is a portion of a distal humerus preserving a shallow and broad olecranon (anconeal or cuboid) fossa and a rounded anterior face. It is missing much of the distal epiphyseal articular surface, ~~however,~~although it is broad relative to the diaphysis to a similar extent to that seen in EMF102. In distal view, the tri-lobate articular outline can be discerned, although the anterior and posterior extremities of the condyles are missing. Although not preserving considerable detail, the proportions of this distal humerus ~~is~~ are similar to that of the holotype and not that of *D. matildae*, the only other Winton Formation sauropod to preserve a distal end of the humerus.

***Australotitan cooperensis*?**

Currently, several sauropod specimens cannot as yet be directly referred to *A. cooperensis* due to their incompleteness or current state of preparation. These specimens are known from the northern and southern Plevna Downs sites and include isolated, associated and articulated remains.

Based on comparisons of these preserved elements with those from northern Winton Formation taxa, they share general features, but none possess features that definitively ally them with those taxa (i.e. *D. matildae*, *W. wattsi* or *S. elliottorum*). Therefore, we ~~suggest that a~~applied the conservative approach ~~be taken and~~of initially ~~allocate~~ allocating them to the local taxon, ~~*Australotitan*~~ *A. cooperensis*, until sufficient overlap is found in skeletal remains to constitute a fully diagnostic allocation.

EMF106 occurs at EML010 and is a collection of small sauropod remains found with EMF164. Identifiable remains of EMF106 include a metapodial articular end and pieces of mid caudal

centra. A portion of a caudal ~~centra~~ centrum is amphicoelous with dense non-pneumatic cancellous bone (Figure 31, ~~D~~G-~~E~~H).

EMF103 occurs at EML011b and is a scattered series of cervical and dorsal vertebrae with a poorly preserved distal femur and isolated dental remains. Based on overall size similarities between the cervical and dorsal vertebrae, along with the femur, it is likely that this specimen represents a single individual; however, the distribution of the skeletal elements and the post-depositional scouring and trampling makes comparing this skeleton with other individuals difficult. The femur does overlap as an appendicular element with EMF102~~;~~. ~~however~~However, the element is not well enough preserved to ally it, or separate it, from *A. cooperensis*. The cervical and dorsal vertebrae are well preserved on the surfaces that faced downward in the site. The upward projecting faces have been scoured and trampled which has dislocated and deformed the positions, and possible interpretations, of the vertebral laminae. Therefore, this precludes meaningful comparisons to the other Winton Formation taxa preserving cervical and dorsal vertebral laminae, until we can retrodeform and model the original positions of these features.

~~-~~EMF166 is an isolated metacarpal found with EMF165 and EMF105. The metacarpal is relatively small in comparison to what would be expected to be from the individual femur (EMF105) or the humerus (EMF165). Based on comparisons with the metacarpals of *D. matildae*, *W. wattsi* and *S. elliottorum*, EMF166 is a metacarpal IV. The proximal and distal ends are rounded through pre-depositional abrasion, marked by a thick layer of plant debris covering the bone prior to preparation. The proximal end describes a roughly tear-drop or rounded triangular shape with the broadest rounded margin being external and the narrowest margin constricted internally. There are remnants of distinct internal condylar processes that have been rounded off through abrasion. The distal external margin is rounded with no distinct indication of distal articular surfaces on the external face suggestive of phalanges. However, the lack of these features could be preservational. In external view, the metacarpal differs from the northern Winton Formation taxa by being more elongate without the proximally and distally expanded and robust epiphyses seen in *D. matildae*, *W. wattsi* and *S. elliottorum.*

EMF109 (EML012) (Figure 6, K and 31, E?) is an associated and articulated skeleton preserved within a massive siltstone concretion located 65 m to the southwest of EML013. Based on what skeletal elements were observable in the concretion this specimen preserves much of the torso

Comentario [MH32]: Looks like a complete caudal centrum indeed.

and tail of the sauropod. The articulated caudal vertebrae were evident in the site, ~~clearly~~ delineated by the concretion itself. However, the ~~main body of the concretion, which houses~~ dorsal vertebrae, ribs and appendicular elements are mostly obscured by concretion. Until this concretion has been prepared, direct referral of it to a described taxon is precluded; however, the distal mid and distal caudal vertebrae have been prepared to a point that allows some initial comparison with the distal caudal vertebrae known from *W. wattsi* (Figure 31).

Of the two known occurrences of distal caudal vertebrae known from the northern Winton Formation both are incipiently bi-convex as originally described (Hocknull et al. 2009), possessing articular ends but do not approach the true bi-convexity seen in *Rinconsaurus* (Calvo & González Riga 2003). This feature is now considered to be a local autapomorphy for *Wintonotitan* because it is known across several titanosauriforms (D'Emic 2012; Poropat et al. 2015a). Having said this, neither *D. matildae* or *S. elliottorum* have associated distal caudal vertebrae preserved, therefore, at this stage, the utility of this feature is equivocal and only useful to exclude *W. wattsi* from a possible candidate taxon for the southern-central Winton Formation specimen.

The distal caudal vertebrae of EMF109 are not incipiently bi-convex, instead being amphicoelous to amphiplatyan, possessing similar morphology to all other anterior and middle caudal vertebrae found across sites in both the northern and southern-central Winton Formation (see Discussion). Therefore, we can exclude *W. wattsi*, as a candidate taxon, however due to the ubiquitous nature of amphicoelous caudal vertebrae of sauropods in the Winton Formation we cannot exclude any of the other three described taxa. Based on what is indicated from the specimen as currently visible, EMF109 will provide significant data to understand the anatomy of these sauropods, being the most complete southern Winton Formation specimen.

EMF100 (Figure 30). EMF100, from EML01 is a small, poorly preserved ulna, missing the majority of the proximal and distal ends. However, comparison of the midshaft diaphyseal cross-section and proximal and distal shape comparisons are possible between EMF100, *A. cooperensis*, *D. matildae* and *W. wattsi*. EMF100 is mediolaterally compressed as seen in *A. cooperensis* and not in *D. matildae* or *W. wattsi*. Furthermore, the shape of the shaft in distal and oblique-distal views ~~are~~ is closer to *A. cooperensis* than it is to *D. matildae* or *W. wattsi*. In proximal view, the anteromedial process is proportionately more elongate relative to the

proximolateral process, albeit missing the proximal portion of the process. However, by projecting the anteromedial and anterolateral processes proximally, the relative expansion of these processes is closer to that of *A. cooperensis* than it is to *D. matildae* or *W. wattsi*.

Discussion

Comparison with other Winton Formation sauropod taxa. *Australotitan cooperensis* can be differentiated from the three semi-contemporaneous northern Winton Formation sauropods, *Diamantinasaurus matildae*, *Wintonotitan wattsi* and *Savannasaurus elliottorum*, in the following ways: *A. cooperensis* is larger than all the three taxa in the scapula, humerus, ulna, femur and pubis (Tables 2-7). The scapula differs from *D. matildae* and *W. wattsi* by possessing sub-parallel dorsal and ventral margins of the scapular blade; not possessing a medial scapular blade tuberosity and; not possessing a distinct lateral mid-ridge of the scapular blade. Instead, this ridge occurs along the ventral margin (Figures 10 and 28). The humerus differs from *D. matildae* by possessing a distinct tri-lobate distal articular epiphysis and a deltopectoral crest that terminates more distally (Figures 15, 16 & 28). Neither *S. elliottorum* nor *W. wattsi* preserve the proximal or distal articular ends so are not directly comparable. The humerus further differs from both *W. wattsi* and *S. elliottorum* by the later taxa bearing an ovo-rectangular midshaft cross-sectional shape (Figure 16). The ulna differs from *D. matildae* and *W. wattsi* by possessing a relatively longer proximal anteromedial process and ~~by possessing~~ a distinct interosseous ridge in the radial fossa (Figures 18, 19 and 28).

Pubes are known from *D. matildae*, *S. elliottorum* and *A. cooperensis*, but are unknown in *W. wattsi*. *A. cooperensis* differs from *D. matildae* by being larger; possessing dorsoventrally thinner pubic blades; possessing an obturator foramen closer to the proximal margin; and a slightly more mediolaterally expanded distal margin (Figures 22 and 28). The pubes of *A. cooperensis* differ from *S. elliottorum* by being larger, more ventrally directed; not possessing a lateral proximodistal mid-ridge (autapomorphy of *S. elliottorum*); and by possessing an obturator foramen that is dorsoventrally oblong instead of dorsoventrally compressed as in *S. elliottorum* (Figures 22 and 28). The latter feature may be due to taphonomic distortion in *S. elliottorum* where the pubis has possibly been compressed in the dorsoventral plane, but if so,

the obturator foramen would then be much larger in *S. elliottorum* relative to *A. cooperensis* and *D. matildae*.

The ischia of *D. matildae*, *W. wattsi*, *S. elliottorum* and *A. cooperensis* are known and all are near complete, making this element one of the best directly comparable elements between all four taxa. All taxa are similar in overall morphology, possessing a distinct 'tear-drop' shaped iliac peduncle in dorsal view; concave acetabular articular region; long ventromedially curved pubic articular surface; and similarly ventromedially curved posterior puboischial blade margin. The ischial blade expands anteroposteriorly as it curves ventrally, then connects with its contralateral element in *D. matildae*, *S. elliottorum* and *A. cooperensis*.

The distomedial margin of the ischium in *W. wattsi* is missing and precludes a definitive mid-line connection between the contralateral ischia. However, based on the close similarity in morphology and the curvature of this element with the other taxa, it is very likely that the ischia extended to contact its contralateral at the midline (Figure 28).

In dorsal view, the posterior-most margin of each ischial blade occurs at near to two-thirds the dorsoventral length of the posterior blade margin. This produces a double-pointed posterior margin of the ischia in dorsal view with a 'v'-shaped embayment at the posteromedial margin of the ischia. This embayment is shallowest in *A. cooperensis* and steepest in *S. elliottorum*, with *D. matildae* intermediate. Although this margin is not completely preserved in *W. wattsi*, it is likely to have been similar based on the close approximation of these elements to one another (Figure 22 and 28). The posterior margin of the ischia in *S. elliottorum* and *A. cooperensis* curve ventrally along the distal plate margin angling the dorsal margin of this distal-most portion posteriorly. This does not occur in *D. matildae*, where the dorsal margin of the distal plate remains dorsally oriented. The orientation of the distal-most plate margin is unknown in *W. wattsi*, ~~however,~~although at the preserved distal-most margin it begins to curve ventrally. If this curvature was to continue, it would produce a similar posteriorly directed distal plate, as seen in *S. elliottorum* and *A. cooperensis*.

The ischium of *A. cooperensis* is larger than in both *S. elliottorum* and *D. matildae*, but smaller than *W. wattsi*. The ischium is the only comparable element across these taxa where *A. cooperensis* is not substantially larger. Both holotype specimens of *A. cooperensis* (EMF102) and *W. wattsi* (QMF7292) are known from associated and semi-articulated remains, which

establishes the allocation of each ischium with other elements of each holotype, therefore the size discrepancy is unlikely an artefact of having come from multiple individuals.

The greater size of the ischium in *W. wattsi* is contrary to the relatively smaller sizes of all other known appendicular elements in common with *A. cooperensis*. The preserved scapula of *A. cooperensis* indicates that it had a much longer scapular blade relative to both *D. matildae* and *W. wattsi*~~;~~ ~~however~~However, this element ~~was~~ is much more gracile in *A. cooperensis*, having a mediolaterally thin scapular blade (Figures 10 and 28). Although incomplete, the reconstructed humerus of *W. wattsi* ~~was~~ is longer than that of *D. matildae* and *S. elliottorum*, but considerably smaller with a narrower midshaft breadth for length in comparison to *A. cooperensis* (Figure 15 and 28). In mid-diaphyseal cross-sectional shape, *W. wattsi* is ovo-rectangular like *S. elliottorum*, but compared to the mediolaterally oblong and anteroposteriorly compressed *A. cooperensis* and *D. matildae* (Figure 16). The ulna of *W. wattsi* has the most robust midshaft cross-sectional shape when compared to the smaller *D. matildae* and larger *A. cooperensis* (Figure 18). The proximal olecranon process is robust, broad and rounded in both *D. matildae* (complete) and *W. wattsi* (incomplete) compared with the gracile, narrow and acute process in *A. cooperensis* (Figures 18, 19 and 28).

The femur of *A. cooperensis* differs from the femur of *D. matildae* by possessing a relatively anteroposteriorly narrower femoral shaft ~~anteroposteriorly~~, including a narrower proximal femoral head. The distal condyles of *A. cooperensis* are beveled more medially in anterior and distal aspects relative to that of *D. matildae*, and all other northern Winton Formation femora compared (Figure 24-26 and 28).

Comparison with non-Winton Formation semi-contemporaneous members of the Titanosauria worldwide (e.g. Latest Albian-early Turonian). Comparisons were not possible with the following semi-contemporaneous titanosaurian taxa due to a lack of overlap in preserved elements: *Austrosaurus mackillopi* (Poropat et al. 2017), *Sarmientosaurus musacchioi* (Martinez et al. 2016), *Drusilasaura deseadensis* (Navarrete et al. 2011), *Jiutaisaurus xidensis* (Wu et al. 2006) and *Borealosaurus wimani* (Hailu et al. 2004). In addition, comparisons were not possible due to poor preservation or a lack of detailed descriptions or figures of the overlapping elements for the following taxa: *Huanghetitan liujiaxiaensis* and *Huanghetitan*

ruyangensis (Junchang et al. 2007; You et al. 2006), *Quetecsaurus rusconii* (González Riga & David 2014) and *Choconsaurus baileywillisi* (Simón et al. 2017).

Several titanosaurians are only comparable by one or two overlapping appendicular elements, and in some cases, size differences are the clearest feature that differentiates these taxa apart. *A. cooperensis* differs from *P. stromeri* (Smith et al. 2001) and *Andesaurus delgadoi* (Mannion & Calvo 2011) by possessing a rounded proximal humeral epiphysis without a distinct proximolateral corner that meets at a right-angle. In addition, *P. stromeri* has a larger humerus with a mediolaterally narrower diaphysis. *A. delgadoi* is smaller and also has a mediolaterally narrower humeral diaphysis.

A. cooperensis ~~differs from *Argentinosaurus huinculensis* by~~ possess~~ing~~ a smaller femur compared to the specimen referred to as *Argentinosaurus huinculensis* (Bonaparte 1996). *A. cooperensis* differs from *Aegyptosaurus baharijensis* (Stromer 1932) by being larger and possessing a mediolaterally broad midshaft for both the femur and humerus. *A. cooperensis* differs from *Dongyangosaurus sinensis* by possessing a pubis that is much longer than the ischium (Junchang et al. 2008). *A. cooperensis* differs from *Ruyangosaurus giganteus* by possessing a more mediolaterally broad and robust femur relative to the long and gracile femur of *R. giganteus* (Lü et al. 2009).

A. cooperensis differs from *E. sciuttoi* (Martínez et al. 2004) by being much larger in all comparative elements (i.e. humerus, ulna, femur, pubis and ischium). *A. cooperensis* possesses a less stocky and robust humerus, a distinct interosseous ridge and an accessory ridge on the distal end of the anterolateral process of the ulna. *A. cooperensis* differs from *P. mayorum* (Carballido et al. 2017) by being much smaller in all comparative elements except for the ulna with which it is of similar length and anterior width. *A. cooperensis* lacks the dorsoventrally deep scapular blade with distinct mid-ridge of *P. mayorum*. Both the humerus and femur are more elongate in anterior outline in *P. mayorum* than in *A. cooperensis*, which is also reflected in a narrower anteroposterior, but broader mediolateral midshaft width.

A. cooperensis is morphologically similar to *E. lilloi* (Mannion & Otero 2012); however, it is larger in all comparative elements (i.e. scapula, humerus, ulna, femur and pubis). The distal epiphysis of the humerus approaches a similar cross-sectional shape, being nearly tri-lobate in distal view; however, *A. cooperensis* has a much greater mediolateral expansion of the distal epiphysis and a laterally flared ectepicondylar margin of the lateral condyle. The proximal

Comentario [MH33]: This can be stated in the Methods section.

epiphysis of the ulna in *E. lilloi* bears a similar reduction of the anterolateral and olecranon processes relative to the much longer anteromedial process; however, the radial fossa does not possess the distinct interosseous ridge ~~n~~or the distal anterolateral accessory ridge present in *A. cooperensis*. The pubes are similarly broadened anteroposteriorly along the pubic blade in both taxa. However, the iliac peduncle of *E. lilloi* is directed more anteriorly and flattened in comparison to the anterodorsally pointed peduncle of *A. cooperensis*. The distal margin of the pubic blade is broader and truncated in *E. lilloi* compared to the rounded distal blade margin in *A. cooperensis*.

Comparisons with other large-bodied titanosaurs. In addition to the above comparisons between semi-contemporaneous titanosaurs, it is also worthy to compare *A. cooperensis* with other large-bodied titanosaurs of comparable size of preserved elements. *Futalognkosaurus dukei* possesses a similar-sized humerus (1510 mm) and near similar femur (1945 mm) (Benson et al. 2014); however, morphological comparisons were not possible. The pubis and ischium can be compared (Calvo 2007) with the pubis having similar overall morphology, but differs from *A. cooperensis* by possessing a anteroposteriorly longer~~, elongated~~ iliac peduncle, and by being thicker along the dorsoventral length of the pubic blade. A lateral ridge along the mid-line of the blade is clearly visible in *F. dukei*, but not in *A. cooperensis*. A lateral ridge along the pubic blade is also present in *S. elliottorum*, and considered an autapomorphy (Poropat et al. 2016). The pubic articulation of the ischium in *F. dukei* is shorter than the long, medially curved articulation seen in *A. cooperensis*, *D. matildae*, *S. elliottorum* and *W. wattsi*.

Both *Antarctosaurus* sp~~p~~. ~~-~~and *T. eocaudata* (Juárez Valieri & Calvo 2011) possess more elongate femora with a more bulbous and anteroposteriorly thicker greater trochanter and femoral head when compared to *A. cooperensis*. *N. gonzalezparejasi* possesses a longer humerus (1760 mm) (Benson et al. 2014) and, unlike *A. cooperensis* has~~;~~ : a proximal humeral epiphysis with a distinct proximolateral corner that meets at right angles; a flattened lateral to bulbous medial humeral head profile in anterior view; a proximodistally reduced deltopectoral crest; and a narrower midshaft diaphysis (Gonzalez Riga et al. 2016). *A. sanjuanensis*'s referred humerus (D'Emic et al. 2011; Gilmore 1946) is the same~~-~~ size (1503 mm) (Benson et al. 2014), with a rounded proximal humeral epiphysis, similar to that of *A. cooperensis*. The referred ischia of *A. sanjuanensis* (Tykoski & Fiorillo 2016) are also similar to *A. cooperensis* including

Con formato: Resaltar

Con formato: Resaltar

Comentario [MH34]: This is Calvo et al. 2007. It is also wrongly cited in the Reference list.

an extensive ischial contact with its contralateral element. Unlike *A. cooperensis*, the posterodistal margin of the ischial blades ~~are~~ is directed posteriorly, past the position of the posterior margin of the iliac peduncle. The scapula of *A. sanjuanensis* possesses a central ridge along the scapular blade that is not seen in *A. cooperensis*. *D. binglingi* has a smaller femur (1770 mm) (Benson et al. 2014), but has similarly oriented distal condyles that are bevell~~l~~ed in an anterolateral to posteromedial orientation when viewed distally (You et al. 2008). *D. binglingi* differs from *A. cooperensis* by possessing a narrower diaphysis and dorsolaterally beveled distal condyles in posterior view.

D. schrani ~~is~~ has longer ~~in length of the~~ humerus (1760 mm) and femur (1910 mm) (Benson et al. 2014)~~,~~ ~~however~~However, is similar in overall appendicular morphology (Ullmann & Lacovara 2016). The scapula shares with *A. cooperensis*~~;~~: a long, straight scapular blade with subparallel dorsal and ventral margins; the absence of a central ridge of the scapular blade; and a mediolaterally thin blade. It also possesses a mediolaterally thin and gracile acromion plate. However, the acromion plate is massively expanded dorsoventrally in excess of that estimated in *A. cooperensis*. Similar to *A. cooperensis*, the humerus of *D. schrani* is proximally and distally broad across the epiphyses as well as being anteroposteriorly narrow and mediolaterally broad at the midshaft. *D. schrani* differs from *A. cooperensis* by the deltopectoral crest ~~not~~ neither reaching as far distally ~~and~~ nor possessing the distinctly tri-lobate distal epiphysis present in *A. cooperensis*. The ulna of *D. schrani* differs from *A. cooperensis* by being more robust and stocky, with near-equal anterolateral and anteromedial processes and an oblong-shaped distal epiphysis. The pubis of *D. schrani* differs from *A. cooperensis* by being considerably thicker along the pubic blade with a dorsoventrally short ischiadic peduncle. The ischium of *D. schrani* differs from *A. cooperensis* by being near-vertically oriented, with the entire dorsal surface of the ischial blade directed posteriorly. As with the pubis, the pubic peduncle is dorsoventrally short. The femur of *D. schrani* is similar to *A. cooperensis*, possessing an anteroposteriorly narrow and mediolaterally broad diaphyseal shaft that leads to mediolaterally expanded proximal and distal epiphyses. The distal epiphyses are bevell~~l~~ed in an anterolateral to posteromedial direction, a feature also seen in *D. binglingi* (You et al. 2008), *L. astibiae* (Díaz et al. 2013) and cf. *L. astibiae* (Vila et al. 2012)~~.~~. However, this feature has been considered to be taphonomic distortion in *D. schrani* created through lithostatic compression (Ullmann & Lacovara 2016).

Considered together, *A. cooperensis* possesses a mosaic of features ~~that it shares~~shared with titanosaurs with similar geographycal (Australia), and temporal range (Latest Albian to ?Turonian), as well as ~~and~~similar body-size. The previously described and comparable Australian taxa (*D. matildae*, *W. wattsi* and *S. elliottorum*) share closer morphological similarities of the pubis and ischium complex with *A. cooperensis* than they do to all other taxa compared. This observation alludes to a potential shared ancestry.

Those taxa of similar geological age or similar limb size tend to share only isolated features of each element with *A. cooperensis* but this is also observed in titanosaurs from older and younger Cretaceous sites, such as the scapular similarities seen in *Y. datangi* from the Lower Cretaceous of China, or the humeral and ischial similarities of *A. sanjuanensis* from the latest Cretaceous of North America. Such a mosaic of characteristics helps define and differentiate *A. cooperensis* from all other taxa and is especially useful in regards to those taxa found within the Winton Formation. However, ~~it is clear from~~ the mosaic of similar and different features found in this taxon, ~~derived~~ which derive from a small number of representative appendicular elements, suggests that these characteristics will not add significantly to a phylogenetic analysis of similarly incomplete and variable taxa.

Phylogenetic position. As evident in the above comparative assessment, phylogenetic analysis of *Australotitan cooperensis* would be premature until better representative skeletal remains of this taxon are available ~~of this taxon~~. However, we can consider its phylogenetic position based on comparing currently published phylogenies and the spread of characteristics hypothesized to define particular clades. The phylogenetics of titanosaurs remains in a state of flux with multiple assessments appearing in recent years investigating the relative position of taxa in a global context, covering Late Jurassic to Late Cretaceous (D'Emic 2012; González Riga et al. 2019; Gonzàlez Riga et al. 2018; Mannion et al. 2017; Mannion et al. 2013; Mannion et al. 2019a; Mannion et al. 2019b).

Based on a recent review of the appendicular skeleton of South American titanosaurs (González Riga et al. 2019) that found appendicular synapomorphies from two independent phylogenetic assessments of titanosaurs (D'Emic 2012; Mannion et al. 2013) we find the following features present in *A. cooperensis* that are considered to be synapomorphies of Titanosauria or clades

Con formato: Resaltar

Con formato: Resaltar

Comentario [MH35]: The paper of Páramo et al (2020) could help your argument.

Páramo A., Mocho P., Ortega F. 2020. Three-dimensional analysis of the titanosaurian limb skeleton: implications for systematic analysis. *Journal of Iberian Geology*.

Con formato: Resaltar

Comentario [MH36]: Also Carballido et al (2017) and Hechenleitner et al (2020)

within it: 1) The humerus length is less than 80% the femur length (= Saltasauridae) (79% for *A. cooperensis*). The length of the femur of *A. cooperensis* has been estimated in multiple different ways. Because we cannot directly confirm the length of the femur in the holotype, and with this percentage being so close to the upper limit of the expected range for saltasaurids, we treat its use as a synapomorphy for *A. cooperensis* within the Saltasauridae as dubious. 2) The humeral deltopectoral crest extends medially across the anterior face of the humerus, but this is not well developed (= Titanosauria). 3) The humeral deltopectoral crest is not expanded distally (≠ Saltasauridae). 4) Humerus with a strong posterolateral bulge around the level of the deltopectoral crest area is not well preserved or discernible in *A. cooperensis* (≠ Saltasauridae). 5) Humeral radial and ulnar condyles are undivided distally (≠ *Alamosaurus* + 'Saltasaurini'). 6) Anterior surface of the distal lateral condyle of the humerus seems to be divided by a notch in *A. cooperensis*; however, this feature is poorly defined (≠ Lithostrotia). 7) -Prominent ulnar olecranon process projecting well above proximal articulation is present in *A. cooperensis* (= Lithostrotia). 8) Anteroposterior to mediolateral width ratio of iliac articular surface of pubis is ≥2.0 (= Titanosauria). 9) Acetabular margin of ischium strongly concave in lateral view such that pubic articular surface forms a proximodorsal projection (= Titanosauria or Lithostrotia). 10) No emargination of ischium distal to pubic articulation (= Titanosauria). 11) Ratio of dorsoventral width of distal end of ischial shaft to minimum shaft dorsoventral greater than 1.5 (≠ Titanosauria). 12) Femur with longitudinal ridge on anterior face of shaft (linea intermuscularis cranialis of (Otero 2010) is preserved on the anterior face of the distal diaphysis in the holotype EMF102 and is well preserved along the entire anterior face of the referred femur in EMF105 (= *Alamosaurus* + 'Saltasaurini'). 13) Femoral distal condyles are bevell~~l~~ed 10° dorsomedially relative to shaft (= Saltasauridae) with the slightly distally projected fibular condyle that is not as exaggerated as seen in *Saltasaurus* and *Bonatitan* (González Riga et al. 2019).

Based on this assessment, *A. cooperensis* possesses a single synapomorphy of the Saltasauridae, being bevell~~l~~ed distal condyles of the femur. One character state supports and another does not support placement within the 'Saltaurini' clade (D'Emic 2012). Two character states support and one does not support placement within the Lithostrotia. Finally, four character states support and two do not support placement within the Titanosauria (Table 8). Such a mosaic of synapomorphies makes any solid phylogenetic footing equivocal.

Comentario [MH37]: So it does not count as difference with saltasaurids

Comentario [MH38]: Width?

Comentario [MH39]: Not mentioned in the results. *Uberabatitan ribeiroi* (a Aeolosaurini) also shows this feature (see Silva et al 2019, Fig. 22)

However, the distribution of the combined synapomorphic features of the appendicular skeleton recovered from two independent phylogenetic assessments of titanosauriformes (D'Emic 2012; Mannion et al. 2013) at least supports our placement of *A. cooperensis* within Titanosauria and suggests ~~some evidence~~ that it could be part of the Lithostrotia. Whether or not *A. cooperensis* is a lithostrotian ~~titanosaur,~~ or a non-lithostrotian titanosaur~~,~~ is remarkably the same situation for two other Winton Formation taxa~~,~~: *S. elliottorum* and *D. matildae* (Mannion et al. 2013; Poropat et al. 2016).

The most recent phylogenetic analyses that include the Winton Formation titanosaurs (González Riga et al. 2019; Gonzàlez Riga et al. 2018; Mannion et al. 2017; Mannion et al. 2019a; Mannion et al. 2019b) provide context for our discussion in two important ways. Firstly, there is growing support for a nearly global distribution of most titanosaurian clades by the Early Cretaceous, and by extension, titanosaurs from Cretaceous Australia could potentially represent one or more of those clades. However, there is also growing support for clades restricted to specific regions, such as Colossosauria, Rincosauria, and Lognkosauria of South America (González Riga et al. 2019). Therefore, the mosaic of features that *A. cooperensis* shares with taxa from older, semi-contemporaneous and geographically distant regions could potentially place it within any of these clades unless homoplasy has played a more significant role in the evolution of sauropod appendicular elements than previously thought (Upchurch 1998).

Secondly, the relative positions of the Australian taxa are unstable, changing position depending on the phylogenetic methodologies and taxa included within each assessment. The relative phylogenetic position of *W. wattsi* as basal to *D. matildae* has changed since the first phylogenetic assessment was undertaken (Hocknull et al. 2009) and further since the addition of *S. elliottorum* (Poropat et al. 2016). *W. wattsi* has been resolved as a non-titanosaurian somphospondylan (Hocknull et al. 2009; Poropat et al. 2015a), but has also been recovered outside of titanosauriformes (Carballido et al. 2011b); more derived than *D. matildae* (Mannion et al. 2013); within the titanosaurian 'Andesauroidea'; or sister taxon to the Titanosauria (Mannion et al. 2019a).

Over time, new phylogenetic assessments have proposed a more basal position for *D. matildae*, first falling outside of the derived Saltasauridae and then further outside Lithostrotia. *D. matildae* has variably been recovered as a derived saltasaurid (Gonzalez Riga et al. 2016; Hocknull et al. 2009; Mannion et al. 2019a; Mannion et al. 2019b; Upchurch et al. 2015); a non-

Con formato: Resaltar

Comentario [MH40]: Is also recovered whithin Titanosauria, in a politomy with *Andesaurus* and Eutitanosauria in Carballido et al (2020), and in a more disparate position in Hechenleitner et al (2020).

Carballido JL., Scheil M., Knötschke N., Sander PM. 2020. The appendicular skeleton of the dwarf macronarian sauropod *Europasaurus holgeri* from the Late Jurassic of Germany and a re-evaluation of its systematic affinities. *Journal of Systematic Palaeontology* 18:739–781.

Hechenleitner EM., Leuzinger L., Martinelli AG., Rocher S., Fiorelli LE., Taborda JRA., Salgado L. 2020. Two Late Cretaceous sauropods reveal titanosaurian dispersal across South America. *Communications Biology* 3.

lithostrotian titanosaurian (González Riga et al. 2019) with *S. elliottorum* as sister taxon (Gonzàlez Riga et al. 2018; Mannion et al. 2017; Mannion et al. 2019a; Mannion et al. 2019b; Poropat et al. 2015b); or close to *Yonglinglong* (Li et al. 2014).

With the addition of more taxa to these newer phylogenetic analyses, especially adding taxa from Asia, the once derived position of *D. matildae* (along with *S. elliottorum*), relative to *W. wattsi* has eroded. Therefore, with such instability in their relative positions, it would be premature to add a further fragmentary taxon to derive another alternative phylogeny.

Our new taxon, along with the others from the Winton Formation, ~~are~~ is unlikely to provide new phylogenetically useful data to these large-scale global analyses until the known ~~better~~ better-preserved specimens such as those currently being prepared are available (Hocknull et al. 2019; Poropat et al. 2019).

All four taxa possess appendicular elements and for those elements with overlap between at least two taxa, they allow comparison between each other and to the appendicular synapomorphies found in Titanosauria (González Riga et al. 2019). The scapulae of *D. matildae* and *W. wattsi* both possess a well-developed ventromedial process of the ventral margin (= Titanosauria) (Hocknull et al. 2009; Poropat et al. 2015a; Poropat et al. 2016; Poropat et al. 2015b) (Figures 9-10 and 28 A-C), although titanosaurian outgroup taxa, including *C. insignis* , also possess this feature (Carballido et al. 2011a; González Riga et al. 2019). The area where this feature would be found in *A. cooperensis* and *S. elliottorum* is missing.

The relative humerus to femur length of *A. cooperensis*, estimated at 79%, is less than 85% for *D. matildae*~~, h~~. However, they are both at or above the limit of this feature being a synapomorphy of Saltasauridae (i.e. less than 80%). Neither *W. wattsi* or *S. elliottorum* preserve a complete humerus and femur for comparison.

The deltopectoral crest extends medially across the anterior face of the humerus in both *A. cooperensis* and *D. matildae* (= Titanosauria) although it does not extend as far as that of derived titanosaurians like *O. skarzynskii* and *S. loricatus.* These features are missing from the preserved humeri of *W. watts* and *S. elliottorum*. Based on what is preserved of the humeri in the four Australian taxa, none of them possess a distally expanded deltopectoral crest or a strong posterolateral bulge level with the deltopectoral crest (≠ Saltasauridae). The distal humeral condyles of *A. cooperensis* and *D. matildae* are undivided (≠ *Alamosaurus* + 'Saltasaurini') and both possess a distal lateral condyle that has a divided anterior surface (≠ Lithostrotia). The

proximal and distal condyles of the humeri of *W. wattsi* and *S. elliottorum* are unknown. The midshaft cross-sectional shape of *W. wattsi* and *S. elliottorum* approximate one another by being anteroposteriorly thick, creating a rounded (ovo-rectangular) outline, whilst in *A. cooperensis* and *D. matildae*, this outline is mediolaterally broad, creating a more oblong outline.

The distal end of the radius is bevelled ~20° proximolaterally relative to the shaft in *D. matildae* (Poropat et al. 2015b) and estimated in *W. wattsi* (Poropat et al. 2015a) although the distal ends in the *W. wattsi* holotype radii are very poorly preserved (= Saltasauridae). The radius is not bevelled in *S. elliottorum* (≠ Saltasauridae), and the radius is unknown in *A. cooperensis*. A prominent olecranon process is present in *A. cooperensis* and *D. matildae* (= Lithostrotia), but is unknown in *S. elliottorum* and not preserved in *W. wattsi.* However, this feature in *W. wattsi* is likely similar to *D. matildae* (Figures 18, 19 and 28) and would then place *W. wattsi* within the Lithostrotia. The relative size of metacarpal I to metacarpal II or III is less than 1.0 in *S. elliottorum* and *D. matildae* (≠ Lithostrotia). This characteristic is not preserved in *W. wattsi* and unknown in *A. cooperensis*.

The anteroposterior length to mediolateral width of the iliac articular surface of the pubis is greater than 2.0 in both *A. cooperensis* and *D. matildae* (= Titanosauria) (Table 8). The pubis is unknown in *W. wattsi* and the iliac articulation of the pubis is missing from both sides of the pelvis of *S. elliottorum*. In *D. matildae*, *A. cooperensis* and *S. elliottorum*, the acetabular margin of the ischium is strongly concave in lateral view such that the pubic articular surface forms a proximodorsal projection (= Titanosauria or Lithostrotia). The acetabular rim of the ischium in *W. wattsi* is broken along its entire length, exposing internal cancellous bone (Figure 22). This indicates the loss of substantial bone around the acetabular rim. Therefore, the morphology of the acetabular rim cannot be accurately defined, or is questionable. The very similar shape of the ischium of all four Australian taxa suggests that the acetabular rim of *W. wattsi* could have been concave, changing this feature from a typically non-titanosaurian character state to a character state found in Titanosauria or Lithostrotia (Figure 28).

There is no emargination of the ischium distal to pubic articulation in *A. cooperensis*, *D. matildae* and *S. elliottorum* (= Titanosauria). This region of the ischium in *W. wattsi* is not preserved, being broken along the pubic articulation and medial region where the contralateral elements may have met. The ischium curves ventrally at the ~~medial broken~~broken medial margin suggesting a significant extension of ischium directed medioventrally, similar to that

observed in *S. elliottorum*. Therefore, it is possible that the ischia did meet at a symphysis with no emargination, thus a feature synapomorphic in Titanosauria. The ratio of dorsoventral width of the distal end of ischial shaft to minimum shaft dorsoventral width is greater than 1.5 in *A. cooperensis*, *S. elliottorum*, *D. matildae* and estimated to be so in *W. wattsi* (≠ Titanosauria) (Tables 8 and 9).

The femur is only known in *A. cooperensis* and *D. matildae*. The femur of *A. cooperensis* possesses a longitudinal ridge on the anterior face of shaft (linea intermuscularis cranialis (= *Alamosaurus* + 'Saltasaurini'), but this is absent in *D. matildae* (≠ *Alamosaurus* + 'Saltasaurini'). The distal condyles are bevelled 10° dorsomedially with a slightly distally projected fibular condyle, unlike that of highly derived saltasaurids (González Riga et al. 2019). Summarising the above comparative phylogenetic appraisal of the four Australian taxa by using synapomorphies derived from three independent phylogenetic character assessments (Tables 8 and 9), we find only one character-state of the sixteen, that are found in all four taxa, that is not a synapomorphy of Titanosauria. Therefore, there is support for the placement of all four Australian taxa within the Titanosauria. In the ischium, the ratio of dorsoventral (anteroposterior) width of the distal end of the shaft to the minimum shaft dorsoventral (anterior-posterior) width ~~are~~ is ~~all~~ greater than 1.5, which is not a synapomorphy of Titanosauria. The ratios for the four Australian taxa are very similar between *A. cooperensis* (1.63) and *W. wattsi* (1.64 est.), and between *D. matildae* (1.73) and *S. elliottorum* (1.74). Together, these ratios describe very similarly proportioned ischia for all four taxa, which reflects the overall similar morphology of the ischium (Figure 28). The shared similarities of the ischium, regardless of overall body-size differences and other appendicular differences, may point to a synapomorphy uniting all four Australian taxa.

Several other features are shared between the four Australian taxa and are summarised in Table 9. *W. wattsi* shares with *D. matildae* a proximal medial tuberosity of the scapular blade (Figure 9). *W. wattsi* shares with *S. elliottorum* amphicoelous anterior caudal vertebrae that bear pneumatic neural arches and zygopophyses with centra possessing dense cancellous bone (Figures 32-34). These shared features of the ischia, scapulae and caudal vertebrae have not been observed in combination with other members of the Titanosauria so could be considered synapomorphies that unit the Australian taxa. In addition, we observe that all of the known sauropod anterior and middle caudal vertebrae from the Winton Formation, both northern and

Comentario [MH41]: Table 9 would be useful at "Comparison with other Winton Formation sauropod taxa"

Comentario [MH42]: Not mentioned in results. Also present in other non-saltasaurid titanosaurians

Comentario [MH43]: This is redundant.

southern-central sites are ubiquitously amphicoelous (Figures 31-34). Although most of the isolated caudal vertebrae are not taxonomically allocated to a known Australian taxon, it is revealing that they are among the most common of the non-appendicular elements preserved in the Winton Formation, and yet all of them are amphicoelous. This, although circumstantial, one could ~~assume~~ speculate that the anterior and middle caudal vertebrae of *D. matildae* and *A. cooperensis* were likely amphicoelous. ~~This observation~~ Such hypothesis~~-~~ is supported by the presence of amphicoelous middle and distal caudal vertebrae found at the referred localities of *A. cooperensis* (EML010 and EML012) (Figure 31-34) and *D. matildae* (QML1333 / AODL127). Of note here is the lack of sauropod proceolous caudal vertebrae from the Winton Formation. Considering the global distribution of titanosaur clades by the mid-Cretaceous, and the presence of proceolous caudal vertebrae in taxa from most continents, it seems strikingly at odds with the observed amphicoelous-only caudal vertebrae from Australia.

One feature currently distinguishing the anterior caudal vertebrae of *S. elliottorum* from *W. wattsi* is the presence in *S. elliottorum* of pneumatic fossae (Poropat et al. 2016). These fossae possess pneumatic pores that lead into the centrum; however, they do not enter a camellate internal structure, instead, the internal structure of the centrum is dense cancellous bone. Dorsally, large camellate internal structures are observable in cross-section, occurring within the neural arch and zygopophyses (Figure 34). The presence in amphicoelous anterior caudal vertebrae with pneumatic fossae, pores, pneumatic neural arches and zygopophyses, along with solid cancellous centrum bone are symplesiomorphic characteristics of titanosauriformes and lithostrotian titanosaurs (Mannion et al. 2017; Mannion et al. 2013; Wedel & Taylor 2013; Whitlock et al. 2011), suggesting that the Australian taxa have uniquely retained symplesiomorphic features of the tail but derived titanosaurian to saltasaurid features of the appendicular skeleton. It would seem that all of the Australian taxa did not possess the derived proceolous caudal vertebrae of saltasauri~~n~~d titanosaurs (Zurriaguz & Cerda 2017).

Con formato: Resaltar

Recent CT scans of the anterior caudal vertebrae of *W. wattsi* reveal the presence of pneumatic camellate chambers in the neural arch and zygopophyses with dense cancellous bone within the amphicoelous anterior caudal vertebra of this taxon (REF). However, there is no clear indication of external pneumatic pores (Figure 32 and 33). Thus pneumaticity of the anterior caudal neural arch and zygopophyses paired with dense cancellous bone within the centrum is a characteristic feature now shared between *W. wattsi* and *S. elliottorum.*

The placement of *W. wattsi* within the Titanosauria is contra previous assessments that found it to be a non-titanosaurian somphospondylan (Poropat et al. 2015a). However, a more recent analysis has it occupying a position within the Titanosauria as part of the 'Andesauroidea' or as sister-taxon to the Titanosauria (Mannion et al. 2019a). We recognise the very poor state of preservation in *W. wattsi* which likely contributes to this unstable phylogenetic position, with less than 50% of the characters considered here available in the holotype. However, based on the similarities shared with the other Winton Formation taxa, we propose that *W. wattsi* should be grouped with the three other Winton Formation taxa, within Titanosauria. Refinement of the characters and scoring of the Australian taxa for each of the three separate phylogenetic assessments (D'Emic 2012; Gonzalez Riga et al. 2016; Mannion et al. 2013) along with statistical testing of an Australian clade would test this proposal and will be undertaken as new better preserved specimens come to light.

Recent support for a clade containing ~~*Diamantinasaurus*~~ *D. matildae* and ~~*Savannasaurus*~~ *S. elliottorum* has been advocated (Poropat et al. 2020). As we have demonstrated here, *Australotitan cooperensis* and ~~*Wintonotitan*~~ *W. wattsi* also show clear similarities to each other and with *D. matildae* and *S. elliottorum*. All four possess a mosaic of shared features with some possibly uniting them all in a single clade. We, therefore, expand a hypothesised Australian clade to include all four taxa.

Unfortunately, the current poor skeletal representation of these taxa creates considerable phylogenetic uncertainty, which is a ubiquitous issue across titanosaurian phylogenetics. We propose this hypothesis of relationship with caution, but also with the optimism that it will focus studies that will refine local and regional sauropod diversity first, that subsequently can lead to a better understanding of global sauropod phylogenetics and palaeobiogeography.

Body size and palaeoecology of sauropods in the Winton Formation. Regardless of their phylogenetic relationship, the presence of four recognized sauropod taxa within the Winton Formation is not unsurprising considering the diversity of sauropod taxa from similar ages and latitudes (de Jesus Faria et al. 2015). In South America, seven to nine sauropod taxa are known from the Cenomanian of Argentina, covering a geographical range of approximately 700-1000 km, similar to that between the northern and southern-central Winton Formation. However,

Comentario [MH44]: Within or a sister taxon of Titanosauria?

Comentario [MH45]: Based on the information discussed here, I think it could be better to replace "palaeoecology" with "palaeoenvironment"

proposing a framework for explanations for the diversity of the sauropods from the Winton Formation is still needed.

Firstly, there is a large difference in maximal limb element size between taxa from the northern and southern-central Winton Formation. Secondly, the relative proportions of these limb elements, as a proxy of body-height, differ when also considering pelvic width, as a proxy of body width. Thirdly, each taxon possesses a combination of features of each preserved limb that seems contrary to what would be expected.

Comentario [MH46]: This paragraph seems out of place here.

The appendicular elements of the holotype of *A. cooperensis*, in particular the humerus, ulna and femur, represent the largest appendicular bones so far recovered of any described Australian dinosaur (Figures 35 and 36) (Tables 2-7 and 10). In addition, ~~we have~~the referred fragmentary ~~remains of a~~ femur~~,~~ EMF164~~, to *A. cooperensis*, which~~ represents an even larger individual (Table 10).

An unassigned isolated large sauropod femur (QMF43302, from QML1333) represents the largest sauropod appendicular element from the northern Winton Formation (Figures 25, J-O, 26 and 35). This femur is separated into three sections, including a proximal femoral head, a ~~mediolaterally~~ mediolaterally-crushed and fragmented diaphysis, and a partial distal epiphysis that is missing the distal condyles. Preserved plant debris cover the broken and missing pieces of the proximal and distal epiphyses, indicating that this specimen underwent considerable transport and~~/or~~ abrasion prior to burial and exposure. The distal condyles were broken off and lost prior to burial, whilst the proximal head was damaged, which removed a centimeter or two of cortical bone from around the proximal articular region of the greater trochanter to the femoral head. QMF43302 measures 1505.68 mm in preserved proximodistal length, and we estimate that with the missing regions added, this would make a total length of approximately 1600 mm (Table 7). This is approximately 250+ mm shorter than the reconstructed length of EMF102 and approximately 450+ mm shorter than the estimated length of EMF164 (Table 10). Proximally, the femoral head is proportionately more robust than the femora seen in *A. cooperensis*, but similar to that seen in *D. matildae*. The anterior face of the diaphysis is heavily broken up into mosaic pieces, which obscures the ~~presence or absence of a~~identification of a longitudinal ridge on the anterior face of the shaft (linea intermuscularis cranialis), which would assist in referring the femur to *A. cooperensis* or *D. matildae*. Close inspection of the diaphyseal surface suggests that there is no sign of a ridge, which would then ally the femur closest to *D.*

matildae, noting that the femur of *W. wattsi* and *S. elliottorum* are currently unknown. An associated sauropod specimen (AODF836)~~,~~ that does not have an associated femur~~,~~ is referred to *D. matildae* (Poropat et al. 2016) and was found 250 m to the northwest of QMF43302 (at QML1333).

When the holotype femur of *D. matildae* is compared to QMF43302, it shares the straight and narrow diaphyseal shaft and bulbous proximal head, in contrast to *A. cooperensis* (Figure 35). However, ~~QMF43302,~~ when isometrically scaled to equal the minimum mediolateral width of *D. matildae*, ~~defines a~~the femoral outline of QMF43302~~that~~ is proportionately taller ~~than *D. matildae*~~ (Figure 28). Therefore, although QMF43302 is morphologically most similar to *D. matildae* in comparison to all of the southern-central Winton Formation femora described here, it remains morphologically distinct. A proportionately longer, more gracile femur would likely be reflected by a proportionately long and gracile humerus. When considering the two other possible candidate taxa that QMF43302 could be assigned to, *W. wattsi* and *S. elliottorum*, only ~~*W. wattsi*~~*the former* possesses a proportionately long and gracile humerus (Figures 15 and 28). *S. elliottorum* and *D. matildae* both have proportionately stocky and robust humeri, whilst *W. wattsi* is clearly more gracile in form. *W. wattsi* represents the largest named sauropod taxon from the northern Winton Formation, based on limb element and ischial size. Therefore, it is possible that QMF43302 represents a femur of *W. wattsi*. If true, this assignment would place *W. wattsi* close to *D. matildae* remains at QML1333, albeit not directly associated with each other.

When comparing linear measurements (preserved, reconstructed and estimated) of all of the appendicular elements for all four Cretaceous Australian taxa, *A. cooperensis* has the longest scapula, humerus, ulna, pubis and femur (Table 10). Although the ischium of *A. cooperensis* is the largest ischium based on preserved length, the ischium of *W. wattsi* holotype is near its size with a thicker blade along its preserved length. *W. wattsi* is missing the proximal articular end of the iliac peduncle, acetabular rim, and the mediodistal margin of the ischial symphysis, therefore, depending on how much of the ischium is missing, *W. wattsi* could have an ischium of the same size, if not marginally larger, than *A. cooperensis*.

The humeri and ulnae of *W. wattsi* are poorly preserved, with all elements missing either both epiphyses or when preserved, missing most of the articular surfaces. This means that the longest linear proximodistal length for these elements are underestimates of the length of the bones.

Comentario [MH47]: Associated with what?

Comentario [MH48]: You have to strongly support this. Otherwise, the following interpretation lacks any substance. I don't see the need to go that further on speculation, especially when it is not the focuss of the present investigation.

Comentario [MH49]: Already stated several times. The morphology and state of preservation of each bone are exposed and discussed above. The following paragraphs can be considerably reduced by excluding redundant information

Using the same ~~better~~ better-preserved elements in *D. matildae* as a guide, we were able to align and scale the 3-D model of *D. matildae* limb elements to that of *W. wattsi* to provide a prediction of length. The humerus of *W. wattsi* returned an estimated proximodistal length of 1253 mm whilst the ulna was estimated to measure 919 mm. The longest preserved length of ulnae is 897 mm, some 22 mm shorter than the estimate; therefore, we suspect about 20-50 mm of length has been lost of the proximal and distal epiphyses.

We also estimated the length of the humerus from *S. elliottorum* by isometrically scaling the complete 3-D model of the humerus of *D. matildae* to the preserved humerus shape of *S. elliottorum*, to return an estimated maximum length of 1112 mm. *S. elliottorum* does not preserve an ulna or femur so cannot be compared to these appendicular elements.

Considering the sizes of the best comparable elements across the four taxa in relation to columnar limb elements (i.e. humerus, ulna and femur), *A. cooperensis* represents overall the largest taxon, but more specifically the taxon with the longest limbs (Table 10). *W. wattsi* was second tallest, whilst *D. matildae* and *S. elliottorum* had the shortest limbs and most robust stature.

When comparing the overall pelvic floor between each taxon, as a proxy of body width, it is evident that *A. cooperensis* had the deepest and widest pelvis in absolute size (Figure 22) (Tables 5, 6 and 11). We cannot reconstruct the pelvis of *W. wattsi* because it is missing the pubes and the medial most portion of the ischial contact. However, the ischium is so close in size and similar in morphology to both *A. cooperensis* and *D. matildae* (Figure 28)~~,~~ that we would expect the pelvic floor to be proportiona~~te~~ly as deep as both of these taxa, ~~but~~ and, impressively, as large and as wide as that of *A. cooperensis*. *S. elliottorum* ~~does not possess the same relative depth of the pelvis as seen in *A. cooperensis*, *D. matildae* or predicted for *W. wattsi*. Instead, it is~~shows a relatively broader and shallower pelvis (Figure 28). Although this feature looks to be a real and ~~a~~ unique feature of *S. elliottorum*, there are some areas at, and below, the position of the iliac peduncles of both the pubis and ischium that may reflect vertical taphonomic compression. If so, this compression would artificially reduce the pelvic floor depth creating what would seem to be a shallow appearance in anterior or posterior views (Figure 28).

Large dorsal vertebrae from the skeleton were found directly above the puboischial complex, and the humerus and ribs show signs of directional crushing and distortion~~, t~~. Therefore, taphonomic alteration via trampling is possible thus altering the pelvic dorsoventral profile.

Each limb segment for the four taxa present~~s~~ unusual combinations that do not intuitively correspond with one another, nor can they be easily considered part of a morphocline. *A. cooperensis* is clearly the largest taxon; however, it both possesses the most lightly built and gracile scapula, ulna and puboischial complex, but with massive and solidly built humeri and femora. *W. wattsi* is the second largest taxon with the most solidly built scapulae and ischia, with most robust ulnae in midshaft cross-section, but ~~with~~ the least rotund humeri. *D. matildae* and *S. elliottorum* both possess equally stocky humeri and *D. matildae* the stockiest ulnae. However, *S. elliottorum* possesses a very broad, shallow and lightly built, but completely fused puboischial complex.

~~These~~ This somewhat contrary mosaic of characteristics for each taxon impedes explanations of adaptative ecology or as part of a morphocline. Whether or not these features represent adaptations of body-size, sexual dimorphism, locomotion, habitat (terrestrial versus semi-aquatic) and/or feeding strategies, are all areas of potential explanation, but are all equally confounded by a lack of phylogenetic, temporal and environmental ~~context~~resolution. Simplistic explanations using modern ecological analogies ~~simply~~ cannot be argued for any of the Winton Formation sauropod taxa without a detailed understanding of the environmental context in which each taxon lived, which is severely lacking at present.

The very poor stratigraphic and temporal context of the Australian sauropod type localities as discussed above ~~in the Geological Settings~~ means that we cannot easily explain the taxonomic diversity in a temporal context. However, based on our current understanding of the relative stratigraphic positions of the sauropod taxa within the Winton Formation, *D. matildae* occurs in the northern Winton Formation close to the base of the ~~Winton Formation~~unit (<100 m) up to at least 350 m ~~within the Winton Formation~~, which is close to a third of the total ~~Winton Formation~~ thickness (~1100 m). *W. wattsi* may also be present close to the base of the Winton Formation (<100 m), but this identification is tenuous. It does also occur at a ~~similar~~ greater height, similar to *D. matildae*, suggesting that these two taxa co-occurred throughout the basal 350 m of the northern Winton Formation. *S. elliottorum* currently only occurs from a single site within 100 m of the northern Winton Formation base, whilst *A. cooperensis* is only known from sites that occur between 270-300 m of the southern-central Winton Formation base. It is therefore unlikely that all four taxa represent a single chronocline, with some evidence for three taxa co-occurring during the deposition of the basal 100 m of the northern Winton Formation.

However, there is no definitive evidence demonstrating that any of the taxa were truly sympatric, with no single site demonstrably showing more than one taxon in a single bonebed. Therefore, we cannot definitively place these taxa together with each other at any singular place or time.

The distinctive taphonomic differences observed between sites in the northern and southern-central Winton Formation may provide some clues to palaeoenvironmental differences that could have created enough difference in habitat to select for varying types of megaherbivorous sauropods. The absence of abundant or diverse aquatic fauna, in particular, freshwater insect larvae, freshwater bivalves and snails, crustaceans, fish, lungfish and crocodilians along with the presence of scoured and highly trampled silty-muddy surfaces absent of developed palaeosols, ~~indicates~~ suggests a highly labile sedimentary and turbid aquatic environment in the southern-central Winton Formation sites, compared to the northern Winton Formation sites. These observed differences could be geochronological, but note the caution we discuss above. If geochronological, the differences could represent a succession of palaeoenvironmental changes as the basin fills, with the reduction of topographic relief and development of new freshwater environments with areas terraformed by the largest of the sauropod taxa. If the sites are contemporaneous, then these differences could be due to regional hydroclimatic differences, perhaps relating to the distance of the southern-central Winton Formation environments from the topographically higher watershed to the east.

The greater diversity of flora and aquatic fauna in the northern Winton Formation points to a less turbid and more stable habitat with a greater diversity of vegetation ~~structure~~. The proximity of the northern Winton Formation sites to a greater diversity of older terrestrial (stable) terrains provides another source of geographical diversity that would have likely been a source of biological diversity proximal to the northern Winton Formation and distal to the southern-central Winton Formation sites (Harrington et al. 2019).

We speculate that a spatiotemporal ecocline developed from east to west, from the eastern basin periphery (drainage topographic high) to the center. The basin rapidly filled with volcanoclastic input from the east and transitioned from low terrestrial vegetation productivity (e.g. shallow / coastal marine habitats) to highly productive habitats (e.g. paralic to fluvial and lacustrine environments). Such labile and frequently disturbed environments were likely further disturbed by the sauropods themselves, and this was set within a backdrop of variable or seasonal local

climate (Fletcher et al. 2018) and major mid-Cretaceous global climatic fluctuations (Hay 2011) associated with volcanism (Percival et al. 2020). The combination of frequent disturbance with climatic variability and instability has been proposed as a mechanism that maintained megaherbivore diversity of Quaternary megafauna (Mann et al. 2018).

Body size of *Australotitan cooperensis*. Body mass estimation is a fraught exercise for fragmentary skeletons (Bates et al. 2015; Bates et al. 2009; Bates et al. 2016; Campione & Evans 2012; Campione & Evans 2020; Paul 2019). Recent body mass estimates of giant sauropods (Carballido et al. 2017; Lacovara et al. 2014) using humeral and femoral circumferences (Benson et al. 2014; Campione & Evans 2012; Campione & Evans 2020) have come under scrutiny and are shown to be implausible or inaccurate (Bates et al. 2015; Paul 2019). However, a recent review of these inaccuracies ~~have~~ has suggested that the estimation methods themselves can be reconciled, albeit with reservations when dealing with particular groups of tetrapods, like giant sauropods (Campione & Evans 2020). Therefore, although it is tempting to produce an estimate of body mass for *A. cooperensis* based on the preserved and reconstructed stylopodial circumferences we ~~feel~~ consider that this will not add significant interpretative value to our main purpose of describing and comparing this taxon to other members of the Titanosauria from the Winton Formation and semi-contemporaneous faunas. Based on limb-size, a feature that is easily comparable, we can compare *A. cooperensis* to other sauropods of similar size globally. This is useful because *A. cooperensis* represents the first osteological evidence of a very large titanosaur in Australia of comparable size to taxa from other parts of the Gondwanan supercontinent. We used the limb element sizes provided in (Benson et al. 2014) for our comparisons to *A. cooperensis*.

Humerus and femur lengths, along with humerus and femur circumferences from known taxa were plotted against the type specimen of *A. cooperensis* (EMF102) to see where this new Australian taxon falls in regards to the largest sauropods known from femora and humeri (Figure 36). In a comparison of humerus length with circumference (Figure 36, A), *A. cooperensis* clusters with *D. schrani*, *P. mayorum*, *P. stromeri* and *N. gonzalezparejasi*. In comparison of femoral length with femoral circumference (Figure 36, B), *A. cooperensis* clusters with *D. schrani* and *Brachiosaurus altithorax*. In comparison of femoral length with humeral length (Figure 36, C), *A. cooperensis* clusters with *Futalognkosaurus dukei*.

Comentario [MH50]: A "Body size estimation and comparison" in Methods section would simplify reading this part of the discussion

Comentario [MH51]: See also the discussion in Otero et al (2020).

Otero A., Carballido JL., Pérez Moreno A. 2020. The appendicular osteology of Patagotitan mayorum (Dinosauria, Sauropoda). *Journal of vertebrate Paleontology* 40:1–19.

Comentario [MH52]: This paragraph should be part of the Results.

Considering the larger referred femur (EMF164), our estimated femur length of this individual 2146 mm, which would confirm the limb element size of *A. cooperensis* close to *D. schrani* and *F. dukei*, but smaller than *P. mayorum*. Body mass estimates for these two titanosaurs vary considerably, from the minimum estimate for *F. dukei* of 23601 kg to the maximum estimate for *D. schrani* of 74487 kg (Campione & Evans 2020). This reflects the uncertainty discussed above and thus demonstrates the issues relating to body mass estimation in extremely large tetrapods.

Conclusions

A new dinosaurian fossil field from the southern-central Winton Formation (Eromanga Basin) has yielded a new giant titanosaurian sauropod, *Australotitan cooperensis*. It represents the largest dinosaur yet known ~~from osteological remains~~ in Australia and confirms the presence of gigantic titanosaurian sauropods in eastern Gondwana during the mid-Cretaceous. The currently described Winton Formation sauropod taxa share with titanosaurians from across the globe a highly fragmentary nature, which creates considerable ambiguity when searching for well-supported phylogenetic placement of each taxon or providing useful explanations for morphological and taxonomic diversity.

The creation of 3-D surface models from specimens has allowed the development of a coloured schematic as a new method for annotating directly onto the bones where features are not easily distinguished. In addition, the use of a range of 3-D alignment and rendering modes offers better geometric comparison whilst allowing the identification of taphonomic ~~and preservation and deformation variations~~biases. These interpretations of taphonomic alteration and preservation are essential for successive morphological interpretations~~, t~~. Therefore, they need to be captured and communicated in 3-D on the digital models created. This will also allow these interpretations to be tested, re-interpreted, and new versions to be published in subsequent research. We see this method as providing a pathway to share all forms of interpretation undertaken on specimens within the context of a 3-D geometric replica of the original.

~~Taking~~ In a comparative approach, we used previously identified synapomorphic features of the appendicular skeleton and found that all four taxa could be classified as members of the Titanosauria and possibly as basal members of it, or as basal lithostrotians. Focusing on the shared preserved elements for the Winton Formation taxa, we ~~find~~ found a mosaic of

Comentario [MH53]: Is there a more specific word, such as locality or quarry site?

characteristics that differentiate them from each other and from taxa elsewhere. We also find a mosaic of appendicular features that are shared across titanosaurs of similar size or semi-contemporaneous age, indicating that the appendicular skeleton is useful for taxonomic differentiation, but perhaps not as useful in reconciling more granular phylogenetic placements. Other characteristics that are shared between the Winton Formation sauropod taxa; such as the shared morphology of the ischium in *A. cooperensis*, *D. matildae* and *W. wattsi*; shared pneumatic anterior caudal vertebrae in *S. elliottorum* and *W. wattsi*; and ubiquitous presence of amphicoelous caudal vertebrae from described and undescribed specimens allude to a shared common ancestry for all of the Winton Formation taxa. We, therefore, propose a hypothesis of common ancestry for all four taxa, as a single clade, occurring in Australia during the mid-Cretaceous.

Perhaps these taxa represent a radiation of sauropods adapting to new~~ly created~~ and rapidly changing environments through frequent disturbance, as the Winton Formation developed across the massive Eromanga Basin. As it transitioned from paralic through to alluvial and lacustrine habitats during a period of global climatic change (REFS), local and regional differences were accentuated, evolving a variety of megaherbivores to occupy these newly productive habitats. Alternatively, the taxa may reflect a complex morphocline or ecocline across variable environments already established across the basin during the Cenomanian. ~~We feel that the current stratigraphic occurrences likely rule out a chronocline, but we cannot prove sympatry for any of the sauropod taxa as yet.~~ Future research should focus on building greater detail of the local stratigraphic and palaeoenvironmental context, for both previous and new sites, because until this is achieved, phylogenetic position alone will be of limited interpretative value.

Con formato: Resaltar

Comentario [MH54]: Barely explored in the discussion

Acknowledgements

We acknowledge and pay respect to the Wangkumura and Boonthamurra People on whose traditional lands these dinosaurs were discovered. We thank Wangkumura elder, Malcolm Ebsworth for his assistance and guidance during the fieldwork on Plevna Downs Station. We would like to acknowledge those who first contributed to this work, both in the field and laboratory, including, Joanne Wilkinson, Kristen Spring, Elizabeth Cannon, Jo Pegler, Scott

Turner, Alex Cook, Ralph Molnar, Paul Sereno and the Mackenzie family, in particular Sandy (jnr) Mackenzie who found the first dinosaur bone.

We thank all of the volunteers and supporters of the Queensland Museum and Eromanga Natural History Museum who have made significant contributions in the field and laboratory: Jim Macmillan, Maxine Macmillan, Stephen Tully, Annabel Tully, Tom Meakin, Janine Meakin, Scott Pegler, Denise O'Boyle, Jill Corrigan, June Gunn, Doug Miller, June Richardson, Joan Rasmussen, Angelica Wilson, Maria Zammitt, Graham Wilson, Clare Steele, Phil Wharton, Ursula Wharton, Jacki Erickson, Corey Richards, Laurie Beirne, Liz Towns, Pam Towns, Keith McGlashin, Pat Turner, Geoff Turner, Nan Mackenzie, Sandy (snr) Mackenzie, Jonathan Cramb, Susan Rigby, Noel Cannon, Wendy Groves, Kimberley Smith, Tanya Hudson, Louise McGowan, the Skinner family, and the Eromanga & Quilpie Communities. We thank Nikki Newman and Queensland X-Ray for CT scanning the specimens described here. We thank Kristen Spring (QM), Trish Sloan and David Elliott (AAOD) for access to specimens for comparative purposes. SAH thanks Adamm Yates for his assistance with Winton Formation fossils from the Northern Territory.

Funding Statement – Field work, preparation and digital capture and processing was supported by Eromanga Natural History Museum, Outback Gondwana Foundation, Santos, Eromanga Earth Moving, Bill Pegler, Eromanga Contracting, IOR and Eagle Gallery, Queensland Museum, Queensland Museum Foundation, Project DIG and ARC Linkage Grant LP100100339.

References

Allen CM, and Campbell IH. 2012. Identification and elimination of a matrix-induced systematic error in LA–ICP–MS 206Pb/238U dating of zircon. *Chemical Geology* 332-333:157-165. 10.1016/j.chemgeo.2012.09.038

Almond CS. 1983. Stratigraphic Drilling Report - GSQ Eromanga 1. *Queensland Government Mining Journal* 84:358-368.

Andersen T, Elburg MA, and Magwaza BNJE-SR. 2019. Sources of bias in detrital zircon geochronology: Discordance, concealed lead loss and common lead correction. 197:102899.
Balfe PE. 1978. Stratigraphic Drilling Report - Manuka 1. *Queensland Government Mining Journal* 70:258-269.
Bates KT, Falkingham PL, Macaulay S, Brassey C, and Maidment SC. 2015. Downsizing a giant: re-evaluating *Dreadnoughtus* body mass. *Biol Lett* 11:20150215. 10.1098/rsbl.2015.0215
Bates KT, Falkingham PL, Rarity F, Hodgetts D, Purslow A, and Manning PL. 2010. Application of high-resolution laser scanning and photogrammetric techniques to data acquisition, analysis and interpretation in palaeontology. *Int Arch Photogramm Remote Sens Spat Inf Sci* 38.
Bates KT, Manning PL, Hodgetts D, and Sellers WI. 2009. Estimating mass properties of dinosaurs using laser imaging and 3D computer modelling. *PLoS One* 4:e4532. 10.1371/journal.pone.0004532
Bates KT, Mannion PD, Falkingham PL, Brusatte SL, Hutchinson JR, Otero A, Sellers WI, Sullivan C, Stevens KA, and Allen V. 2016. Temporal and phylogenetic evolution of the sauropod dinosaur body plan. *R Soc Open Sci* 3:150636. 10.1098/rsos.150636
Behrensmeyer AK. 1978. Taphonomic and ecologic information from bone weathering. *Paleobiology* 4:150-162.
Bell PR, Brougham T, Herne MC, Frauenfelder T, and Smith ET. 2019a. *Fostoria dhimbangunmal*, gen. et sp. nov., a new iguanodontian (Dinosauria, Ornithopoda) from the mid-Cretaceous of Lightning Ridge, New South Wales, Australia. *Journal of Vertebrate Paleontology*:e1564757.
Bell PR, Fanti F, Hart LJ, Milan LA, Craven SJ, Brougham T, and Smith E. 2019b. Revised geology, age, and vertebrate diversity of the dinosaur-bearing Griman Creek Formation (Cenomanian), Lightning Ridge, New South Wales, Australia. *Palaeogeography, Palaeoclimatology, Palaeoecology* 514:655-671.
Bell PR, Herne MC, Brougham T, and Smith ET. 2018. Ornithopod diversity in the Griman Creek Formation (Cenomanian), New South Wales, Australia. *PeerJ* 6:e6008.
Benson RB, Campione NE, Carrano MT, Mannion PD, Sullivan C, Upchurch P, and Evans DC. 2014. Rates of dinosaur body mass evolution indicate 170 million years of sustained ecological innovation on the avian stem lineage. *PLoS Biol* 12:e1001853. 10.1371/journal.pbio.1001853
Berrell RW, Alvarado-Ortega J, Yabumoto Y, and Salisbury SW. 2014. The first record of the ichthyodectiform fish *Cladocyclus* from eastern Gondwana: a new species from the Lower Cretaceous of Queensland, Australia. *Acta Palaeontologica Polonica* 59:903-920.
Bitelli G, Rinaudo F, Gonzalez-Aguilera D, and Grussenmeyer P. 2020. *Data Acquisition and Processing in Cultural Heritage*: ISPRS International Journal of Geo-Information.
Bonaparte J. 1996. Cretaceous tetrapods of Argentina. *Münch Geowis Abhand* 30:73-130.
Bonnan MF. 2007. Linear and geometric morphometric analysis of long bone scaling patterns in Jurassic neosauropod dinosaurs: their functional and paleobiological implications. *Anat Rec (Hoboken)* 290:1089-1111. 10.1002/ar.20578
Bonnan MFJP. 2004. Morphometric analysis of humerus and femur shape in Morrison sauropods: implications for functional morphology and paleobiology. 30:444-470.
Boothby P. 1989. DIO Navalla 1 Well Completion Report. Delhi Petroleum Pty Ltd. Report CR 20109. Brisbane, Queensland: Department of Natural Resources and Mines Queensland
Borsuk-Bialynicka M. 1977. A new camarasaurid sauropod *Opisthocoelicaudia skarzynskii* gen. n., sp. n. from the Upper Cretaceous of Mongolia. *Palaeontologia Polonica* 37:5-64.
Brecko J, and Mathys A. 2020. Handbook of best practice and standards for 2D+ and 3D imaging of natural history collections. *European Journal of Taxonomy* 623:1–115. https://doi.org/10.5852/ejt.2020.623
Britt BB, Eberth DA, Scheetz RD, Greenhalgh BW, and Stadtman KL. 2009. Taphonomy of debris-flow hosted dinosaur bonebeds at Dalton Wells, Utah (Lower Cretaceous, Cedar Mountain Formation,

USA). *Palaeogeography, Palaeoclimatology, Palaeoecology* 280:1-22. 10.1016/j.palaeo.2009.06.004
Bryan SE, Cook A, Allen CM, Siegel C, Purdy D, Greentree J, and Uysal T. 2012. Early-mid Cretaceous tectonic evolution of eastern Gondwana: from silicic LIP magmatism to continental rupture. *Episodes* 35:142-152.
Callieri M, Ranzuglia G, Dellepiane M, Cignoni P, and Scopigno RJCAQMA. 2012. Meshlab as a complete open tool for the integration of photos and colour with high-resolution 3D geometry data.406-416.
Calvo JO. 2007. Anatomy of *Futalognkosaurus dukei* Calvo, Porfiri, González Riga & Kellner, 2007 (Dinosauria, Titanosauridae) from the Neuquén Group (Late Cretaceous), Patagonia, Argentina. *Arquivos do Museu Nacional, Rio de Janeiro* 65:511-526.
Calvo JO, González-Riga BJ, and Porfiri JD. 2007. A New Titanosaur Sauropod From The Late Cretaceous Of Neuquén, Patagonia, Argentina. *Arquivos do Museu Nacional, Rio de Janeiro* 65:485-504.
Calvo JO, and González Riga BJ. 2003. *Rinconsaurus caudamirus* gen. et sp. nov., a new titanosaurid (Dinosauria, Sauropoda) from the Late Cretaceous of Patagonia, Argentina. *Revista geológica de Chile* 30:333-353.
Campione NE, and Evans DC. 2012. A universal scaling relationship between body mass and proximal limb bone dimensions in quadrupedal terrestrial tetrapods. *BMC Biol* 10:60. doi:10.1186/1741-7007-10-60
Campione NE, and Evans DC. 2020. The accuracy and precision of body mass estimation in non-avian dinosaurs. *Biol Rev Camb Philos Soc* 95:1759-1797. 10.1111/brv.12638
Carballido JL, Pol D, Cerda I, and Salgado L. 2011a. The osteology of *Chubutisaurus insignis* del Corro, 1975 (Dinosauria: Neosauropoda) from the 'middle'Cretaceous of central Patagonia, Argentina. *Journal of Vertebrate Paleontology* 31:93-110.
Carballido JL, Pol D, Otero A, Cerda IA, Salgado L, Garrido AC, Ramezani J, Cuneo NR, and Krause JM. 2017. A new giant titanosaur sheds light on body mass evolution among sauropod dinosaurs. *Proc Biol Sci* 284. 10.1098/rspb.2017.1219
Carballido JL, Rauhut OWM, Pol D, and Salgado L. 2011b. Osteology and phylogenetic relationships of *Tehuelchesaurus benitezii* (Dinosauria, Sauropoda) from the Upper Jurassic of Patagonia. *Zoological Journal of the Linnean Society* 163:605-662. 10.1111/j.1096-3642.2011.00723.x
Cignoni P, Callieri M, Corsini M, Dellepiane M, Ganovelli F, and Ranzuglia G. 2008. Meshlab: an open-source mesh processing tool. Eurographics Italian chapter conference. p 129-136.
Cignoni P, Montani C, Rocchini C, Scopigno R, and Tarini MJTVC. 1999. Preserving attribute values on simplified meshes by resampling detail textures. 15:519-539.
Cignoni P, Rocchini C, and Scopigno R. 1998. Metro: measuring error on simplified surfaces. Computer graphics forum: Wiley Online Library. p 167-174.
Cook A. 2005. First record of fossil freshwater gastropods within the Winton Formation. *Memoirs of the Queensland Museum* 51:406.
Cook AG, and Jell JS. 2013. Paleogene and Neogene. In: Jell PA, ed. *Geology of Queensland*. Brisbane, Queensland: Geological Survey of Queensland., 577-652.
Cook AG, McKellar JL, and Draper JJ. 2013. Post-orogenic Mesozoic basins and magmatism. In: Jell PA, ed. *Geology of Queensland*. Brisbane, Queensland: Geological Survey of Queensland, 515-576.
Coote SM. 1987. GSQ Blackall 2 - Preliminary Lithological and Composite Log. In: Queensland GSo, editor. Brisbane: Queensland Government.
Coutts DS, Matthews WA, and Hubbard SM. 2019. Assessment of widely used methods to derive depositional ages from detrital zircon populations. *Geoscience Frontiers*. 10.1016/j.gsf.2018.11.002

Curry Rogers K. 2009. The postcranial osteology of *Rapetosaurus krausei* (Sauropoda: Titanosauria) from the Late Cretaceous of Madagascar. *Journal of Vertebrate Paleontology* 29:1046-1086. 10.1671/039.029.0432

D'Emic MD. 2012. The early evolution of titanosauriform sauropod dinosaurs. *Zoological Journal of the Linnean Society* 166:624-671. 10.1111/j.1096-3642.2012.00853.x

D'Emic MD, Wilson JA, and Williamson TE. 2011. A sauropod dinosaur pes from the latest Cretaceous of North America and the validity of *Alamosaurus sanjuanensis* (Sauropoda, Titanosauria). *Journal of Vertebrate Paleontology* 31:1072-1079. 10.1080/02724634.2011.595856

Day RW, Whitaker WG, Murray CG, Wilson IH, and Grimes KG. 1983. Queensland Geology. A companion volume to the 1:2 500 000 scale geological map (1975). *Geological Survey of Queensland* Publication 383.

de Jesus Faria CC, Riga BG, dos Anjos Candeiro CR, da Silva Marinho T, David LO, Simbras FM, Castanho RB, Muniz FP, and Gomes da Costa Pereira PVL. 2015. Cretaceous sauropod diversity and taxonomic succession in South America. *Journal of South American Earth Sciences* 61:154-163. 10.1016/j.jsames.2014.11.008

Delhi Petroleum PL. 1966. Delhi-Santos Mt Howitt 1 Well Report. In: Queensland GSo, editor. Brisbane: Queensland Government.

Delhi Petroleum PL. 1991. 1990 Oxley Seismic Survey ATP 259 Queensland Final Report. Delhi Petroleum Pty Ltd. Report CR 23106 Brisbane, Queensland: Department of Natural Resources and Mines Queensland.

Dettmann ME, Clifford HT, and Peters M. 2009. *Lovellea wintonensis* gen. et sp. nov.- Early Cretaceous (late Albian), anatomically preserved, angiospermous flowers and fruits from the Winton Formation, western Queensland, Australia. *Cretaceous Research* 30:339-355. 10.1016/j.cretres.2008.07.015

Díaz VD. 2013. Revisión del dinosaurio saurópodo lirainosaurus astibiae (titanosauria) del cretácico superior de la península ibérica: comparación con otros titanosaurios del suroeste de europa. Hipótesis filogenéti. Universidad del País Vasco-Euskal Herriko Unibertsitatea.

Díaz VD, Suberbiola XP, and Sanz JL. 2013. Appendicular skeleton and dermal armour of the Late Cretaceous titanosaur *Lirainosaurus astibiae* (Dinosauria: Sauropoda) from Spain. *Palaeontologia Electronica* 16:1-18.

Draper JJ. 2002. *Geology of the Cooper and Eromanga basins, Queensland*: Department of Natural Resources and Mines.

Elliott D. 2004. In the name of Science. *Australian Age of Dinosaurs*:33-41.

Elliott D, and Cook A. 2004. A Bug's Life. *Australian Age of Dinosaurs*:13.

Espurt N, Callot JP, Totterdell J, Struckmeyer H, and Vially R. 2009. Interactions between continental breakup dynamics and large- scale delta system evolution: Insights from the Cretaceous Ceduna delta system, Bight Basin, Southern Australian margin. *Tectonics* 28.

Exoma Energy PL. 2013. Wardoo 1 Well Completion Report. In: Queensland GSo, editor. Brisbane: Queensland Government.

Exon NF, and Senior BR. 1976. The Cretaceous of the Eromanga and Surat Basins. *BMR Journal of Australian Geology and Geophysics* 1:33-50.

Faggotter S, Salisbury S, and Yabumoto Y. 2007. A new possible haleocomorph fish from the mid-Cretaceous (Albian-Cenomanian) Winton Formation of Isisford, central-western Queensland, Australia. 11th Conference on Australian Vertebrate Evolution, Palaeontology and Systematics, 2007: Geological Society of Australia. p 55-55.

Falkingham PL. 2012. Acquisition of high resolution three-dimensional models using free, open-source, photogrammetric software. *Palaeontologia Electronica* 15:15.

Filippi LS, García RA, and Garrido AC. 2011. A new titanosaur sauropod dinosaur from the Upper Cretaceous of North Patagonia, Argentina. *Acta Palaeontologica Polonica* 56:505-520. 10.4202/app.2010.0019

Finlayson B. 1984. 1983-4 Gray Seismic Survey ATP 259 Queensland Final Report. Delhi Petroleum Pty Ltd. Report CR 15494. Brisbane, Queensland: Department of Natural Resources and Mines Queensland.

Fletcher TL, Moss PT, and Salisbury SW. 2018. The palaeoenvironment of the Upper Cretaceous (Cenomanian–Turonian) portion of the Winton Formation, Queensland, Australia. *PeerJ* 6:e5513. 10.7717/peerj.5513

Fletcher TL, and Salisbury SW. 2014. Probable oribatid mite (Acari: Oribatida) tunnels and faecal pellets in silicified conifer wood from the Upper Cretaceous (Cenomanian–Turonian) portion of the Winton Formation, central-western Queensland, Australia. *Alcheringa: An Australasian Journal of Palaeontology* 38:541-545.

Flynn MJ. 1985. 1984 Brahe Seismic Survey ATP 259 Queensland Final Report. Delhi Petroleum Pty Ltd. Report CR 16024 Brisbane, Queensland: Department of Natural Resources and Mines Queensland.

Forbes BG. 1966. The geology of the Marree 1:250 000 map area. *South Australia Geological Survey, Report of Investigations* 28.

Gallina PA, and Apesteguía S. 2015. Postcranial anatomy of *Bonitasaura salgadoi* (Sauropoda, Titanosauria) from the Late Cretaceous of Patagonia. *Journal of Vertebrate Paleontology* 35:e924957. 10.1080/02724634.2014.924957

Garrad D, and Russel T. 2014. Petroleum Geology and Prospectivity of ATP 927 Cooper-Eromanga Basin, SW Queensland including the Interpretation of 2014 Reprocessed 2D Seismic Data. Real Energy Queensland Pty Ltd. Report CR 88747. Brisbane, Queensland: Department of Natural Resources and Mines Queensland.

Gauld T. 1981. DIO Wareena 1 Well Completion Report. Delhi Petroleum Pty Ltd. CR 9549. Brisbane, Queensland: Department of Natural Resources and Mines Queensland.

Gilmore CW. 1946. *Reptilian fauna of the North Horn Formation of central Utah*: US Government Printing Office.

Girardeau-Montaut D. 2016. CloudCompare. EDF R&D Telecom ParisTech.

Gomani EM. 2005. Sauropod Dinosaurs from the Early Cretaceous of Malawi, Africa. *Palaeontologia Electronica* 8:1-37.

González Riga BJ, and Astini RA. 2007. Preservation of large titanosaur sauropods in overbank fluvial facies: A case study in the Cretaceous of Argentina. *Journal of South American Earth Sciences* 23:290-303. 10.1016/j.jsames.2007.02.005

González Riga BJ, and David LO. 2014. A new titanosaur (Dinosauria, Sauropoda) from the Upper Cretaceous (Cerro Lisandro Formation) of Mendoza Province, Argentina. *Ameghiniana* 51:3-25. 10.5710/amegh.26.12.1013.1889

Gonzalez Riga BJ, Lamanna MC, Ortiz David LD, Calvo JO, and Coria JP. 2016. A gigantic new dinosaur from Argentina and the evolution of the sauropod hind foot. *Sci Rep* 6:19165. 10.1038/srep19165

González Riga BJ, Lamanna MC, Otero A, David LDO, Kellner AWA, and Ibiricu LM. 2019. An overview of the appendicular skeletal anatomy of South American titanosaurian sauropods, with definition of a newly recognized clade. *An Acad Bras Cienc* 91.

Gonzàlez Riga BJ, Mannion PD, Poropat SF, Ortiz David LD, and Coria JP. 2018. Osteology of the Late Cretaceous Argentinean sauropod dinosaur *Mendozasaurus neguyelap*: implications for basal titanosaur relationships. *Zoological Journal of the Linnean Society* 184:136-181. 10.1093/zoolinnean/zlx103

Grant C, and Blackmore A. 1991. Self mulching behavior in clay soils-Its definition and measurement. *Soil Research* 29:155-173.

Gray ARG, McKillop M, and McKellar JL. 2002. Eromanga Basin Stratigraphy. . In: Draper JJ, ed. *Geology of the Cooper and Eromanga Basins, Queensland*. Brisbane, Queensland: Queensland Department of Natural Resources and Mines., 55.

Greentree J. 2011. Palaeoenvironmental setting of dinosaur trackways in the context of the closing stages of Eromanga Basin evolution Honours Honours. Queensland University of Technology.
Hailu Y, Qiang J, Lamanna MC, Jinglu L, and Yinxian L. 2004. A titanosaurian sauropod dinosaur with opisthocoelous caudal vertebrae from the early Late Cretaceous of Liaoning Province, China. *Acta Geologica Sinica* 78:907-911.
Hall LS, Hill, A., Troup, A., Korsch, R., Radke, B., Nicoll, R. S., Palu, T., Wang, L. & Stacey, A. 2015. Cooper Basin Architecture and Lithofacies: Regional Hydrocarbon Prospectivity of the Cooper Basin, Part 1. Canberra: Geoscience Australia.
Harrington L, Zahirovic S, Salles T, Braz C, and Müller RD. 2019. Tectonic, geodynamic and surface process driving forces of Australia's paleogeography since the Jurassic. In: Keep M, and Moss SJ, editors. The Sedimentary Basins of Western Australia V: Proceedings of the Petroleum Exploration Society of Australia Symposium. Perth, WA. p 29.
Harris JD. 2007. The appendicular skeleton of *Suuwassea emilieae* (Sauropoda: Flagellicaudata) from the Upper Jurassic Morrison Formation of Montana (USA). *Geobios* 40:501-522. 10.1016/j.geobios.2006.02.002
Hay WW. 2011. Can humans force a return to a 'Cretaceous' climate? *Sedimentary Geology* 235:5-26. 10.1016/j.sedgeo.2010.04.015
Helby R, Morgan RP, and Partridge AD. 1987. A palynological zonation of the Australian Mesozoic. *Association of Australasian Palaeontologists Memoir* 4:1-94.
Herne MC, Nair JP, Evans AR, and Tait AM. 2019. New small-bodied ornithopods (Dinosauria, Neornithischia) from the Early Cretaceous Wonthaggi Formation (Strzelecki Group) of the Australian-Antarctic rift system, with revision of Qantassaurus intrepidus Rich and Vickers-Rich, 1999. *Journal of Paleontology* 93:543-584.
Herne MC, Tait AM, Weisbecker V, Hall M, Nair JP, Cleeland M, and Salisbury SW. 2018. A new small-bodied ornithopod (Dinosauria, Ornithischia) from a deep, high-energy Early Cretaceous river of the Australian–Antarctic rift system. *PeerJ* 5:e4113.
Hocknull S. 1997. Cretaceous freshwater bivalves from Queensland. *Memoirs of the Queensland Museum* 42:223-226.
Hocknull S. 2000. Mesozoic freshwater and estuarine bivalves from Australia. *Memoirs of the Queensland Museum* 45:405-426.
Hocknull S. 2005. Poor Wally. *Australian Age of Dinosaurs Museum of Natural History* 3:66-83.
Hocknull S, and Cook A. 2008. Hypsilophodontid (Dinosauria: Ornithischia) from latest Albian, Winton Formation, central Queensland. *Memoirs of the Queensland Museum* 52:212.
Hocknull SA, Lewis R, Arnold LJ, Pietsch T, Joannes-Boyau R, Price GJ, Moss P, Wood R, Dosseto A, and Louys J. 2020. Extinction of eastern Sahul megafauna coincides with sustained environmental deterioration. *Nat Commun* 11:1-14.
Hocknull SA, White MA, Tischler TR, Cook AG, Calleja ND, Sloan T, and Elliott DA. 2009. New Mid-Cretaceous (Latest Albian) Dinosaurs from Winton, Queensland, Australia (New Australian Dinosaurs). *PLoS One* 4:e6190. 10.1371/journal.pone.0006190
Hocknull SA, Wilkinson M, Lawrence RA, Newman N, and R. M. 2019. On the shoulders of titans: Introducing new Cretaceous dinosaur fossil fields from southwest Queensland, Australia, and demonstrating the utility of scanning (surface and ct) in taphonomic and ichnofossil interpretation. Society of Vertebrate Paleontology. Brisbane: Journal of Vertebrate Paleontology, Program and Abstracts. p 119.
Hocknull SA, Zhao J-X, Feng Y-X, and Webb GE. 2007. Responses of Quaternary rainforest vertebrates to climate change in Australia. *Earth and Planetary Science Letters* 264:317-331. 10.1016/j.epsl.2007.10.004
Hoffman KL, and Brain TJ. 1991. Stratigraphic Drilling Report - GSQ McKinlay 1. In: Queensland GSo, editor. Brisbane: Queensland Government.

Hoffmann K. 1989. The influence of pre-Jurassic tectonic regimes on the structural development of the southern Eromanga Basin, Queensland.
Hollands CB, Nanson GC, Jones BG, Bristow CS, Price DM, and Pietsch TJ. 2006. Aeolian–fluvial interaction: evidence for Late Quaternary channel change and wind-rift linear dune formation in the northwestern Simpson Desert, Australia. *Quaternary Science Reviews* 25:142-162. 10.1016/j.quascirev.2005.02.007
Horstwood MSA, Košler J, Gehrels G, Jackson SE, McLean NM, Paton C, Pearson NJ, Sircombe K, Sylvester P, Vermeesch P, Bowring JF, Condon DJ, and Schoene B. 2016. Community-Derived Standards for LA-ICP-MS U-(Th-)Pb Geochronology - Uncertainty Propagation, Age Interpretation and Data Reporting. *Geostandards and Geoanalytical Research* 40:311-332. 10.1111/j.1751-908X.2016.00379.x
Idnurm M, and Senoir BR. 1978. Palaeomagnetic ages of late cretaceous and tertiary weathered profiles in the Eromanga Basin, Queensland. *Palaeogeography, Palaeoclimatology, Palaeoecology* 24:263-277. https://doi.org/10.1016/0031-0182(78)90010-X
Ingram JA. 1971. Eromanga, Qld Geological Map Sheet SG/54-12 1:250 000 Geological Series-Explanatory Notes. *Bureau of Mineral Resources Geology and Geophysics* 1.
Jell PA. 2004. Fossil insects of Australia. *Memoirs of the Queensland Museum* 50:1-124.
Johnstone S, Schwartz T, and Holm-Denoma C. 2019. A Stratigraphic Approach to Inferring Depositional Ages From Detrital Geochronology Data. Front. *Earth Sci* 7:57.
Juárez Valieri RD, and Calvo JO. 2011. Revision of MUCPv 204, a Senonian basal titanosaur from Northern Patagonia. . *Paleontología y dinosarios desde América Latina*. Mendoza: Editorial de la Universidad Nacional de Cuyo, Mendoza, 143-152.
Junchang L, Azuma Y, Rongjun C, Wenjie Z, and Xingsheng J. 2008. A new titanosauriform sauropod from the early Late Cretaceous of Dongyang, Zhejiang Province. *Acta Geologica Sinica-English Edition* 82:225-235.
Junchang L, Li X, Xingliao Z, Weiyong H, Yanhua W, Songhai J, and Qiang J. 2007. A new gigantic sauropod dinosaur with the deepest known body cavity from the Cretaceous of Asia. *Acta Geologica Sinica- English Edition* 81:167-176.
Kazhdan M, and Hoppe HJAToG. 2013. Screened poisson surface reconstruction. 32:1-13.
Keany M, Holford S, and Bunch M. 2016. Constraining Late Cretaceous exhumation in the Eromanga Basin using sonic velocity data %J The APPEA Journal. 56:101-126. https://doi.org/10.1071/AJ15009
Kemp A. 1991. Australian Mesozoic and Cainozoic lungfish. In: Vickers-Rich P, Monaghan JM, Baird RF, and Rich TH, eds. *Vertebrate palaeontology of Australasia*. Melbourne, Victoria: Monash University, 465-496.
Kemp A. 1997. Four species of Metaceratodus (Osteichthyes: Dipnoi, Family Ceratodontidae) from Australian Mesozoic and Cenozoic deposits. *Journal of Vertebrate Paleontology* 17:26-33.
Kilbourne BM, and Makovicky PJJJoA. 2010. Limb bone allometry during postnatal ontogeny in non-avian dinosaurs. 217:135-152.
King S, and Mee B. 2004. The seismic stratigraphy and petroleum potential of the Late Cretaceous ceduna Delta, ceduna Sub-basin, Great australian bight.
Klötzli U, Klötzli E, Günes Z, and Kosler J. 2009. Accuracy of laser ablation U- Pb zircon dating: Results from a test using five different reference zircons. *Geostandards and Geoanalytical Research* 33:5-15.
Košler J, Sláma J, Belousova E, Corfu F, Gehrels GE, Gerdes A, Horstwood MS, Sircombe KN, Sylvester PJ, and Tiepolo M. 2013. U- Pb detrital zircon analysis–Results of an inter- laboratory comparison. *Geostandards and Geoanalytical Research* 37:243-259.
Kreutzer LA. 1988. Megafaunal butchering at Lubbock Lake, Texas: a taphonomic reanalysis. *Quaternary Research* 30:221-231.

Krieg GW, Callen RA, Gravestock DI, and Gatehouse CG. 1990. Geology. In: Tyler MJ, Twidale CR, Davies M, and Wells CB, eds. *Natural History of the Northern Deserts*. Adelaid, South Australia: Royal Society of South Australia Occassional Publications, 1-26.

Lacovara KJ, Lamanna MC, Ibiricu LM, Poole JC, Schroeter ER, Ullmann PV, Voegele KK, Boles ZM, Carter AM, Fowler EK, Egerton VM, Moyer AE, Coughenour CL, Schein JP, Harris JD, Martinez RD, and Novas FE. 2014. A gigantic, exceptionally complete titanosaurian sauropod dinosaur from southern Patagonia, Argentina. *Sci Rep* 4:6196. 10.1038/srep06196

Lautenschlager S. 2016. Reconstructing the past: methods and techniques for the digital restoration of fossils. *R Soc Open Sci* 3:160342. 10.1098/rsos.160342

Lawrence MG. 1998. SSL Wareena 4 Well Completion Report. Santos Ltd. ReportCR 30831. Brisbane, Queensland: Department of Natural Resources and Mines Queensland.

Le Cabec A, and Toussaint M. 2017. Impacts of curatorial and research practices on the preservation of fossil hominid remains. *J Anthropol Sci* 95:7-34. 10.4436/JASS.95002

Le Loeuff J. 2005. Osteology of *Ampelosaurus atacis* (Titanosauria) from southern France. *Thunder-lizards The sauropodomorph dinosaurs*, 115-137.

Leahey LG, Molnar RE, Carpenter K, Witmer LM, and Salisbury SW. 2015. Cranial osteology of the ankylosaurian dinosaur formerly known as *Minmi* sp.(Ornithischia: Thyreophora) from the Lower Cretaceous Allaru Mudstone of Richmond, Queensland, Australia. *PeerJ* 3:e1475.

Leahey LG, and Salisbury SW. 2013. First evidence of ankylosaurian dinosaurs (Ornithischia: Thyreophora) from the mid-Cretaceous (late Albian–Cenomanian) Winton Formation of Queensland, Australia. *Alcheringa: An Australasian Journal of Palaeontology* 37:249-257. 10.1080/03115518.2013.743703

Lehman TM, and Coulson AB. 2002. A juvenile specimen of the sauropod dinosaur *Alamosaurus sanjuanensis* from the Upper Cretaceous of Big Bend National Park, Texas. *Journal of Paleontology* 76:156-172.

Li LG, Li DQ, You HL, and Dodson P. 2014. A new titanosaurian sauropod from the Hekou Group (Lower Cretaceous) of the Lanzhou-Minhe Basin, Gansu Province, China. *PLoS One* 9:e85979. 10.1371/journal.pone.0085979

Lloyd J, Collins AS, Payne JL, Glorie S, Holford S, and Reid AJ. 2016. Tracking the Cretaceous transcontinental Ceduna River through Australia: The hafnium isotope record of detrital zircons from offshore southern Australia. *Geoscience Frontiers* 7:237-244. https://doi.org/10.1016/j.gsf.2015.06.001

Longman HA. 1927. The giant dinosaur: *Rhoetosaurus brownei*. *Memoirs of the Queensland Museum* 9:1-18.

Lowman R. 2010. SSL Wareena 5 Well Completion Report. Santos Ltd. Report CR 62290. Brisbane, Queensland: Department of Natural Resources and Mines Queensland.

Lü J, Xu L, Jia S, Zhang X, Zhang J, Yang L, You H, and Ji Q. 2009. A new gigantic sauropod dinosaur from the Cretaceous of Ruyang, Henan, China. *Geological Bulletin of China* 28:1-10.

Ludbrook N. 1985. Trigonioididae (Mollusca: Bivalvia) from the Cretaceous of Lake Eyre North, South Australia. *Trans R Soc South Aust* 109:77-82.

Lyman RL. 1994. Accumulation and dispersal of vertebrate remains. In: Lyman RL, ed. *Vertebrate Taphonomy*. Cambridge: Cambridge University Press, 161-222.

Mann DH, Groves P, Gaglioti BV, and Shapiro BA. 2018. Climate-driven ecological stability as a globally shared cause of Late Quaternary megafaunal extinctions: the Plaids and Stripes Hypothesis. *Biol Rev Camb Philos Soc*. 10.1111/brv.12456

Mannion PD, Allain R, and Moine O. 2017. The earliest known titanosauriform sauropod dinosaur and the evolution of Brachiosauridae. *PeerJ* 5:e3217. 10.7717/peerj.3217

Mannion PD, and Calvo JO. 2011. Anatomy of the basal titanosaur (Dinosauria, Sauropoda) Andesaurus delgadoi from the mid-Cretaceous (Albian-early Cenomanian) Río Limay Formation, Neuquén

Province, Argentina: implications for titanosaur systematics. *Zoological Journal of the Linnean Society*:no-no. 10.1111/j.1096-3642.2011.00699.x

Mannion PD, and Otero A. 2012. A reappraisal of the Late Cretaceous Argentinean sauropod dinosaur *Argyrosaurus superbus*, with a description of a new titanosaur genus. *Journal of Vertebrate Paleontology* 32:614-638. 10.1080/02724634.2012.660898

Mannion PD, Upchurch P, Barnes RN, and Mateus O. 2013. Osteology of the Late Jurassic Portuguese sauropod dinosaur *Lusotitan atalaiensis* (Macronaria) and the evolutionary history of basal titanosauriforms. *Zoological Journal of the Linnean Society* 168:98-206. 10.1111/zoj.12029

Mannion PD, Upchurch P, Jin X, and Zheng W. 2019a. New information on the Cretaceous sauropod dinosaurs of Zhejiang Province, China: impact on Laurasian titanosauriform phylogeny and biogeography. *R Soc Open Sci* 6:191057. 10.1098/rsos.191057

Mannion PD, Upchurch P, Schwarz D, and Wings O. 2019b. Taxonomic affinities of the putative titanosaurs from the Late Jurassic Tendaguru Formation of Tanzania: phylogenetic and biogeographic implications for eusauropod dinosaur evolution. *Zoological Journal of the Linnean Society*.

Maroulis JC, Nanson GC, Price DM, and Pietsch T. 2007. Aeolian–fluvial interaction and climate change: source-bordering dune development over the past~ 100 ka on Cooper Creek, central Australia. *Quaternary Science Reviews* 26:386-404.

Martínez RD, Giménez O, Rodríguez J, Luna M, and Lamanna MC. 2004. An articulated specimen of the basal titanosaurian (Dinosauria: Sauropoda) *Epachthosaurus sciuttoi* from the early Late Cretaceous Bajo Barreal formation of Chubut Province, Argentina. *Journal of Vertebrate Paleontology* 24:107-120. 10.1671/9.1

Martinez RD, Lamanna MC, Novas FE, Ridgely RC, Casal GA, Martinez JE, Vita JR, and Witmer LM. 2016. A Basal Lithostrotian Titanosaur (Dinosauria: Sauropoda) with a Complete Skull: Implications for the Evolution and Paleobiology of Titanosauria. *PLoS One* 11:e0151661. 10.1371/journal.pone.0151661

Mateus O, Mannion PD, and Upchurch P. 2014. *Zby atlanticus*, a New Turiasaurian Sauropod (Dinosauria, Eusauropoda) from the Late Jurassic of Portugal. *Journal of Vertebrate Paleontology* 34:618-634. 10.1080/02724634.2013.822875

Mond A. 1974. Simpson Desert North, Northern Territory: 1:250,000 Geological Series - Explanatory Notes. Record SG5304. . Geoscience Australia, Canberra.

Monteil E. 2006. Australian Mesozoic and Cenozoic Palynology Zonations – update to the 2004 Geologic Time Scale. In: Australia G, editor. Canberra, Australia: Geosciences Australia.

Moore PS, and Pitt GM. 1985. Cretaceous subsurface of the southwestern Eromanga Basin: a review. In: Lindsay JM, ed. *Stratigraphy, Palaeontology, Malacology – papers in honour of Dr Nell Ludbrook*. Adelaide, South Australia: South Australia Department of Mines and Energy, 269–286.

Moore PS, Pitt GM, and Dettmann ME. 1986. The Early Cretaceous Coorikiana Sandstone and Toolebuc Formation: their recognition and stratigraphic relationship in the south-western Eromanga Basin. . In: Gravestock DI, Moore PS, and Pitt GM, eds. *Contributions to the geology and hydrocarbon potential of the Eromanga Basin*. Canberra, ACT: Geological Society of Australia Special Publication 97-114.

Musser AM, Luo Z-X, Martinelli AG, Lamanna MC, Weisbecker V, Wroe S, and Salisbury SW. 2009. First Australian non-mammalian cynodont: new evidence for the unusual nature of Australia's Cretaceous vertebrate faunas. In: Travuillon KJ, Worthy TH, Hand SJ, and Creaser P, editors. 12th Conference on Australian Vertebrate Evolution, Palaeontology and Systematics. Sydney, New South Wales: Geological Society of Australia. p 47.

Navarrete C, Casal G, and Martínez R. 2011. *Drusilasaura deseadensis* gen. et sp. nov., un nuevo titanosaurio (Dinosauria-Sauropoda), de la Formación Bajo Barreal, Cretácico Superior del norte de Santa Cruz, Argentina. *Revista Brasileira de Paleontologia* 14:1-14.

Otero A. 2010. The Appendicular Skeleton of *Neuquensaurus*, a Late Cretaceous Saltasaurine Sauropod from Patagonia, Argentina. *Acta Palaeontologica Polonica* 55:399-426. 10.4202/app.2009.0099

Otero A. 2018. Forelimb musculature and osteological correlates in sauropodomorpha (Dinosauria, Saurischia). *PLoS One* 13:e0198988.

Otero A, Moreno AP, Falkingham PL, Cassini G, Ruella A, Militello M, and Toledo N. 2020. Three-dimensional image surface acquisition in vertebrate paleontology: a review of principal techniques. *Publicación Electrónica de la Asociación Paleontológica Argentina* 20 1–14. http://dx.doi.org/10.5710/PEAPA.04.04.2020.310

Pangaea Resources PL. 2013. Well completion report well, abandonment report QLD_ATP_1041P_Minion_9. In: Queensland GSo, editor. Brisbane: Queensland Government.

Paul G. 2019. Determining the largest known land animal: A critical comparison of differing methods for restoring the volume and mass of extinct animals. *Annals of Carnegie Museum* 85:335–358.

Pentland AH, Poropat SF, Tischler TR, Sloan T, Elliott RA, Elliott HA, Elliott JA, and Elliott DA. 2019. *Ferrodraco lentoni* gen. et sp. nov., a new ornithocheirid pterosaur from the Winton Formation (Cenomanian–lower Turonian) of Queensland, Australia. *Scientific Reports (Nature Publisher Group)* 9:1-13.

Percival LME, Helmond NAGM, Selby D, Goderis S, and Claeys P. 2020. Complex Interactions Between Large Igneous Province Emplacement and Global- Temperature Changes During the Cenomanian- Turonian Oceanic Anoxic Event (OAE 2). *Paleoceanography and Paleoclimatology* 35. 10.1029/2020pa004016

Pietroni N, Tarini M, Cignoni PJIToV, and Graphics C. 2009. Almost isometric mesh parameterization through abstract domains. 16:621-635.

Poropat SF, Mannion PD, Upchurch P, and Elliott DA. 2019. New sauropod dinosaur discoveries in the lower upper Cretaceous Winton Formation (Cenomanian– Lower Turonian) of Queensland, Australia: implications for titanosaurian evolution. Society of Vertebrate Palaeontology. Brisbane, Australia: Journal of Vertebrate Paleontology Program and Abstracts. p 171.

Poropat SF, Mannion PD, Upchurch P, Hocknull SA, Kear BP, and Elliott DA. 2015a. Reassessment of the non- titanosaurian somphospondylan *Wintonotitan wattsi* (Dinosauria: Sauropoda: Titanosauriformes) from the mid- Cretaceous Winton Formation, Queensland, Australia. *Papers in Palaeontology* 1:59-106. 10.1002/spp2.1004

Poropat SF, Mannion PD, Upchurch P, Hocknull SA, Kear BP, Kundrat M, Tischler TR, Sloan T, Sinapius GH, Elliott JA, and Elliott DA. 2016. New Australian sauropods shed light on Cretaceous dinosaur palaeobiogeography. *Sci Rep* 6:34467. 10.1038/srep34467

Poropat SF, Mannion PD, Upchurch P, Tischler TR, Sloan T, Sinapius GH, Elliott JA, and Elliott DAJJoVP. 2020. Osteology of the Wide-Hipped Titanosaurian Sauropod Dinosaur Savannasaurus Elliottorum from the Upper Cretaceous Winton Formation of Queensland, Australia.e1786836.

Poropat SF, Nair JP, Syme CE, Mannion PD, Upchurch P, Hocknull SA, Cook AG, Tischler TR, and Holland T. 2017. Reappraisal of *Austrosaurus mckillopi* Longman, 1933 from the Allaru Mudstone of Queensland, Australia's first named Cretaceous sauropod dinosaur. *Alcheringa: An Australasian Journal of Palaeontology*:1-38. 10.1080/03115518.2017.1334826

Poropat SF, Upchurch P, Mannion PD, Hocknull SA, Kear BP, Sloan T, Sinapius GH, and Elliott DA. 2015b. Revision of the sauropod dinosaur *Diamantinasaurus matildae* Hocknull et al. 2009 from the mid-Cretaceous of Australia: implications for Gondwanan titanosauriform dispersal. *Gondwana Research* 27:995-1033.

Ransley T, and Smerdon B. 2012. Hydrostratigraphy, hydrogeology and system conceptualisation of the Great Artesian Basin. In: CSIRO, editor. A technical report to the Australian Government from the CSIRO Great Artesian Basin Water Resource Assessment. Canberra, Australia: CSIRO Water for a Healthy Country Flagship Australia.

Raymond O, Liu S, Gallagher R, Zhang W, and Highet L. 2012. Surface Geology of Australia 1: 1 million scale dataset, 2012 edition. . In: Australia G, editor. Canberra, Australia: Geoscience Australia. p 20.

Robinson S. 1988. DIO Wareena 2 Well Completion Report. Delhi Petroleum Pty Ltd. Report CR 19911. Brisbane, Queensland: Department of Natural Resources and Mines Queensland.

Rodgers J, Wehr F, and Hunt J. 1991. Tertiary uplift estimation from velocity data in the Eromanga Basin. *Exploration Geophysics* 22:321-324.

Royo-Torres R, Cobos A, and Alcala L. 2006. A giant European dinosaur and a new sauropod clade. *Science* 314:1925-1927. 10.1126/science.1132885

Salisbury S. 2003. On the shoulders of a giant. *Australian Age of Dinosaurs*:12-19.

Salisbury SW. 2005. A new vertebrate assemblage from the mid-Cretaceous (Albian–Cenomanian) Winton Formation, central-western Queensland. In: Reed L, Bourne D, Megirian D, Prideaux G, Young G, and Wright A, editors. Proceedings of Conference of Vertebrate Evolution, Systematics and Palaeontology. Adelaide, South Australia: Alcheringa. p 465.

Salisbury SW, Herne MC, Lamanna MC, Nair JP, Syme C, and Witmer LM. 2019. An exceptionally preserved small-bodied ornithopod dinosaur from the Lower Cretaceous (Upper Albian) Winton Formation of Isisford, central-western Queensland, Australia, and the diversification of Gondwanan ornithopods. Society of Vertebrate Paleontology. Brisbane: Journal of Vertebrate Paleontology Program and Abstracts. p 185.

Salisbury SW, Molnar RE, Frey E, and Willis PM. 2006. The origin of modern crocodyliforms: new evidence from the Cretaceous of Australia. *Proceedings of the Royal Society B: Biological Sciences* 273:2439-2448.

Salisbury SW, Romilio A, Herne MC, Tucker RT, and Nair JP. 2016. The Dinosaurian Ichnofauna of the Lower Cretaceous (Valanginian–Barremian) Broome Sandstone of the Walmadany Area (James Price Point), Dampier Peninsula, Western Australia. *Journal of Vertebrate Paleontology* 36:1-152. 10.1080/02724634.2016.1269539

Sauermilch I, Whittaker JM, Bijl PK, Totterdell JM, and Jokat W. 2019. Tectonic, Oceanographic, and Climatic Controls on the Cretaceous- Cenozoic Sedimentary Record of the Australian-Antarctic Basin. *Journal of Geophysical Research: Solid Earth* 124:7699-7724. 10.1029/2018jb016683

Scanlon JD, and Hocknull SA. 2008. A dolichosaurid lizard from the latest Albian (mid-Cretaceous) Winton Formation, Queensland, Australia. Transactions of the Kansas Academy of Science (Fort Hays Studies Special Issue-Proceedings of the Second Mosasaur Meeting). p 131-136.

Seedsman KR. 1998. 1997 SQ 97 Seismic Survey ATP 259 Queensland Interpretation Report. Santos Ltd. Report CR 31073. Brisbane, Queensland: Department of Natural Resources and Mines Queensland.

Senior B. 1970. Barrolka, Qld Geological Map Sheet SG/54-11 1:250 000 Geological Series-Explanatory Notes. *Bureau of Mineral Resources Geology and Geophysics* 1.

Senior B, and Mabbutt J. 1979. A proposed method of defining deeply weathered rock units based on regional geological mapping in southwest Queensland. *Journal of the Geological Society of Australia* 26:237-254.

Senior D. 1968. Durham Downs, Qld Geological Map Sheet SG/54-15 1:250 000 Geological Series-Explanatory Notes. *Bureau of Mineral Resources Geology and Geophysics* 1.

Sharman GR, and Malkowski MA. 2020. Needles in a haystack: Detrital zircon U Pb ages and the maximum depositional age of modern global sediment. *Earth-Science Reviews* 203. 10.1016/j.earscirev.2020.103109

Silva J, Marinho TS, Martinelli AG, and Langer MC. 2019. Osteology and systematics of *Uberabatitan ribeiroi* (Dinosauria; Sauropoda): a Late Cretaceous titanosaur from Minas Gerais, Brazil. *Zootaxa* 4577:zootaxa 4577 4573 4571. 10.11646/zootaxa.4577.3.1

Simón E, Salgado L, and Calvo JO. 2017. A New Titanosaur Sauropod from the Upper Cretaceous of Patagonia, Neuquén Province, Argentina. *Ameghiniana* 55:1-29. 10.5710/AMGH.01.08.2017.3051

Smith JB, Lamanna MC, Lacovara KJ, Dodson P, Smith JR, Poole JC, Giegengack R, and Attia YJS. 2001. A giant sauropod dinosaur from an Upper Cretaceous mangrove deposit in Egypt. 292:1704-1706.

Stromer R. 1932. Ergebnisse der Forschungsreisen Prof. E. Stromers in den Wüsten Ägyptens. II. Wirbeltierreste der Baharîje-Stufe (unterstes Cenoman). 11. Sauropoda. *Abhandlungen der Bayerischen Akademie der Wissenschaften, Mathematisch-Naturwissenschaftliche Abteilung* 10:1-21.

Thulborn RA, and Wade M. 1984. Dinosaur trackways in the Winton Formation (mid-Cretaceous) of Queensland. *Memoirs of the Queensland Museum* 21:413-517.

Totterdell JM, and Krassay AA. 2003. Sequence stratigraphic correlation of onshore and offshore Bight Basin successions. In: Australia G, editor. Canberra: Australian Government.

Tucker RT, Roberts EM, Darlington V, and Salisbury SW. 2017. Investigating the stratigraphy and palaeoenvironments for a suite of newly discovered mid-Cretaceous vertebrate fossil-localities in the Winton Formation, Queensland, Australia. *Sedimentary Geology* 358:210-229. 10.1016/j.sedgeo.2017.05.004

Tucker RT, Roberts EM, Henderson RA, and Kemp AI. 2016. Large igneous province or long-lived magmatic arc along the eastern margin of Australia during the Cretaceous? Insights from the sedimentary record. *Bulletin* 128:1461-1480.

Tucker RT, Roberts EM, Hu Y, Kemp AI, and Salisbury SW. 2013. Detrital zircon age constraints for the Winton Formation, Queensland: contextualizing Australia's Late Cretaceous dinosaur faunas. *Gondwana Research* 24:767-779.

Turner M. 1997. SSL Wareena 3 Well Completion Report. Santos Ltd. Report CR 30488. Brisbane, Queensland: Department of Natural Resources and Mines Queensland.

Tykoski RS, and Fiorillo AR. 2016. An articulated cervical series of Alamosaurus sanjuanensis Gilmore, 1922 (Dinosauria, Sauropoda) from Texas: new perspective on the relationships of North America's last giant sauropod. *Journal of Systematic Palaeontology* 15:339-364. 10.1080/14772019.2016.1183150

Ullmann PV, and Lacovara KJ. 2016. Appendicular osteology of *Dreadnoughtus schrani*, a giant titanosaurian (Sauropoda, Titanosauria) from the Upper Cretaceous of Patagonia, Argentina. *Journal of Vertebrate Paleontology* 36:e1225303. 10.1080/02724634.2016.1225303

Upchurch P. 1998. The phylogenetic relationships of sauropod dinosaurs. *Zoological Journal of the Linnean Society* 124:43-103.

Upchurch P, Mannion PD, and Taylor MP. 2015. The anatomy and phylogenetic relationships of "*Pelorosaurus*" *becklesii* (Neosauropoda, Macronaria) from the Early Cretaceous of England. *PLoS One* 10:e0125819. 10.1371/journal.pone.0125819

Vanderstaay AGB. 2000. Soils of Western Queensland, Technical notes Western Queensland best practice guidelines. . In: Roads. QGDoM, editor. Brisbane, Queensland: Queensland Government.

Vergne R, Pacanowski R, Barla P, Granier X, and Schlick C. 2010. Radiance scaling for versatile surface enhancement. Proceedings of the 2010 ACM SIGGRAPH symposium on Interactive 3D Graphics and Games. p 143-150.

Vidal D, and Díez Díaz V. 2017. Reconstructing hypothetical sauropod tails by means of 3D digitization: Lirainosaurus astibiae as case study. *Journal of Iberian Geology* 43:293-305. 10.1007/s41513-017-0022-6

Vila B, Galobart À, Canudo J, Le Loeuff J, Dinarès-Turell J, Riera V, Oms O, Tortosa T, and Gaete RJP, Palaeoclimatology, Palaeoecology. 2012. The diversity of sauropod dinosaurs and their first

taxonomic succession from the latest Cretaceous of southwestern Europe: clues to demise and extinction. 350:19-38.
Voorhies MR. 1969. *Taphonomy and population dynamics of an early Pliocene vertebrate fauna, Knox County, Nebraska*: University of Wyoming Laramie.
Watson PJ. 1973. Lovelle Downs 1, Well Completion Report (Hematite Petroleum Ltd.). In: Queensland GSo, editor. Brisbane: Queensland Government.
Wedel MJ, and Taylor MPJPO. 2013. Caudal pneumaticity and pneumatic hiatuses in the sauropod dinosaurs Giraffatitan and Apatosaurus. 8:e78213.
White MA, Bell PR, Poropat SF, Pentland AH, Rigby SL, Cook AG, Sloan T, and Elliott DA. 2020. New theropod remains and implications for megaraptorid diversity in the Winton Formation (lower Upper Cretaceous), Queensland, Australia. 7:191462. doi:10.1098/rsos.191462
Whitlock JA, D'EMIC MD, and Wilson JAJP. 2011. Cretaceous diplodocids in Asia? Re- evaluating the phylogenetic affinities of a fragmentary specimen. 54:351-364.
Wilford J, Searle R, Thomas M, Pagendam D, and Grundy M. 2016. A regolith depth map of the Australian continent. *Geoderma* 266:1-13.
Wilkinson M, Hocknull SA, and Mackenzie R. 2019. What is and can be known about the Winton Formation? Understanding the geology of the Winton Formation and integrating newly discovered fossil fields from south-west Queensland, Australia. . Society of Vertebrate Paleontology. Brisbane, Queensland: Journal of Vertebrate Paleontology Program and Abstracts. p 219.
Wu W-H, Dong Z-M, Sun Y-W, Li C-T, and Li T. 2006. A New Sauropod Dinosaur from the Cretaceous of Jiutai, Jilin, China. *Global Geology* 25:6-9.
You H, Li D, Zhou L, and Ji Q. 2006. *Huanghetitan liujiaxiaensis*, a new sauropod dinosaur from the Lower Cretaceous Hekou Group of Lanzhou Basin, Gansu Province, China. *Geological Review* 52:668-674.
You H, Li D, Zhou L, and Ji Q. 2008. *Daxiatitan binglingi*: a giant sauropod dinosaur from the Early Cretaceous of China. *Gansu Geology* 17:1-10.
Zurriaguz VL, and Cerda IA. 2017. Caudal pneumaticity in derived titanosaurs (Dinosauria: Sauropoda). *Cretaceous Research* 73:14-24. 10.1016/j.cretres.2017.01.001

TABLES

Table 1. Cenomanian – ?Turonian fauna from the Winton Formation. Superscript numbers refer to citations: [1](Cook 2005), [2](Hocknull 1997), [3](Hocknull 2000), [4]Hocknull pers. obs. (2002, 2009, 2019), [5](Ludbrook 1985), [6](Fletcher & Salisbury 2014), [7](Jell 2004), [8](Elliott & Cook 2004), [9](Salisbury 2003), [10](Kemp 1991), [11](Kemp 1997), [12](Berrell et al. 2014), [13](Faggotter et al. 2007), [14](Mond 1974), [15](Salisbury 2005), [16](Scanlon & Hocknull 2008), [17](Salisbury et al. 2006), [18](Pentland et al. 2019), [19](Hocknull et al. 2009), [20] (Poropat et al. 2016), [21](Hocknull et al. 2019), [22](Poropat et al. 2019), [23](Elliott 2004), [24](White et al. 2020), [25](Thulborn & Wade 1984), [26](Hocknull & Cook 2008), [27](Salisbury et al. 2019), [28](Leahey & Salisbury 2013), [29](Musser et al. 2009).

	Northern Winton Formation (Winton, QLD)	Eastern Winton Formation (Isisford, QLD)	Southern Winton Formation (Eromanga-Quilpie, QLD)	Western Winton Formation (Northern Territory)	South-western Winton Formation (South Australia)
Freshwater Gastropods	*Melanoides* sp. indet.[1]				
Freshwater Bivalves	*Hyridella (Protohyridella) goodiwindiensis* [2,3] *Hyridella (Hyridella) macmichaeli* [2,3] *Megalovirgus wintonensis* [2,3] new genus et sp.[4]		*Hyridella (Hyridella) macmichaeli*[4,21]		*Pledgia eyrensis*[5]
Insects	?orbatid mite[6] Odonata[7,8] Mecoptera[7,8] Coleoptera[9]				
Fish	Teleostii[4] *Metaceratodus wollastoni*[10,11] *Metaceratodus ellioti*[10, 11] shark[4]	*Cladocyclus geddesi*[12] ?haleocomorph[13]		*Metaceratodus wollastoni*[4, 10, 11]	*Metaceratodus wollastoni*[10, 11] *Metaceratodus ellioti*[10, 11] shark[14]
Plesiosaur	Plesiosaur[15]				
Squamates	cf. *Coniasaurus*[16]				
Turtles	Chelidae[15,19]		Chelidae[4,21]		
Crocodiles	Crocodilia indet.[15,19]	*Isisfordia duncani*[17]			
Pterosaurs	*Ferodraco lentoni*[18]				
Sauropods	*Diamantinasaurus matildae*[19,20] *Savannasaurus elliottorum*[20] *Wintonotitan wattsi*[19] sauropod tracks[21,22]		*Australotitan cooperensis* [21](here) sauropod trample[21]		

Theropods	*Australovenator wintonensis*[19] Theropod~~an~~ indet.[23] Megaraptoran[24] Theropod tracks[25]		Theropod tracks[21]		
Ornithopods	Ornithopod indet.[26] Ornithopod tracks[25]	new[27]	Ornithopod tracks[21]		
Ankylosaurs	Thyreophora indet.[28]				
Mammalia	?cynodont[29]				
Dinosauria				Indeterminate bone[4]	

3187

Comentario [MH55]: Unplublished new species?

Comentario [MH56]: Not all cynodonts are mammals.

Table 2. Scapula measurements of Winton Formation sauropods.

	Preserved	Reconstructed
EMF102 *Australotitan cooperensis*		
Maximum proximodistal length	1220.5+	2182.98
Maximum acromial plate dorsoventral height (c)	498.94+	
Minimum scapular blade dorsoventral height (a)	264.89 (at base)	264.89
Maximum scapular blade dorsoventral height	313.36+	
Maximum proximodistal scapular blade length	911.12+	
Maximum mediolateral scapular blade thickness (b)	65.86	65.86
(b)/(a) – relative thickness of blade	0.25	0.25
(a) / (c) – relative acromion plate to minimum scapular blade height		0.48
AODF603 *Diamantinasaurus matildae*		
Maximum proximodistal length (d)	1485.48	
Maximum acromial plate dorsoventral height	354.46+	
Minimum scapular blade dorsoventral height (a)	283.15 (mid-blade)	
Maximum scapular blade dorsoventral height	407.37+ (distal expansion)	
Maximum proximodistal scapular blade length (c)	876.94	
Maximum mediolateral scapular blade thickness (b)	59.13	
(b)/(a) – relative thickness of blade	0.21	
QMF7292 *Wintonotitan wattsi*		
Maximum proximodistal length	1088.48+	
Maximum acromial plate dorsoventral height (c)	563.14	
Minimum scapular blade dorsoventral height (a)	235.34 (at mid-blade)	
Maximum scapular blade dorsoventral height	287.53+ (distal expansion)	
Maximum proximodistal scapular blade length	652.19+	
Maximum mediolateral scapular blade thickness (b)	77.42	
(b)/(a) – relative thickness of blade	0.33	
(a) / (c) – relative acromion plate to minimum scapular blade height	0.42	

Footnotes. All measurements in mm.

3194 **Table 3. Humerus measurements of Winton Formation sauropods.**

	Left (Preserved)	Right (Preserved)	Model
EMF102 *Australotitan cooperensis*			
Maximum proximodistal length (d)	1394.87+	1494.73	1500.25
Maximum medial, proximodistal length		1479.75	1448.58
Maximum lateral, proximodistal length	1329.61+	1390.54	1433.06
Maximum mediolateral width of proximal epiphysis		<723.26	667.95
Maximum anteroposterior length of proximal epiphysis		79.42+	114.23
Maximum mediolateral width across distal condyles	<561.87	514.83+	516.78
Maximum anteroposterior length of distal medial condyle	118.92+	186.25	173.11
Maximum anteroposterior length of distal centro-condyle	126.46+	187.27+	204.31
Maximum anteroposterior length of distal lateral condyle	99.44+	158.15+	172.02
Maximum midshaft mediolateral width (a)		333.34	335.81
Minimum midshaft anteroposterior length (b)		101.80	101.67
Minimum mediolateral width (c)		292.8	
Proximal epiphysis circumference		1564.36+	1621.54
Midshaft circumference (incl. base of deltopectoral crest (dpc))		1021.55+	1041.69
Minimum diaphyseal circumference		759	759
Distal condyles circumference	1238.31	1351.50+	1368.78
(b)/(a) – midshaft length to width		0.30	0.30
(c)/(d)		0.19	
AODF603 *Diamantinasaurus matildae*			
Maximum proximodistal length (d)	1122.35+	1056.34+	1154.11
Maximum medial, proximodistal length	1105.9	961.84+	1131.86
Maximum lateral, proximodistal length	1049.68	1056.55	1105.53
Maximum mediolateral width of proximal epiphysis	487.66	392.75+	510.27
Maximum anteroposterior length of proximal epiphysis		119.75	119.75
Maximum mediolateral width across distal condyles	379.56+	403.44+	448.37
Maximum anteroposterior length of distal medial condyle		208.16	208.16
Maximum anteroposterior length of distal lateral condyle		195.19	195.19
Maximum midshaft mediolateral width (a)	229.38	230.38	230.38
Minimum midshaft anteroposterior length (b)		81.4	81.4

Minimum mediolateral width (c)			234.11
Proximal epiphysis circumference	735.29+	1047.71+	1338.46
Midshaft circumference (incl. base of dpc)	331.62+	580.83	580.83
Minimum diaphyseal circumference			559.26
Distal condyles circumference	627.37+	1099.51	1128.89
(b)/(a) – midshaft length to width		0.35	0.35
(c)/(d)			0.20
QMF7292 *Wintonotitan wattsi*			
Maximum proximodistal length (d)	787.55+	617.05+	924.45+
Maximum medial, proximodistal length	n/a	575.09+	785.63+
Maximum lateral, proximodistal length	726.01+	n/a	878.31+
Maximum mediolateral width of proximal epiphysis	333.58+	n/a	333.58+
Maximum anteroposterior length of proximal epiphysis	71.7+	n/a	71.7+
Maximum mediolateral width across distal condyles	n/a	n/a	n/a
Maximum anteroposterior length of distal medial condyle	n/a	n/a	n/a
Maximum anteroposterior length of distal lateral condyle	n/a	n/a	n/a
Maximum midshaft mediolateral width (a)	183.49+	100.14+	241.15
Minimum midshaft anteroposterior length (b)	115.72	94.71+	115.72
Minimum mediolateral width (c)			248.81
Proximal epiphysis circumference			n/a
Midshaft circumference (incl. base of dpc)	447.16+	187.92+	674.30
Minimum diaphyseal circumference			583.48
Distal condyles circumference			n/a
(b)/(a) – midshaft length to width			0.48
(c)/(d)			?
AODF660 *Savannasaurus elliottorum*			
Maximum proximodistal length (d)	577.34+	1020.78+	1112 est.
Maximum medial, proximodistal length	n/a	864.07+	864.07+
Maximum lateral, proximodistal length	n/a	878.6+	878.6+
Maximum mediolateral width of proximal epiphysis	n/a	300.73+	300.73+
Maximum anteroposterior length of proximal epiphysis	n/a	n/a	n/a
Maximum mediolateral width across distal condyles	n/a	n/a	n/a
Maximum anteroposterior length of distal medial condyle	n/a	n/a	n/a
Maximum anteroposterior length of distal lateral condyle	n/a	n/a	n/a
Maximum midshaft mediolateral width (a)	232.6+	243.55	243.55

Minimum midshaft anteroposterior length (b)	136.77	<171.97	136.77
Minimum mediolateral width (c)			223.30
Proximal epiphysis circumference	n/a	n/a	n/a
Midshaft circumference (incl. base of dpc)	666.49+	<727.66	713.04
Minimum diaphyseal circumference			601.54
Distal condyles circumference	n/a	n/a	n/a
(b)/(a) – midshaft length to width			0.56
(c)/(d)			?

Footnotes. All measurements in mm.

Table 4. Ulna measurements of Winton Formation sauropods.

	Preserved	Reconstructed
EMF102 *Australotitan cooperensis*		
Maximum proximodistal length	1043.90+	1056.35
Olecranon – anteromedial process length	501.34+	518.46
Olecranon – anterolateral process length	298.85	298.85
Maximum distal condylar width	225.05+	241.67
Minimum distal condylar width	122.65+	134.72
Angle formed (amp-oc-alp)	48°	48°
Angle formed (oc-alp-amp)	102°	102°
Angle formed (alp-amp-oc)	29°	29°
AODF603 *Diamantinasaurus matildae*		
Maximum proximodistal length	727.83	
Olecranon – anteromedial process length	359.09	
Olecranon – anterolateral process length	321.98	
Maximum distal condylar width	204.37	
Minimum distal condylar width	157.53	
Angle formed (amp-oc-alp)	51°	
Angle formed (oc-alp-amp)	71°	
Angle formed (alp-amp-oc)	57°	
QMF7292 *Wintonotitan wattsi*		
Maximum proximodistal length	897.39+	
Olecranon – anteromedial process length	n/a	
Olecranon – anterolateral process length	326.42+	
Maximum distal condylar width	n/a	
Minimum distal condylar width	n/a	
Angle formed (amp-oc-alp)	n/a	
Angle formed (oc-alp-amp)	n/a	
Angle formed (alp-amp-oc)	n/a	

Footnotes. All measurements in mm.

Comentario [MH57]: Delete the last 5

3203

3204 **Table 5. Pubes measurements of Winton Formation sauropods.**

	Preserved	Preserved	Reconstructed
EMF102 *Australotitan cooperensis*	Left	Right	
Maximum pubis length	1262.77	1206.7+	
Maximum proximolateral to distolateral length (b)	1118.73	1035.18+	
Maximum length of ischial peduncle	628.22	615.27+	
Maximum anteroposterior acetabular length	389.58	n/a	
Maximum mediolateral mid-blade distance (a)	514.98	405.26+	
Maximum mediolateral distal-blade length	513.46	492.96+	
Maximum anteroposterior iliac peduncle length (c)	414.21	n/a	
Maximum mediolateral iliac peduncle width (d)	158.51	n/a	
Maximum obturator foramen length	113.87	112.41	
Maximum obturator foramen width	86.43	73.28	
Distance between anterior margin of iliac peduncles			1564.32
(a)/(b)	0.46		
(c)/(d)	2.61		
AODF603 *Diamantinasaurus matildae*			
Maximum pubis length	1056.28	1082.88	
Maximum proximolateral to distolateral length (b)	942.25	957.12	
Maximum length of ischial peduncle	413.24	379.21+	
Maximum anteroposterior acetabular length	441.29	348.15	
Maximum mediolateral mid-blade distance (a)	386.65	370.9	
Maximum mediolateral distal-blade length	305.24	357.74	
Maximum anteroposterior iliac peduncle length (c)	297.65	280.55	
Maximum mediolateral iliac peduncle width (d)	113.20	99.86	
Maximum obturator foramen length	71.92	80.76	
Maximum obturator foramen width	57.45	60.55	
Distance between anterior margin of iliac peduncles			1219.42
(a)/(b)	0.41	0.39	
(c)/(d)	2.63	2.81	
AODF660 *Savannasaurus elliottorum*			
Maximum pubis length	894.13+	997.18	
Maximum proximolateral to distolateral length (b)	651.8+	802.88	
Maximum length of ischial peduncle	458.9+	366.82+	
Maximum anteroposterior acetabular length	n/a	209.65	
Maximum mediolateral mid-blade distance (a)	415.58	420.97	
Maximum mediolateral distal-blade length	409.5	407.46	
Maximum anteroposterior iliac peduncle length (c)	n/a	n/a	
Maximum mediolateral iliac peduncle width (d)	n/a	n/a	
Maximum obturator foramen length	n/a	98.02	
Maximum obturator foramen width	n/a	52.75	
Distance between anterior margin of iliac peduncles			1083.71+

(a)/(b)		0.52	
~~(c)/(d)~~		~~n/a~~	

Footnotes. All measurements in mm.

Table 6. Ischia measurements of Winton Formation sauropods.

	Preserved	Preserved	Reconstructed
EMF102 *Australotitan cooperensis*	Left	Right	
Maximum ischial length	901.23	879.87+	
Maximum proximolateral to distomedial length	644.46	577.35+	
Maximum length of pubic peduncle	600.37	614.43	
Maximum anteroposterior acetabular length (a)	213.94	n/a	
Maximum anteroposterior mid-blade length (b)	274.97	250.05+	
Maximum dorsoventral (anteroposterior) distal-shaft width (c)	423.05	n/a	
Minimum dorsoventral (anteroposterior) ischial blade width (d)	259.15		
Maximum anteroposterior iliac peduncle length	227.81	n/a	
Maximum mediolateral iliac peduncle width	117.49	n/a	
Distance between iliac peduncles	mirrored		1171.71
Posterior-most medial projection to posterior-most point on iliac peduncle	602.5		
Posterior-most medial projection to anterior-most pubic peduncle	425.6		
(a)/(b)	0.78		
(c)/(d)	1.63		
AODF603 *Diamantinasaurus matildae*			
Maximum ischial length		668.7	
Maximum proximolateral to distomedial length		558.54	
Maximum length of pubic peduncle		366.73+	
Maximum anteroposterior acetabular length (a)		182.93	
Maximum anteroposterior mid-blade length (b)		207.04	
Maximum dorsoventral (anteroposterior) distal-shaft width (c)		381.12	
Minimum dorsoventral (anteroposterior) ischial blade width (d)		220.23	
Maximum anteroposterior iliac peduncle length		176.69	
Maximum mediolateral iliac peduncle width		91.63	
Distance between iliac peduncles			1002 estimated (est.)
Posterior-most medial projection to posterior-most point on iliac peduncle		559.04	
Posterior-most medial projection to anterior-most pubic peduncle		372.3	
(a)/(b)		0.88	
(c)/(d)		1.73	
QMF7292 *Wintonotitan wattsi*			
Maximum ischial length	776.9+		
Maximum proximolateral to distomedial length	643.5+		

Maximum length of pubic peduncle	337.6+		
Maximum anteroposterior acetabular length (a)	271.3		
Maximum anteroposterior mid-blade length (b)	276.6		
Maximum dorsoventral (anteroposterior) distal-shaft width (c)	274.1+ (420 est.)		
Minimum dorsoventral (anteroposterior) ischial blade width (d)	255.23		
Maximum anteroposterior iliac peduncle length	n/a		
Maximum mediolateral iliac peduncle width	n/a		
Distance between iliac peduncles	n/a		1065 est.
Posterior-most medial projection to posterior-most point on iliac peduncle	616.92		
Posterior-most medial projection to anterior-most pubic peduncle	413.69		
(a)/(b)	0.98		
(c)/(d)	1.64 est.		
AODF660 *Savannasaurus elliottorum*			
Maximum ischial length	578.28+	656.08	
Maximum proximolateral to distomedial length	546.49+	601.44	
Maximum length of pubic peduncle	449.59+	375.46+	
Maximum anteroposterior acetabular length (a)	n/a	198.89	
Maximum anteroposterior mid-blade length (b)	235.67	227.67	
Maximum dorsoventral (anteroposterior) distal-shaft width (c)	415.22	403.22	
Minimum dorsoventral (anteroposterior) ischial blade width (d)	238.32	233.5	
Maximum anteroposterior iliac peduncle length	n/a	189.59	
Maximum mediolateral iliac peduncle width	n/a	82.11	
Distance between iliac peduncles			1045.87+ 1078 est.
Posterior-most medial projection to posterior-most point on iliac peduncle	611.7		
Posterior-most medial projection to anterior-most pubic peduncle	392.47		
(a)/(b)		0.87	
(c)/(d)	1.74	1.73	

Footnotes. All measurements in mm.

3214 **Table 7. Femur measurements of Winton Formation sauropods.**

	Preserved	Estimate 1 reconstruction	Estimate 2 EMF105
EMF102 *Australotitan cooperensis* (holotype)			
Maximum proximodistal length (b)	n/a	1886.02	1888.32
Maximum medial, proximodistal length	1587.76+ (right)	1854.44	1791.32
Maximum lateral, proximodistal length	1582.46+ (right)	1833.52	1795.69
Maximum mediolateral width of proximal epiphysis	525.53+ (left)	626.93	611.85
Maximum anteroposterior length of proximal epiphysis	161.9+ (left)	213.16	276.88
Maximum mediolateral width across distal condyles	584.79	588.76	611.23
Maximum anteroposterior length of distal medial condyle	357.72+	363.64	375.12
Maximum anteroposterior length of distal lateral condyle	316.29+	324.63	332.69+
Maximum midshaft mediolateral width (a)	<466.03	460.09	409.63
Minimum midshaft anteroposterior width	166.21+	189.56	167.69
Proximal epiphysis circumference	1148.61+	1389.47	1427.78
Midshaft circumference	992.70+	1095.46	1018.37
Minimum diaphyseal circumference	932.8	932.8	915.9
Distal condyles circumference	1772.86+	1937.46	1757.5+
(a)/(b)		0.24	0.21
EMF105 *Australotitan cooperensis* (referred)			
Maximum proximodistal length (b)	1412.32	1412.32	
Maximum medial, proximodistal length	1310.42	1310.42	
Maximum lateral, proximodistal length	1379.44	1379.44	
Maximum mediolateral width of proximal epiphysis	469.77	469.77	
Maximum anteroposterior length of proximal epiphysis	219.82+	232.41	
Maximum mediolateral width across distal condyles	470.88	470.88	
Maximum anteroposterior length of distal medial condyle	279.32+	320.49	
Maximum anteroposterior length of distal lateral condyle	251.04+	296.94	
Maximum midshaft mediolateral width (a)	298.99	298.99	
Minimum midshaft anteroposterior width	143.16	143.16	
Proximal epiphysis circumference	1123.53+	1134.25	
Midshaft circumference	733.74	733.74	
Minimum diaphyseal circumference	717.91	717.91	

Distal condyles circumference	1273.13+	1443.93	
(a)/(b)	0.21		
AODF604 *Diamantinasaurus matildae*			
Maximum proximodistal length (b)	1357.87		
Maximum medial, proximodistal length	1297.88		
Maximum lateral, proximodistal length	1336.72		
Maximum mediolateral width of proximal epiphysis	412.5		
Maximum anteroposterior length of proximal epiphysis	187.42		
Maximum mediolateral width across distal condyles	488.57		
Maximum anteroposterior length of distal medial condyle	255.32		
Maximum anteroposterior length of distal lateral condyle	235.43		
Maximum midshaft mediolateral width (a)	274.21		
Minimum midshaft anteroposterior width	104.54		
Proximal epiphysis circumference	902.19		
Midshaft circumference	661.92		
Distal condyles circumference	1366.26		
(a)/(b)	0.20		
QMF43302 ?*Wintontitan wattsi*			
Maximum proximodistal length (b)	1505.68		
Maximum medial, proximodistal length	1430.59+		
Maximum lateral, proximodistal length	1438.89+		
Maximum mediolateral width of proximal epiphysis	388.78+		
Maximum anteroposterior length of proximal epiphysis	188.98+		
Maximum mediolateral width across distal condyles	436.86		
Maximum anteroposterior length of distal medial condyle	202.89+		
Maximum anteroposterior length of distal lateral condyle	161.68+		
~~Maximum midshaft mediolateral width (a)~~	~~?~~		
~~Minimum midshaft anteroposterior width~~	~~?~~		
~~Proximal epiphysis circumference~~	~~?~~		
~~Midshaft circumference~~	~~?~~		
~~Distal condyles circumference~~	~~?~~		
~~(a)/(b)~~	~~?~~		

Footnotes. All measurements in mm.

Comentario [MH58]: A brief explanation here of what Estimate 1 and 2 mean would be helpful.

Table 8. Synapomorphies of Titanosauria in Australian Taxa.

Synapomorphy	Clade	*Australotitan cooperensis*	*Diamantinasaurus matildae*	*Wintonotitan wattsi*	*Savannasaurus elliottorum*
Scapula					
Scapula, ventral margin with well-developed ventromedial process	Titanosauria	?	✓	✓	?
Humerus					
humerus length less than 80% femur length	Saltasauridae	✓ (~79%)	× (85%)	?	?
deltopectoral crest extends medially across anterior face	Titanosauria	✓ - less than *Saltasaurus* / *Opisthsocoelicaudia*	✓ - less than *Saltasaurus* / *Opisthsocoelicaudia*	?	?
deltopectoral crest strongly expanded distally	Saltasauridae	×	×	×	×
strong posterolateral bulge around level of deltopectoral crest	Saltasauridae	?	×	×	×
radial and ulnar condyles divided distally	*Alamosaurus* + 'Saltasaurini'	×	×	?	?
Anterior surface of distal lateral condyle of humerus undivided	Lithostrotia	×	×	?	?
Radius					
radius distal end beveled ~20° proximolaterally relative to shaft	Saltasauridae	?	✓	✓ - poorly preserved	×
Ulna					
Prominent olecranon process,	Lithostrotia	✓	✓	?✓	?

Comentario [MH59]: The ref to González Riga et al should be here.

Comentario [MH60]: What does this mean?

projecting well above proximal articulation					
Manus					
Metacarpal I:metacarpal II/III proximodistal length ratio ≥1.0	Lithostrotia	?	×	?	×
Pubis					
Anteroposterior to mediolateral width ratio of iliac articular surface of pubis ≥2.0	Titanosauria	✓	✓	?	?
Ischium					
Acetabular margin of ischium strongly concave in lateral view such that pubic articular surface forms proximodorsal projection	Titanosauria or Lithostrotia	✓	✓	?✓	✓
No emargination of ischium distal to pubic articulation	Titanosauria	✓	✓	?✓	✓
Ratio of dorsoventral width of distal end of ischial shaft: minimum shaft dorsoventral width <1.5	Titanosauria	× (1.63)	× (1.73)	× (~1.64)	× (1.74)
Femur					
Femur with longitudinal ridge on anterior face of shaft	*Alamosaurus* + 'Saltasaurini'	✓	×	?	?
Femoral distal condyles beveled	Saltasauridae	✓ - less than *Saltasaurus* /	✓ - less than *Saltasaurus* /	?	?

Comentario [MH61]: ?

Comentario [MH62]: ?

10° dorsomedially relative to shaft		*Bonatitan*	*Bonatitan*		
% of known characters		75%	100%	31-50%	43%
Not Titanosauria		1	1	1	1
Within Titanosauria		8	8	2 + 3 possible	2
Within Lithostrotia or Saltasaurini /Saltasauridae		5	4	1 + 2 possible	1
Not within Lithostrotia or Saltasaurini / Saltasauridae		4	8	3	5

Comentario [MH63]: Final counts, right? They should have a separate heading.

Footnotes. Synapomorphies of Titanosauria from (González Riga et al. 2019)

Table 9. Shared features between two or more Australian species.

Characteristic	*Australotitan*	*Diamantinasaurus*	*Wintontitan*	*Savannasaurus*
Scapula				
Medial tuberosity on the proximal scapular blade	×	✓	✓	?
Proximoventral process	?	✓	✓	?
Humerus				
Midshaft cross-sectional shape	Mediolaterally broad, anteroposteriorly narrow	Mediolaterally broad, anteroposteriorly narrow	Mediolateral breadth similar to anteroposterior length	Mediolateral breadth similar to anteroposterior length
Pubis				
Dorsoventral thickness along pubic blade.	Thin	Thick	?	Thin
Ischium				
Distal ischial blade ventrally curved, dorsal margin posteriorly	✓	×	?✓	✓

Comentario [MH64]: ?

facing.				
Anterior Caudal Vertebrae				
Amphicoelous	✓*	✓*	✓	✓
Pneumatic neural arch and zygopophyses	?	?	✓	✓
Centrum cancellous	✓*	✓*	✓	✓
Humerus / Ischium				
Minimum mediolateral width of humerus / minimum anteroposterior (dorsoventral) width of ischial distal blade	1.13	1.06	0.97	0.94

Footnote: *assumed present due to ubiquitous presence within the Winton Formation (See Discussion).

Comentario [MH65]: I do not see the morphological meaning or the comparative relevance of a ratio humerus fature vs. ischium feature.

Table 10. Maximum appendicular bone lengths for Australian sauropod taxa.

Taxon	Specimen	Humerus	Ulna	Femur
Rhoetosaurus brownei	QMF1659			1376 mm^{pres} 1525 mm$^{est\ (1)}$
Diamantinasaurus matildae	AODF603	1122 mm^{pres}	728 mm^{pres}	1358 mm^{pres}
Wintonotitan wattsi	QMF7292	924 mm$^{recon\ pres}$ 1253 mm$^{recon\ est}$	897 mm$^{recon\ pres}$ 919 mm$^{recon\ est}$	
Wintonotitan wattsi?	QMF43302			1505 mm^{pres} 1600 mm^{est}
Savannasaurus elliottorum	AODF660	1020 mm$^{recon\ pres}$ 1112$^{recon\ est}$		
Australotitan cooperensis	EMF102	1494 mm^{pres}	1044 mm^{pres}	1886 mm$^{recon\ pres}$ 1888 mm$^{recon\ est}$
Australotitan cooperensis (referred)	EMF164			2146 mm^{est}

Footnote: [1] (Longman 1927). Abbreviations; pres = as preserved, est = estimated, recon = as reconstructed.

Comentario [MH66]: Does not appear in the main text. I recommend excluding it and modify the title accordingly: From "...for Australian sauropod taxa" to "…for sauropod taxa from Winton Fm".

Table 11. Relative humerus length to distance between iliac peduncles for Winton Formation taxa.

Taxon	Specimen	Humerus (a)	Pelvic Width (b)	a/b
Savannasaurus elliottorum	AODF660	1020+ mm$^{\text{recon pres}}$ 1112 mm$^{\text{recon est}}$	1046+ mm$^{\text{pres}}$ 1078 mm$^{\text{recon est}}$	1.03
Diamantinasaurus matildae	AODF603	1122 mm$^{\text{pres}}$	1002 mm$^{\text{recon est}}$	1.12
Wintonotitan wattsi	QMF7292	924+ mm$^{\text{recon pres}}$ 1253 mm$^{\text{recon est}}$	1065 mm$^{\text{est(1)}}$	1.18
Australotitan cooperensis	EMF102	1494 mm$^{\text{pres}}$	1171 mm$^{\text{recon est}}$	1.27

Footnotes: (1) estimate of pelvic width based on isometrically scaling *A. cooperensis* puboischial elements to match *W. wattsi* ischium.

Comentario [MH67]: As above said, I do not see the morphological meaning or the comparative relevance of a ratio humerus feature vs. ischium feature.

FIGURES

Figure 1. **Vertebrate fossil sites of the Winton Formation (Eromanga Basin).** Geographical map data from (http://pid.geoscience.gov.au/dataset/ga/61754) used under CC-BY 4.0 AU. Geological datasets, including the distribution and interpretation of the Quaternary, Winton and Mackunda formations and their associated and interpreted structures were combined using QGIS 3.14.1 software (http://qgis.org) with data retrieved for; Northern Territory from STRIKE (http://strike.nt.gov.au/wss.html) under CC-BY 4.0; South Australia from SARIG (http:/map.sarig.sa.gov.au) under CC-BY 3.0 AU; Queensland from QGlobe (http://qldglobe.information.qld.gov.au) under CC-BY 4.0; New South Wales and overall Eromanga Basin structure retrieved from (Raymond et al. 2012) (http://ga.gov.au) used under CC-BY 3.0 AU. Great Artesian (Australian) (Ransley & Smerdon 2012).

Comentario [MH68]: Mackunda looks orange in the map, maybe due to some overlapping layer.

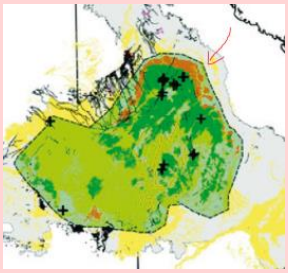

Figure 2. **Distribution of vertebrate fossil sites within the Winton Formation with regionally mapped geology and geological structures relating to the fossil sites described here**. A. The Winton Formation is here divided into five provinces of known vertebrate fossil sites, including a northern (Winton-Opalton region), central-eastern (Isisford), southern-central (Eromanga-Quilpie region), south-western (Kati Thunda / Lake Eyre) and western (Munga-Thirri / Simpson Desert). South-eastern semi-contemporaneous Griman Creek Formation (Lightning Ridge). B. New vertebrate fossil sites of the southern-central Winton Formation described here including the type locality for *Australotitan cooperensis* gen. et sp. nov. (EML011). Cross-sectional line (NW-SE) shown in Figure 4, A. Seismic line (83-NJZ) cross-sectional interpretation shown in Figure 4, B. Geographical map data from (http://pid.geoscience.gov.au/dataset/ga/61754) used under CC-BY 4.0 AU. Geological datasets, including the distribution and interpretation of the Quaternary, Alluvium, Sand Dunes, Glendower, Winton and Mackunda Formations and their associated and interpreted structures

Comentario [MH69]: The star for Sauropod Type Locality is not visible here.

were combined using QGIS 3.14.1 software (http://qgis.org) with data retrieved for; Northern Territory from STRIKE (http://strike.nt.gov.au/wss.html) under CC-BY 4.0; South Australia from SARIG (http:/map.sarig.sa.gov.au) under CC-BY 3.0 AU; Queensland from QGlobe (http://qldglobe.information.qld.gov.au) under CC-BY 4.0; New South Wales and overall Eromanga Basin structure retrieved from (Raymond et al. 2012) (http://ga.gov.au) used under CC-BY 3.0 AU. Great Artesian (Australian) Basin (Ransley & Smerdon 2012). Detailed southern-central geological structures, bores, wells and seismic data retrieved from ~~Qglobe~~ QGlobe (http://qldglobe.information.qld.gov.au) under CC-BY 4.0.

Figure 3. **Distribution of weathering depths of regolith and soil depth, relative to the Winton Formation**. A. Regolith depth illustrates the significantly deep weathering throughout central and southern Eromanga Basin, which has significantly influenced the Winton Formation in terms of geochemical alteration and post-diagenetic alterations at vertebrate fossil localities. B. Soil depth illustrates relatively deep soil profiles associated with vertebrate fossils sites from the Winton Formation, reflecting the impact of soil forming processes on available outcrop and vertebrate fossil preservation and exposure. Geographical map data from (http://pid.geoscience.gov.au/dataset/ga/61754) used under CC-BY 4.0 AU. Soil Depth dataset retrieved from CSIRO Soil and Landscape Grid National Soil Attribute Maps (https://data.csiro.au/dap/) under CC-BY 4.0. Regolith Depth dataset (Wilford et al. 2016) retrieved from CSIRO Soil and Landscape Grid National Soil Attribute Maps (https://data.csiro.au/dap/) under CC-BY 4.0. Outline of Winton and Mackunda formations retrieved for; Northern Territory from STRIKE (http://strike.nt.gov.au/wss.html) under CC-BY 4.0; South Australia from SARIG (http:/map.sarig.sa.gov.au) under CC-BY 3.0 AU; Queensland from QGlobe (http://qldglobe.information.qld.gov.au) under CC-BY 4.0; New South Wales and overall Eromanga Basin structure retrieved from (Raymond et al. 2012) (http://ga.gov.au) used under CC-BY 3.0 AU. Great Artesian (Australian) Basin (Ransley & Smerdon 2012).

Figure 4. **Interpretations of Winton Formation thickness associated with the vertebrate fossil sites described here, including the type locality for *Australotitan cooperensis* gen. et sp. nov.** A. Cross-sectional thickness of the Cenozoic/Quaternary deposits overlying the Winton Formation. Cross-section adapted from Figure 11d of (Hall 2015) under CC-BY 4.0. Mt. Howitt 1 well, which occurs close to the northern-most Plevna Downs vertebrate fossil sites (e.g. EML019), provides an approximate estimation of 300 m of Winton Formation thickness. However, the thickness of the preserved Winton Formation rapidly increases away from the crest of the anticline on the eastern and western flanks of the Mt. Howitt Anticline. B. Seismic Line 83-NJZ databeen reinterpreted by Santos Pty Ltd for this research project and includes the interpreted base of the Winton Formation by M.W. The base of the Winton Formation interpreted in Wareena 1 from petro-physical data is 270-300 metres. Interpretation of seismic line 83-NJZ indicates the dinosaur sites EML 010-013 are at a similar structural level to Wareena 1, near the crest of the anticline. Therefore, the type locality for *A. cooperensis* gen. et

sp. nov. is interpreted to be 270-300? m from the base of the Winton Formation (see text for additional justification). Seismic Line data available CC-BY 4.0 from ~~Qglobe~~ QGlobe and GSQ Open Data Portal (http://qldglobe.information.qld.gov.au and http://geoscience.data.qld.gov.au/seismic/ss095410).

Figure 5. **Winton Formation Thickness and Age**. A. Chronostratigraphic scheme showing the palynostratigraphic zones and lithostratigraphic units discussed in the text. B. Mackunda and Winton Formation outcrop distribution map showing dominant structural elements associated with sauropod type localities, position of stratigraphic cores and petroleum wells used to estimate the thickness of Winton Formation at the four sauropod type localities, 1: *Wintonotitan wattsi* type locality QML313, 2: *Diamantinasaurus matildae / Australovenator wintonensis* type locality AODL085, 3: *Savannasaurus elliottorum* type locality AODL082, 4: *Diamantinasaurus matildae* (referred) and QMF43302 discussed here from QML1333. C. Closeup of the northern Winton Formation sauropod type localities associated with stratigraphic cores, petroleum wells, geological structures (faults and anticlines). Dashed lines A-A' and B-B' indicate cross-sections provided in D. D. Two generalised cross-sections of the Winton Formation, west (A-A') and east (B-B') of the Cork Fault, showing the relative position of the sauropod type localities in relation to the estimated base of the Winton Formation. Red diamonds indicate the core depth of zircon samples with the age in millions of years (Ma) provided for the youngest graphical detrital zircon age peak (YPP) (Bryan et al. 2012; Tucker et al. 2016). Abbreviations: CA, Canaway Anticline; CF, Cork Fault; CNF, Canaway Fault; CS, Cooper Syncline; EA, Eyriewald Anticline; F, unnamed Fault; HA, Mt. Howitt Anticline; WS, Wetherby Structure. C. Geographical map data from (http://pid.geoscience.gov.au/dataset/ga/61754) used under CC-BY 4.0 AU. Winton and Mackunda formations retrieved for South Australia from SARIG (http:/map.sarig.sa.gov.au) under CC-BY 3.0 AU; Queensland from QGlobe (http://qldglobe.information.qld.gov.au) under CC-BY 4.0; New South Wales from (Raymond et al. 2012) (http://ga.gov.au) used under CC-BY 3.0 AU. Stratigraphic and petroleum wells, water bores and geological structures retrived from Qglobe (http://qldglobe.information.qld.gov.au) under CC-BY 4.0.

Figure 6. **Preservational examples of leaves, wood debris, bone debris, trampled sediments and articulated remains from southern Plevna Downs sites (EML011, 012 and 013)**. A-F. Leaves preserved indicate a dominance of conifers (Pinophyta) and ferns (Pterophyta). A. EMF177, conifer twig with leaves. B. EMF175, ?Bennettitalean leaf. C. EMF176, conifer twig with poorly preserved leaves. D. EMF174, Pterophyte leaf (?*Cladophlebis* sp.). E. EMF172, Pterophyte leaf (?*Sphenopteris* sp.). F. EMF173, conifer leaf 'mat'. G & H. Woody (wd) debris impressions in layers showing preferred orientation within thick sections of cemented siltstone. I. Bone (bn) and woody debris in cross-section with bone occurring at the base of the woody debris beds (arrow indicating upward direction). Underside of bone either corroded or eroded

off creating a scoured (sc) underside (EML013). J. Massive ichnological features showing trampled and cemented (cem) siltstone horizon, sediment deformation buldges (def) and partial sauropod foot imprints (tr) (EML011). K. Articulated sauropod skeleton from EML012 preserved within a siltstone concretion, including the torso and tail. Idenfiable elements include ribs (rib), dorsal vertebrate (dor), pelvic elements (pel) and caudal vertebrae (cdl). Scale bars?

Figure 7. **EML011, type locality of *Australotitan cooperensis* gen. et sp. nov. site sedimentology and taphonomy**. A. Site overview showing excavation pit, distant weathered geochemically weathered Glendower (Gl) and more proximal weathered Winton (Wf) and Quaternary alluvial (Qa) deposits. B. Semi-articulated pubes and ischia from *A. coopernesis~~cooperensis~~* gen. et sp. nov. with mediodorsal surfaces of each pubis facing upwards with the dislocated ischia in close articular approximation. C. In situ ovo-lobate deformation (def) of pubis. D. Cross-section (a-b) of sediment beneath pelvis showing downwardly deformed laminations (lam) of the siltstone (slt) above E. E. ~~a~~ A lower surface-scoured sandstone (ss) layer. F. Associated humerus (hum), ulna (uln) and scapula (sca) of *A. cooperensis* gen. et sp. nov. within the shallow stratigraphy of the site, including the surface vertosol (blacksoil, bs) that transitions into underlying Winton Formation siltstone (slt) with the bonebed (bb). A thin sandstone (ss) layer occurs below the siltstone and bonebed. Scale bars ~~—~~ = 10cm (C~~, D,~~ -E) and 100 cm (B & F).

Figure 8. **Examples of sauropod bone preservation and taphonomic alteration, including coloured reference scheme for 3-D models**. A-H. EMF102, right femur showing vertical displacement via a localized downward force acting upon the bone to deform the shaft. A. 3-D model showing the upward-facing in situ surface. B. 3-D model in medial view showing the relative downward deformation that has occurred to the bone from horizontal orientation. C. 3-D model in distomedial view showing a triangular-shaped depressed deformation of the femoral shaft that connects to the larger ovo-lobate deformation structure impacting the proximal shaft of the femur (D-F). G. Depth of deformation of the depressed (surface) cortical bone. H. Edge-detected 3-D model outline with interpreted outline of depression and indicating sauropod manus-like shape. I-J. EMF102, right ulna showing deformation of the distal shaft (I) and the digitally retrodeformed shaft (J). K-N. The right humerus illustrating the outward collapse of the deltopectoral crest (that occurred during excavation) (L & M) and the digitally retrodeformed deltopectoral crest (K & M). O. Coloured reference scheme for 3-D models illustrating preservational, taphonomic and 3-D model observations. Abbreviations: brk, broken or missing connecting surfaces; col, collapsed deltopectoral crest; cor, corroded surface; def, deformation; los, bone loss; mat, obscuring matrix; mod, poor model alignment/surface; mos, mosaic-fractured cortical bone surface; pla, plaster/infill; sur, surface/cortical bone missing; undef, undeformed. Scale bars = 20 cm.

Comentario [MH70]: In the two previous captions the abbreviations are within the text. Please use a single criterion.

Figure 9. **Scapulae of *Australotitan cooperensis* (EMF102), *Wintonotitan wattsi* (QMF7292) and *Diamantinasaurus matildae* (AODF603).** Each element is rendered using four methods from top to bottom, natural; ambient occlusion with radiance scaling; coloured schematic (see Figure 5); and orthogonal outline edge detection. A. & B. 3-D model of *A. cooperensis* left scapula in lateral (A) and medial (B) views. C. & D. 3-D model of *W. wattsi* left scapula in lateral (C) and medial (D) views. E. & F. 3-D model of *D. matildae* right scapula in lateral (E) and medial (F) views. G.-I. Proximoventral views showing mid scapular blade cross-sectional profile in *A. cooperensis* (G), *W. wattsi* (H) and *D. matildae* (I). Abbreviations: cr, central ridge of scapular blade; mt, medial tuberosity; pvp, proximoventral process; vr, ventral ridge of scapular blade. Scale bars = 20 cm.

Figure 10. **Scapulae of *Australotitan cooperensis* (EMF102), *Diamantinasaurus matildae* (AODF603) and *Wintonotitan wattsi* (QMF7292) in lateral view, ~~and~~ showing relative cross-sectional profile across the scapular blade.** A. *A. cooperensis* preserved scapula aligned within the reconstructed scapula. Aligned models rendered using transparency tool and orthogonal outline edge detection. B. *D. matildae* (mirrored right 3-D model). C. *W. wattsi*. Dashed vertical lines indicate position of cross-section. Dotted lines indicate estimation of missing scapular blade. All three scapulae are isometrically scaled to the minimum scapular blade dorsoventral height. Abbreviations as per Figure 8.

Figure 11. **Humeri of *Australotitan cooperensis* (EMF102).** A-B. Left partial humerus in anterior (A) and posterior (B) views. C.-S. Right humerus in anterior (C & D), posterior (E & F), distal (G) and oblique anterodistal (H-S) views. C, F and H are retrodeformed. 3-D image rendering methods used included, natural, ~~(~~A (left), B (right), C, D (middle), E (middle), F, G (middle), H & R; ambient occlusion with radiance scaling, A (middle), B (middle), D (left), E (right), G (left) & I; and coloured schematic (see Figure 5), A (right), B (left), D (right), E (left), G (right) & S. Scale bars = 20 cm.

Figure 12. **Humeri of *Diamantinasaurus matildae* (AODF603).** A-B. Left humerus in proximal (A) and anterior (B) views. C-F. Right humerus in proximal (C), anterior (D), posterior (E) and distal (F) views. G-L. Reconstructed left humerus using the left and right (mirrored) humeri in medial (G), posterior (H), anterior (I), lateral (J), proximal (K) and distal (L) views. 3-D image rendering methods used included, natural, ~~(~~A-D (left), E-F (right); ambient occlusion with radiance scaling, A-F (middle); coloured schematic (see Figure 5), A-D (right), E-F (left) and orthogonal outline edge detection (G-L). Scale bars = 20 cm.

Figure 13. **Humeri of *Wintonotitan wattsi* (QMF7292).** A-B. Partial right humerus in posterior (A) and anterior (B) views. C-D. Partial left humerus in anterior (C) and posterior (D) views. E-J. Reconstructed right humerus using partial left (mirrored) and right humeri in medial (E), posterior (F), anterior (G), lateral (H), proximal (I) and distal (J) views. 3-D image rendering

Comentario [MH71]: Please, provide orientation for the distal view (G).

Con formato: Resaltar

Con formato: Resaltar

Comentario [MH72]: Please, provide orientation for the proximal and distal views (A, C, F, L and K).

Comentario [MH73]: Please, provide orientation for the proximal and distal views (I-J)

Comentario [MH74]: Appears as **C & D** and **C, D** in caption of Fig 11 and as **C-D** here. Please, unify criteria,

Con formato: Resaltar

methods used included, natural, A & C (right), B & D (left); ambient occlusion with radiance scaling, A-D (middle); coloured schematic (see Figure 5), A & C (left), B & D (right); orthogonal outline edge detection (E-J). Scale bars = 20 cm.

Figure 14. **Humeri of *Savannasaurus elliottorum* (AODF660).** A-B. Left partial humerus in anterior (A) and posterior (B) views. C-D. Right partial humerus in anterior (C) and posterior (D) views. E-J. Reconstructed right humerus using partial left (mirrored) and right humeri in medial (E), posterior (F), anterior (G), lateral (H), proximal (I) and distal (J) views. 3-D image rendering methods used included, natural, A & C (left), B & D (right); ambient occlusion with radiance scaling, A-D (middle); coloured schematic (see Figure 5), A & C (right), B & D (left); orthogonal outline edge detection (E-J). Scale bars = 20 cm.

Figure 15. **Comparisons of Winton Formation sauropod humeri**. A-F. *A. cooperensis* (EMF102) right humerus in medial (A), anterior (B), posterior (C), lateral (D), proximal (E) and distal (F) views. G-L. *D. matildae* (AODF602), reconstructed as right humerus, in medial (G), anterior (H), posterior (I), lateral (J), proximal (K) and distal (L) views. M-R. *W. wattsi* (QMF7292) reconstructed as right humerus, in medial (M), anterior (N), posterior (O), lateral (P), proximal (Q) and distal (R) views. S-X. *S. elliottorum* (AODF660), reconstructed as right humerus, in medial (S), anterior (T), posterior (U), lateral (V), proximal (W) and distal (X) views. Y-AB. Reconstructed right humeri of *A. cooperensis* (Y), *W. wattsi* (Z), *D. matildae* (AA) and *S. elliottorum* (AB) scaled to minimum mediolateral width of the midshaft. Dotted lines estimating missing portions and shape of humerus. All 3-D models rendered using orthogonal outline edge detection. Scale bars = 20 cm.

Figure 16. **Comparisons of Winton Formation sauropod humeri in cross-section, scaled to minimum mediolateral midshaft width.** A. *Australotitan cooperensis*. B. *Diamantinasaurus matildae*. C. *Savannasaurus elliottorum*. D. *Wintonotitan wattsi*.

Figure 17. **Ulnae of *Australotitan cooperensis* (EMF102), *Diamantinasaurus matildae* (AODF603) and *Wintonotitan wattsi* (QMF7292).** A-D. *A. cooperensis* ulna in proximal (A), anterolateral (B), medial (C) and distal (D) views. E-H. *D. matildae* ulna in proximal (E), anteromedial (F), lateral (G) and distal (H) views. I-P. *W. wattsi* ulnae in proximal (I & M), anterolateral (J), anteromedial (N), medial (K), lateral (O) and distal (L & P) views. 3-D image rendering methods used included, natural, A, B, E, F, I, J, M & N (left), C, D, G, H, K, L, O, P (right); ambient occlusion with radiance scaling, A-P (middle); coloured schematic (see Figure 5), A, B, E, F, I, J, M, N (right), C, D, G, H, K, L, O, P (left). Abbreviations: alp, anterolateral process; amp, anteromedial process; ior, interosseous ridge of radial fossa; oc, olecranon process; rf, radial fossa; uac, distal ulnar accessory process. Scale bars = 20 cm.

Comentario [MH75]: Only for left humerus?

Comentario [MH76]: Please, provide orientation for the proximal and distal views (I-J)

Comentario [MH77]: Please, provide orientation for the proximal and distal views.

Comentario [MH78]: Please, provide orientation for the proximal and distal views.

Figure 18. **Comparisons of Winton Formation sauropod ulnae in cross-section, scaled to minimum midshaft width.** A. *Australotitan cooperensis*. B. *Diamantinasaurus matildae*. C. *Savannasaurus elliottorum*. D. *Wintonotitan wattsi* (reconstructed from both preserved ulnae). Abbreviations as in Figure 16. Dashed line indicates position of cross-section. Dotted line indicates estimation of missing bone.

Figure 19. **Comparisons of Winton Formation sauropod ulnae in preserved right ulna outline, scaled to minimum midshaft width.** A-E. *A. cooperensis* in lateral (A), anterolateral (B), anteromedial (C), medial (D) and posterior (E). F-J. *D. matildae* in lateral (F), anterolateral (G), anteromedial (H), medial (I) and posterior (J). K-O. *W. wattsi* (reconstruction) in lateral (K), anterolateral (L), anteromedial (M), medial (N) and posterior (O). 3-D images rendered using orthogonal outline edge detection.

Figure 20. **Pubes and ischia of *Australotitan cooperensis* (EMF102)**. A-B. Right pubis and ischium in ventrolateral (A) and dorsomedial (B) views. C-D. Left pubis and ischium in ventrolateral (C) and dorsomedial (D) views). E. Preserved left pubis and ischium in lateral view, red dotted line indicating region of deformation. F. Retrodeformed and digitally restored right pubis and ischium. 3-D image rendering methods used included, natural, A & D (right), B & C (left); ambient occlusion with radiance scaling, A-D (middle); coloured schematic (see Figure 5), A & D (left), B & C (right); vertex and texture uncoloured (E & F). Scale bars = 20 cm.

Figure 21. **Pubes and ischia of *Australotitan cooperensis* (EMF102) continued**. A. In-field 3-D model of pubes and ischia at EML011. B-C. After preparation, 3-D model of pubes and ischia reoriented to connect at pubic and ischial symphyses pre-displacement in dorsal (B) and anterior (C) views. D-E. Mirror of left pubis and ischium (least distorted) to reconstruct overall pelvic floor shape in anterior (D) and dorsal (E) views. Red dotted line indicates estimated extent of pubic and ischial blade contralateral bone with central diamond-shaped gap. F-H. Digitally restored pubes and ischia in dorsal (F), anterior (G) and posterior (H) views. 3-D image rendering methods used included, natural, A-E and vertex and texture uncoloured (F-H). Scale bars = 20 cm.

Figure 22. **Comparisons of Winton Formation sauropod pubes and ischia in dorsal, lateral, anterior and posterior views.** A. & E. *W. wattsi*, B, F, I & L. *D. matildae*, C, G, J & M. *A. cooperensis*, D, H, K & N. *S. elliottorum*. 3-D image rendering methods used included, ambient occlusion with radiance scaling, A-H (top); orthogonal outline edge detection, A-D (bottom) and I-N. Scale bars = 20 cm.

Figure 23. **Femora of *Australotitan cooperensis* gen. et sp. nov. (EMF102) and referred ~~femur~~ specimen (EMF105)**. A-C. EMF102, left proximal femur head in proximal (A),

Comentario [MH79]: Please, provide orientation of the cross sections and view of the ulna.

Comentario [MH80]: Please, provide orientation for the dosal views.

Comentario [MH81]: Please, provide orientation for the dorsal views.

Comentario [MH82]: Provide orientation for the proximal and distal views. It seems that in all (A, D, G-H and K) the posterior face is up.

posterior (B) and anterior (C) views. D-G. EMF102, right, near complete femur in proximal (D), posterior (E), anterior (F) and distal (G) views. EMF105, right femur in proximal (H), posterior (I), anterior (J) and distal (K) views. 3-D image rendering methods used included, natural, B, D, F, I, K (left), A, C, E, G, H, J (right); ambient occlusion with radiance scaling, A-K (middle); coloured schematic (see Figure 5), B, D, F, I, K (right), A, C, E, G, H, J (left). Scale bars = 20 cm.

Figure 24. **Femoral orthogonal outlines of *Australotitan cooperensis* gen. et sp. nov. (EMF102) as preserved and reconstructed, and referred femur (EMF105)**. A-E. EMF102 as preserved in medial (A), anterior (B), posterior (C), oblique lateral (D) and lateral (E). F-J. Reconstructed femur using left and right specimens in medial (F), anterior (G), posterior (H), lateral (I) and distal (J). EMF105 as preserved in medial (K), anterior (L), posterior (M), lateral (N) and distal (O). All images scaled to equal minimum mediolateral midshaft width. 3-D image rendering methods used orthogonal outline edge detection. Scale bars = 20 cm.

Comentario [MH83]: Please, provide orientation for the proximal and distal views (J-O)

Figure 25. **Northern Winton Formation femora, including the femur of *Diamantinasaurus matildae* holotype (AODF603).** A-C. AODF603 right femur in proximal (A), posterior (B) and distal (C) views. Anterior face of femur within fiberglass cradle and not available to this study. D-F. QMF43302 distal right femur in anterior (D), posterior (E) and distal (F) views. G-I. QMF43302 distal right femur in anterior (G), posterior (H) and distal (I) views. J-O. QMF43302 partial right femur in anterior (J), posterior (K), oblique medial (L), lateral (M-N) and medial (O) views. Posterior face of femur within fiberglass cradle and not available to this study. 3-D image rendering methods used included, natural, A, B, C, E, F, G, J, (left), D, H, I, K (right), L & M; ambient occlusion with radiance scaling A-K (middle), N & O; coloured schematic (see Figure 5), A, B, C, E, F, G, J, (right), D, H, I, K (left). Scale bars = 20 cm.

Comentario [MH84]: Please, provide orientation for the proximal and distal views.

Figure 26. **Northern Winton Formation femora in orthogonal outlines, including the femur of *Diamantinasaurus matildae* holotype (AODF603).** A-C. AODF603 right femur in proximal (A), posterior (B) and distal (C) views. D-G. QMF43302 partial right femur in medial (D), anterior (E), posterior (F) and lateral (G) views. H-L. QMF43302 distal right femur in medial (H), anterior (I), distal (J), lateral (K) and posterior (L). QMF43302 distal right femur in medial (M), anterior (N), distal (O), lateral (P) and posterior (Q). Scale bars = 20 cm.

Comentario [MH85]: Please, provide orientation for the proximal and distal views.

Figure 27. **3-D digital model restorations of the appendicular elements of *Australotitan cooperensis* holotype AOF603**. A-B. Scapula in lateral (A) and medial views (B). C-D. Humerus in anterior (C) and posterior (D) views. E-G. Ulna in anterolateral (E), posterior (F) and anteromedial (G) views. H-I. Pubes and ischia in dorsal (H) and lateral (I) views. J-K. Femur in posterior (J) and anterior (K) views. 3-D image rendering method was x-ray overlay of aligned 3-D models in orthogonal view.

Comentario [MH86]: Please, provide orientation for dorsal view.

Figure 28. **Comparative 'x-ray' renders of isometrically aligned skeletal elements shared between *Australotitan cooperensis* and other Winton Formation sauropods**. A-C. Comparison of preserved scapulae in lateral view. A. *A. cooperensis* aligned to *D. matildae*. B. *A. cooperensis* aligned to *W. wattsi*. C. *W. wattsi* aligned to *D. matildae*. D-I. Comparison of preserved humeri in anterior view. D. *A. cooperensis* aligned to *D. matildae*. E. *A. cooperensis* aligned to *S. elliottorum*. F. *A. cooperensis* aligned to *W. wattsi*. G. *W. wattsi* aligned to *S. elliottorum*. H. *D. matildae* aligned to *S. elliottorum*. I. *D. matildae* aligned to *W. wattsi*. J-L. Comparison of preserved ulnae in mediolateral view. J. *A. cooperensis* aligned to *D. matildae*. K. *A. cooperensis* aligned to *W. wattsi*. L. *D. matildae* aligned to *W. wattsi*. M-O. Comparison of preserved ischium. M. *A. cooperensis* aligned to *W. wattsi*. N. *D. matildae* aligned to *W. wattsi*. O. *S. elliottorum* aligned to *W. wattsi*. P-S. Comparison of preserved femora in posterior view. P. QMF43302 aligned to EMF105. Q. QMF43302 aligned to *D. matildae*. R. EMF105 aligned to *D. matildae*. S. Reconstructed femur of *A. cooperensis* (EMF102) aligned to referred femur EMF105.

Figure 29. **EMF165, a distal humerus referred to *A. cooperensis***. A. Anterior view. B. Posterior view. C. Distal view. 3-D image rendering methods used included, natural, A & C (left), B (right); ambient occlusion with radiance scaling A-C (middle); coloured schematic (see Figure 5) A & C (right), B (left). Scale bars = 20 cm.

Comentario [MH87]: Please, provide orientation for the distal view.

Figure 30. **EMF100 (EML01), a small partial ulna with similar morphological features to *A. cooperensis***. A-B. Ulna in mediolateral (A) and medial (B) views. C-J. Comparisons between EMF100(D) with *A. cooperensis* (C & J), *W. wattsi* (E & H) and *D. matildae* (F & J), scaled to minimum midshaft width. Mediolateral shape (top left), medial shape (top right), proximal shape (middle left), distal shape (middle right), midshaft cross-sectional shape (bottom left, cross-section position indicated by dotted line in top) and distal margin outline (bottom right). 3-D image rendering methods used included, natural, A (left), B (right); ambient occlusion with radiance scaling A& B (middle), C-J top and middle row; coloured schematic (see Figure 5) A (right), B (left); and orthogonal outline edge detect (bottom row). Scale bars = 20 cm.~~20cm~~

Comentario [MH88]: Please, provide orientation for the proximal and distal views.

Figure 31. **Sauropod caudal vertebrae from southern-central Winton Formation sites compared to *Wintonotitan wattsi* (QMF7292).** A. EMF109, series of articulated distal caudal vertebrae as part of an articulated skeleton (see Figure 7K), right lateral view. B. QMF7292, *Wintonotitan wattsi* holotype distal caudal vertebral series, right lateral view. C. Closeup of the most complete distal caudal in the series for *W. wattsi*, in oblique cranio-lateral view. D. QMF7292, *W. wattsi* holotype middle caudal vertebra, in oblique cranioventral view. E. EMF109 (EML012) middle caudal vertebra, in oblique cranioventral view. F. EMF171 (EML028) middle caudal vertebra, in oblique cranioventral view. G-H. Partial proximal distal caudal, EMF106, from EML010 in anterior (~~D~~G?) and lateral (~~E~~H?) views. Scale bars = 10 cm.~~10cm.~~

Figure 32. **Anterior caudal vertebra from *Wintonotitan wattsi* holotype (QMF7292).** A. Cranial view. B. Caudal view. C. Left lateral view. D. Right lateral view. 3-D image rendering methods used included, ambient occlusion with radiance scaling A & D (left), B & C (right); coloured schematic (see Figure 5) A & D (right), B & C (left). Scale bars = 20 cm.

Figure 33. **Anterior caudal vertebra from *Wintonotitan wattsi* holotype (QMF7292) showing pneumatic cavities within the neural arch.** A. A series of absorption contrast CT scan images taken from dorsal view through the prezygopophyses, neural arch and centrum. Revealing the internal cavities of the zygopophyses and neural arch that have been infilled with a dense material (iron-oxide pseudomorph of pyrite). B. A series of maximum intensity CT scan images taken from dorsal view through the prezygopophyses, through the neural arch and into the centrum. C & D. Coloured volume renders of the anterior caudal vertebra, clipped longitudinally through the vertebra at the position of the left prezygopophysis (C) and right prezygopophysis (D) to reveal the internal pneumatic cavities that have been partially infilled with iron-oxide pseudomorph of pyrite. Abbreviations: pne; pneumatic cavities, pyr; dense material infill (pseudomorph of pyrite). Scale bars?

Figure 34. **Anterior caudal vertebra from *Savannasaurus elliottorum* holotype (QMF7292).** A. Right lateral view. B. left lateral view. C. Cranial view. D. Caudal view. E. Right lateral view. F. Left lateral view. G. Anterior view. H. Posterior view. I-K. Anterior caudal vertebra of *S. elliottorum* (I & J) compared to *W. wattsi* (K) isometrically scaled to minimum central cranial-caudal length. All in left lateral orthogonal outline view. 3-D image rendering methods used included, natural; A, D, F, G (right), B, C, E, H (left); ambient occlusion with radiance scaling, A-H (middle); coloured schematic (see Figure 5), A, D, F, G (left) & B, C, E, H (right); Orthogonal outline edge detect, A-D (far left), F-H (far right) & I-K. Scale bars = 20 cm.

Figure 35. **Comparison of preserved size, estimated size, and shape in Winton Formation sauropod humeri, ulnae and femora (rendered as right elements).** A-D. Humeri in anterior view; A. *A. cooperensis*, B. *W. wattsi*, C. *D. matildae* and D. *S. elliottorum*. E-F. Ulnae in anterolateral view; E. *A. cooperensis*, F. *D. matildae*, G. *W. wattsi* (reconstruction). H-K. Femora in anterior view; H. *D. matildae*, I. ?*W. wattsi* (QMF7292), J. *A. cooperensis* (EMF105), K. *A. cooperensis* (reconstructed, EMF102). L-P. Femora in posterior view; L. *A. cooperensis* (EMF164), M. *A. cooperensis* (reconstruction, EMF102)), N. *A. cooperensis* (EMF105), O. ?*W. wattsi* (QMF7292) and *D. matildae*. Top rows are all natural vertex colour renders and bottom row are all orthogonal edge detected outlines. Dotted lines indicate estimated missing regions for incomplete specimens. Scale bar = 20 cm.

Figure 36. **Scatterplots of stylopodial measurements (mm)**.

A. Humerus length plotted against humerus circumference. B. Femoral length plotted against femoral circumference. C. Femoral length plotted against humeral length. Red stars indicate positions of holotype specimens of *D. matildae* (Dm) and *A. cooperensis* (Ac), with the grey star representing the estimated position for *A. cooperensis* referred femur EMF164. Abbreviations of sauropod taxa: Ah, *Argentinosaurus huiculensis*; Ai, *Atlasaurus imelakei*; As, *Alamosaurus sanjuanensis*; Ay, *Argyrosaurus superbus*; Aw, *Antarctosaurus wichmannianus*; Ba, *Brachiosaurs altithorax*; Ci, *Chubutisaurus insignis*; Dc, *Dreadnoughtus schrani*; El, *Elaltitan lilloi*; Fd, *Futalognkosaurus dukei*; Gb, *Giraffatitan brancai*; La, *Lourinhasaurus alenquerensis*; Ll, *Ligabuesaurus leanzai*; Ng, *Notocolossus gonzalezpare~~j~~i~~h~~asi*; Pl, *Paralititan stromeri*; Pm, *Patagotitan mayorum*; Tb, *Tehuelchesaurus benitezii*; Te, *Traukutitan eocaudata*. Measurement data from (Benson et al. 2014)